Search for anisotropy of ultrahigh-energy cosmic rays

A. A. Mikhaĭlov[a)] and M. I. Pravdin
Institute of Space Research and Aeronomy, 677891 Yakutsk, Russia

(Submitted 18 July 1997)
Pis'ma Zh. Éksp. Teor. Fiz. **66**, No. 5, 289–292 (10 September 1997)

It is shown that a statistically significant anisotropy exists in the arrival directions of cosmic rays with energies $\sim 1\times 10^{17}$ eV and 4×10^{18} eV.
© *1997 American Institute of Physics.* [S0021-3640(97)00117-5]

PACS numbers: 96.40.−z, 95.85.Ry

We have examined the arrival directions of extensive air showers (EASs) produced by ultrahigh-energy cosmic rays and registered by the Yakutsk EAS apparatus.[1] In the period 1974–1995 the apparatus detected more than 500 000 showers with energies of 3×10^{16}–2×10^{20} eV. To make a more accurate estimate of the parameters of the EASs the events for analysis were chosen according to the following criteria: arrival at zenith angles $\theta<60°$ and actuation of at least three master stations with a particle density ρ at each detector greater than 0.8 particles/m^2 in measurements since 1982 and greater than 2 particles/m^2 in measurements going back to 1974. In the measurements going back to 1974 showers with energies above 10^{18} eV were analyzed for the period from November to May (the months during which the apparatus operated most smoothly), and in the measurements since 1982 showers with energies below 10^{18} eV were analyzed for the same months. This left approximately 230 000 showers with energies above 3×10^{16} eV. The energy of the primary particle engendering an EAS was determined to within $\sim$30% and the arrival angle was determined to within $\sim 3-7°$. The energy of the showers was determined in terms of the particle density ρ at a distance of 600 m from the axis of the shower, taking into account the surrounding air temperature T and pressure P ($E=4.8\times 10^{17}\rho_{600}(\theta,P,T)$ eV).[2]

The entire observed energy range was divided into 10 uniform intervals, and the harmonics were determined, taking into account the exposure of the apparatus, according to the arrival directions of the showers in right ascension. The exposure of the apparatus was determined to within 1 min in right ascension and its amplitude is $\sim$1.3%. The results of the harmonic analysis — the amplitudes and phases of the first harmonic — are shown in Fig. 1. It is seen from the figure that, although a statistically significant amplitude was not observed, the phases in some neighboring intervals are correlated with one another to within the limits of error: for 3×10^{16}–3×10^{17} eV and 2×10^{18}–4×10^{19} eV.

Combining the first four energy intervals we obtain a statistically significant amplitude and phase of the first harmonic for the interval $3\times 10^{16}-3\times 10^{17}$ eV: $r_1=1.35\pm 0.36\%$, $\varphi_1=123°$, and $n=152280$ (number of events). The probability of this happening accidentally is $P\sim 0.0009$. In what follows, we shall denote the energy range $3\times 10^{16}-3\times 10^{17}$ eV by the letter $E1$ and the harmonic obtained there by the vector $\mathbf{R}1(1.3;\ 123°)$.

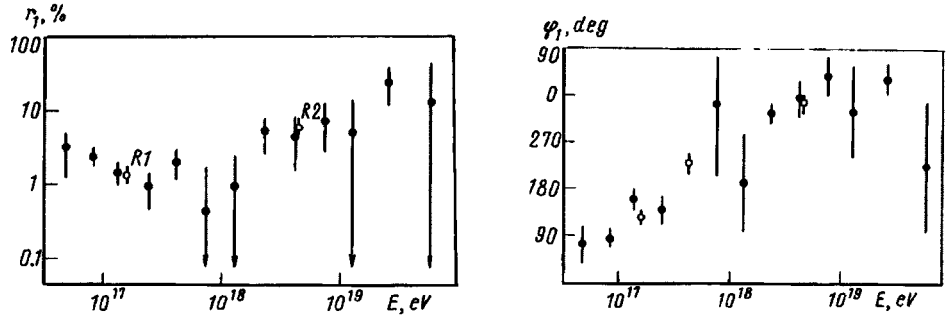

FIG. 1. Results of harmonic analysis. $R1$, $R2$ — statistically significant amplitudes in the energy ranges $E1$ (from 3×10^{16} to 3×10^{17} eV) and $E2$ (from 2×10^{18} to 4×10^{19} eV).

For the energy range 2×10^{18}–4×10^{19} eV the phases in five independent energy intervals fall within a 73° interval in right ascension (326°–37°) and they are directed toward the galactic plane. The probability of this happening accidentally equals $P\leqslant0.001$. The fact that the phases are directed toward the galactic plane most likely indicates that cosmic rays with energies up to 4×10^{19} eV are galactic rays, confirming our previous results (see, for example, Ref. 3). Combining these energy intervals we obtain a statistically significant amplitude and phase for the first harmonic: $r_1=6.4\pm1.8\%$, $\varphi_1=347°$, and $n=5683$, the probability of this happening accidentally being $P\sim0.0027$. In what follows, we designate the energy range 2×10^{18}–4×10^{19} eV by the letter $E2$ and the harmonic obtained there by the vector $\mathbf{R}2(6.4;\ 347°)$.

We performed an additional analysis in order to verify that the observed anisotropy is not accidental. The daily and seasonal variations of the surrounding air temperature T and pressure P could influence the arrival-direction distribution of the number of showers. This effect can be substantial for small energy ranges. We shall consider first the arrival directions of showers in the energy range $E1$.

1. If the threshold for selecting events with respect to density ρ at the master stations is increased, then the following amplitudes r_1 and phases φ_1 of the first harmonic are obtained: a) $r_1=1.5\pm0.5\%$, $\varphi_1=133°$, and $n=72586$ for $\rho>1.2$ particles/m^2; b) $r_1=0.6\pm1\%$, $\varphi_1=157°$, and $n=19534$ for $\rho>2$ particles/m^2. Analysis shows that when the detection threshold was changed, the phase of the anisotropy changed very little: $\varphi_1=123°$.

Figure 2 shows the distributions of the vectors of the first harmonic in terms of the solar-diurnal (S'), sidereal-diurnal (S), and antisidereal-diurnal (A) variations. Assuming that the spurious sidereal anisotropy is due to solar-diurnal variations which are constant in phase, we estimated the true sidereal anisotropy by the method of Ref. 4. This estimate gives the vector $\mathbf{r}_1=0.4\pm0.6\%$, $\varphi_1=151°$. This vector, which is determined from only the arrival time of the showers, is consistent with the main vector $\mathbf{R}1(1.3;\ 123°)$, obtained with the individual arrival directions of the showers taken into account.

Next we shall analyze both energy ranges $E1$ and $E2$.

The amplitudes and phases of the first harmonic of the arrival directions of showers

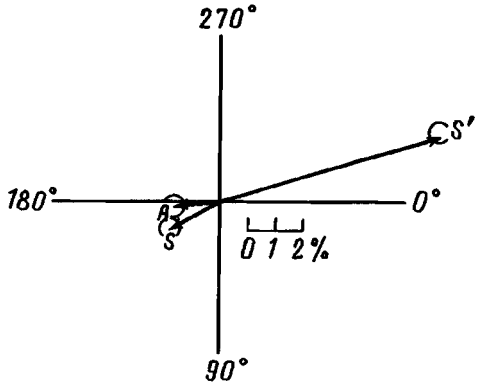

FIG. 2. First harmonics for the solar-diurnal (S'), sidereal-diurnal (S), and antisidereal-diurnal (A) variations. The circles show the errors in the harmonics.

in right ascension for shorter periods of observation are displayed in Fig. 3 (the years at the end of the observation periods, starting with 1982 for the $E1$ region and 1974 for the $E2$ region, are shown in parentheses). As one can see from Fig. 3, in the $E1$ energy range the amplitudes and phases lie within their error limits from the resultant vector **R**1(1.3; 123°) and they lie in the same half plane. The probability that all vectors lie in the same half plane is $P=5\times10^{-4}$. A similar pattern is observed in the $E2$ energy range. The probability that all vectors lie in the same half plane is $P=1\times10^{-3}$.

The amplitudes and phases of the first harmonic of the arrival directions of showers for separate observation months over the entire period are displayed in Fig. 4 (the numbers of the months are given in parentheses). As one can see from the figures, in both energy ranges $E1$ and $E2$ all vectors are always located within their error limits from the main vectors **R**1(1.3; 123°) and **R**2(6.4; 347°) and they lie in the same half plane as the

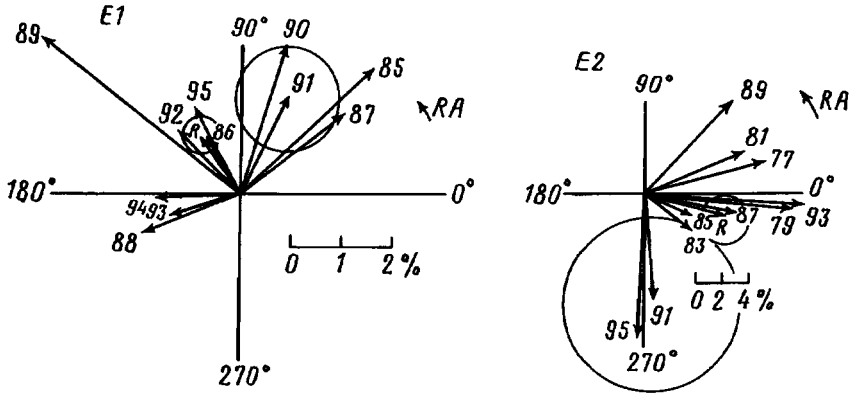

FIG. 3. First harmonics obtained from short observation periods in the energy ranges $E1$ and $E2$. The numbers indicate the years at the end of the observation periods.

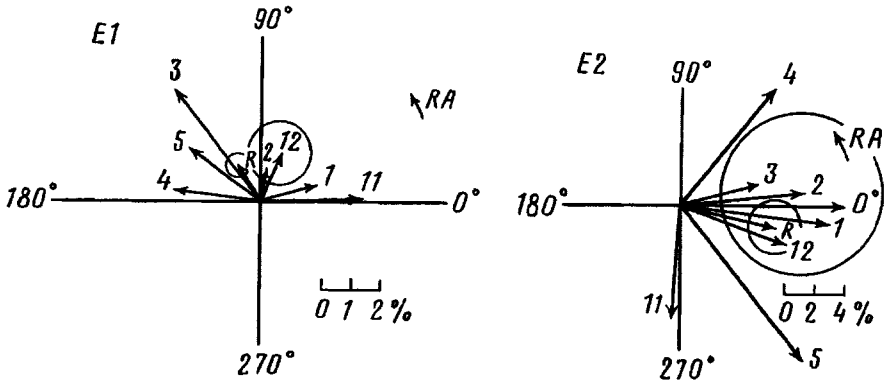

FIG. 4. First harmonics obtained from separate months of observations in the energy ranges $E1$ and $E2$ (the numbers represent the months). Circles — errors in the harmonics.

main vectors. The probabilities of this happening accidentally in the cases $E1$ and $E2$ are equal 8×10^{-3}.

Analysis of the data for separate observation years and months confirms the initially obtained vectors **R**1(1.3; 123°) and **R**2(6.4; 347°).

Of course, it is difficult to say that the effect of temperature and pressure on the particle distribution has been taken into account completely. But it should be kept in mind that the vectors **R**1(1.3; 123°) and **R**2(6.4; 347°) are in antiphase, and any factor that decreases the significance of one vector can automatically increase the significance of the other vector.

In conclusion, a statistically significant anisotropy has been found with amplitudes and phases $r_1=1.35\pm0.36\%$ and $\varphi_1=123°$ for energies of $\sim10^{17}$ eV and $r_1=6.4\pm1.8\%$ and $\varphi_1=347°$ for energies of $\sim4\times10^{18}$ eV. Efforts to take the effective atmospheric conditions into account in order to determine the anisotropy more accurately will continue.

[a)]e-mail: mikhailov@sci.yakutia.ru

---

[1]N. N. Efremov, A. A. Mikhailov, M. I. Pravdin, and I. Ye. Sleptsov, *Proceedings of the International Symposium on Extremely High-Energy Cosmic Rays: Astrophysics and Future Observations*, Tokyo, 1996, p. 418.
[2]V. N. Afanasiev, M. N. Dyakonov, V. P. Egorova *et al.*, *Proceedings of the International Symposium on Extremely High-Energy Cosmic Rays: Astrophysics and Future Observations*, Tokyo, 1996, p. 32.
[3]N. N. Efimov and A. A. Mikhaĭlov, JETP Lett. **54**, 67 (1991).
[4]F. J. Farley and J. R. Storey, Proc. Roy. Soc. A **67**, 996 (1954).

Translated by M. E. Alferieff

Unification of interactions in a model with composite particles

L. V. Prokhorov[a)]
Scientific-Research Institute of Physics, St. Petersburg State University, 198904 St. Petersburg, Russia

(Submitted 30 June 1997)
Pis'ma Zh. Éksp. Teor. Fiz. **66**, No. 5, 293–298 (10 September 1997)

A model for the unification of interactions with composite quarks, leptons, and Higgs fields is proposed on the basis of the $SU(5)$ group. The model explains in a natural manner the appearance of generations, mixing of cato-quarks, proton decay, and so on. A number of effects are predicted, specifically, the existence of a fourth generation of particles.
© *1997 American Institute of Physics.* [S0021-3640(97)00217-X]

PACS numbers: 12.60.Rc

INTRODUCTION

Experimental indications that quarks may not be elementary particles[1] make it necessary to take a new look at the unification problem. Models with composite particles (quarks, leptons, and Higgs fields) merit special attention. Arguments in favor of a composite nature of quarks and leptons are briefly reproduced below.[2]

This conjecture follows from two facts which are now reliably established: 1) Quarks and leptons interact weakly in the same manner, and 2) the electroweak interaction is described by a theory with non-Abelian local gauge symmetry. This means that quarks and leptons transform identically under the operations of this group. How is this possible? After all, quarks and leptons are completely different particles: Quarks interact strongly and leptons do not. This can happen in only two cases. First, it can happen if quarks and leptons belong to the same multiplet of an enveloping gauge group which contains as subgroups the strong and electroweak interactions. This is the grand unification path.[3] Second, it can happen if the quarks and leptons are composite particles and contain the same subparticles which interact only weakly (i.e., which realize the fundamental representation of the group $SU(2)\times U(1)$). The second alternative has been developed less actively, since it presupposed a knowledge of the forces which bind the subparticles. The experiment of Ref. 1 has given the first indication of the size of quarks ($\Lambda_c \sim 1.6$ TeV), making it possible to look at the problem from a new point of view.

CHOICE OF GAUGE GROUP

Let us suppose that quarks and leptons are composite particles. There immediately arises the question of the forces which bind the subparticles. The simplest assumption is that, besides the groups of strong and electroweak interactions, there is an additional group (for example, the hypercolor group $SU(n)_{c'}$, $n \geqslant 3$) that binds the subparticles similarly to the color group $SU(3)_c$. This path, however, merely transfers the problem to

 © 1997 American Institute of Physics

shorter distances where it must be solved anew. Indeed, now the subparticles ψ must carry two indices $\psi^{i}_{\alpha'}$ and $\psi^{\alpha}_{\alpha'}$, where $i=1,\ 2$ (electroweak interactions), $\alpha=1,2,3$ (strong interactions), $\alpha'=1,2,\ldots,n$ (hypercolor), and it must be assumed that these multiplets are parts of the fundamental representation $\Psi^{A}(\psi^{i}_{\alpha'},\psi^{\alpha}_{\alpha'},\ldots)$ of an enveloping group that includes $SU(n)_{c'}$, $SU(3)_{c}$, and $SU(2)\times U(1)$ as subgroups. But now there once again arises the problem of the forces that confine the subparticles Ψ, similarly to the situation when the symmetry group $G=SU(5)\supset SU(3)_{c}\times SU(2)\times U(1)$ was chosen as the minimum possible group. For this reason, we shall start with the $SU(5)$ group without introducing additional gauge fields. Superconductivity can serve as an argument in favor of this solution: In a theory with the $U(1)$ gauge group, Cooper pairs with nonzero binding energy appear without the introduction of additional forces. The assumption made obviously presupposes a quite complicated structure of the vacuum.

MODEL

Let us assume that the theory is determined by the gauge group $SU(5)$. Its elementary representation ζ^{a} $(\zeta^{1},\ldots,\zeta^{5})$ corresponds to a quintuplet of fundamental fermions. From these fermions composite fermions can be constructed (decuplet and singlet):

$$\omega^{ab}=\epsilon^{abc_1c_2c_3}\zeta^{*}_{c_1}\zeta^{*}_{c_2}\zeta^{*}_{c_3},\quad \omega=\epsilon^{a_1\cdots a_5}\zeta^{*}_{a_1}\ldots\zeta^{*}_{a_5}, \tag{1}$$

where $\epsilon^{a_1\cdots a_5}$ is the antisymmetric unit tensor of the $SU(5)$ group; the bilinear fields are $\Phi=\zeta^{*}_{a}\zeta^{a}$ (singlet), $\Phi^{b}_{a}=\zeta^{*}_{a}\zeta^{b}-\frac{1}{5}\Phi\,\delta^{b}_{a}$ (24-plet), and $\varepsilon^{abc}=\epsilon^{abca_1a_2}\zeta^{*}_{a_1}\zeta^{*}_{a_2}$ (decuplet); and, the scalar quintet is

$$\varphi^{a}=\epsilon^{aa_1\cdots a_4}\zeta^{*}_{a_1}\ldots\zeta^{*}_{a_4}. \tag{2}$$

There are a total five fundamental and 11 composite fermions as well as a set of scalar fields. If, now, the quintuplet ζ^{a} is identified with the right-handed d-quarks, a positron, and an antineutrino

$$\zeta^{a}_{R}\equiv(q^{\alpha},l^{i})_{R}\equiv(d^{1},d^{2},d^{3},e^{+},\widetilde{\nu})_{R} \tag{3}$$

($\alpha=1,2,3$ enumerates the color indices and $i=4,5$ enumerates the isotopic indices, i.e., the indices of the $SU(2)$ group of the electroweak interactions) and the conjugate quintuplet is identified with their CP-conjugates

$$\widetilde{\zeta}_{aL}\equiv(\widetilde{q}_{\alpha},\widetilde{l}_{i})_{L}\equiv(\widetilde{d}_{1},\widetilde{d}_{2},\widetilde{d}_{3},e^{-},\nu)_{L}, \tag{4}$$

then it is easily seen that the decuplet

$$\omega^{ab}_{L}=\begin{pmatrix} 0 & \widetilde{U}_{3} & -\widetilde{U}_{2} & -U^{1} & -D^{1}\\ . & 0 & \widetilde{U}_{1} & -U^{2} & -D^{2}\\ . & . & 0 & -U^{3} & -D^{3}\\ . & . & . & 0 & -E^{+}\\ . & . & . & . & 0 \end{pmatrix}_{L} \tag{5}$$

together with the fundamental quintuplet give a complete set of fermions of the standard model

$$\begin{pmatrix} U \\ D \end{pmatrix}_L, \quad U_R, d_R, \quad \begin{pmatrix} \nu \\ e^- \end{pmatrix}_L, \quad E_R^- . \tag{6}$$

The composite particles are designated by capital letters; the quarks U_R are obtained by CP-conjugation from the particles $\widetilde{U}_L$ in the upper left-hand corner of the matrix (5).

The Lagrangian of the model is identical to that of QCD for one flavor with the gauge group changing as $SU(3) \to SU(5)$.

Thus, we have a model with the gauge group $SU(5)$ and composite quarks and leptons. In addition to the standard set, there is another fermion ω, which, however, is a $SU(5)$ singlet and does not interact with the gauge fields at low energies (i.e., it is difficult to observe). The components φ^i $(i=1,2)$ of the field (2) can be identified with the Higgs field of the standard model. The fundamental particles and their components are:

Particles		Antiparticles	
fermions			
	$[d^1, d^2, d^3, e^+, \widetilde{\nu}]_R$	$[\widetilde{d}_1, \widetilde{d}_2, \widetilde{d}_3, e^-, \nu]_L$	
$U^\alpha(\widetilde{d}\widetilde{d}\nu)_L$	$U^\alpha(de^+\widetilde{\nu})_R$	$\widetilde{U}_\alpha(\widetilde{d}e^-\nu)_L$	$\widetilde{U}_\alpha(dd\widetilde{\nu})_R$
$D^\alpha(\widetilde{d}\widetilde{d}e^-)_L$			$\widetilde{D}_\alpha(dde^+)_R$;
$E^+(\widetilde{d}\widetilde{d}\widetilde{d})_L$			$E^-(ddd)_R$
$\omega(\widetilde{d}\widetilde{d}\widetilde{d}e^-\nu)$			$\widetilde{\omega}(ddde^+\widetilde{\nu})$;
Higgs fields			
$\varphi_+(\widetilde{d}\widetilde{d}\widetilde{d}\nu)$	$\varphi_+^+(ddd\widetilde{\nu})$		
$\varphi_0(\widetilde{d}\widetilde{d}\widetilde{d}e^-)$	$\varphi_0^+(ddde^+)$.		

(7)

(8)

It is interesting to watch how masses appear in the proposed model. For example, in the transition

$$e_L^- \underset{\to\to\to}{\varphi_0^+(ddde^+)} E_R^- \tag{9}$$

the left-handed electron annihilates with a right-handed positron of the Higgs field φ_0^+ (see Eqs. (7) and (8); it is assumed that $\langle \varphi_0^+ \rangle_0 \neq 0$, $\langle \varphi_0 \rangle_0 \neq 0$). The mass of the d quark is generated similarly:

$$d_R \underset{\to\to\to}{\varphi_0(\widetilde{d}\widetilde{d}\widetilde{d}e^-)} D_L . \tag{10}$$

Proton decay is described just as simply:

$$P\{U(\widetilde{d}\widetilde{d}\nu)U(\widetilde{d}\widetilde{d}\nu)D(e^-\widetilde{d}\widetilde{d})\} \to \{U(\widetilde{d}\widetilde{d}\nu)\widetilde{U}(\widetilde{d}e^-\nu)E^+(\widetilde{d}\widetilde{d}\widetilde{d})\} = \pi^0\{U\widetilde{U}\}E^+, \tag{11}$$

i.e., an exchange of a $\tilde{d}$ quark and an electron e_L^- (or $\tilde{d}$ and ν) between the U and D quarks of a proton is equivalent to the transition $P \to \pi^0 e^+$.

Particle generations appear naturally in the model. For example, the replacement of an elementary $\tilde{d}$ quark in a D quark by a composite $\tilde{D}$ quark signifies the appearance of a fermion of a new type, which is naturally identified as an S quark $S_L(\tilde{d}\tilde{D}e^-) \equiv S_L(\tilde{d}(dde^+)e^-)$, and a fermion with two quarks replaced is identified as a B quark $B_L(\tilde{D}\tilde{D}e^-)$. The μ and τ leptons arise similarly: $M_R^-(ddD)$ and $T_R^-(dDD)$.

The model predicts the existence of a fourth generation of particles

$$Q(\tilde{D}\tilde{D}E^-), \quad L^-(DDD); \tag{12}$$

the first one being a quark and the second a lepton.

A neutrino can transform in the vacuum into an ω particle

$$\nu \overset{\varphi_0(\tilde{d}\tilde{d}\tilde{d}e^-)}{\to\to\to} \omega, \tag{13}$$

i.e., ω can be identified with ν_R, and neutrinos possess mass. Older-generation neutrinos are obtained by replacing the elementary quarks in ω by composite quarks, for example,

$$\nu_{\mu R} = \omega(\tilde{d}\tilde{d}\tilde{D}e^-\nu). \tag{14}$$

The mixing $d,\ s,\ b \to d',\ s',\ b'$ occurs via transitions of the type

$$D_L(\tilde{d}\tilde{d}e^-) \overset{\varphi_0^+(ddde^+)}{\to\to\to} S_L(\tilde{d}(dde^+)e^-) \tag{15}$$

as a result of the annihilation of the $\tilde{d}$ and d quarks D_L and φ_0^+. In the limit of zero neutrino masses, mixing of neutrinos does not occur and in this approximation the Cabibbo angle for leptons equals zero.

We note that the d quarks in an electron E_R^- cannot be in an S state: Color antisymmetry presupposes the same symmetry of the wave function relative to transpositions of the spins and coordinates of the quarks. Since the spin of E_R^- equals 1/2, its wave function cannot be symmetric with respect to the spin variables. This also concerns other composite particles (U, D). This is not a difficulty, since the quantum numbers of E_R^- are dictated by the quantum numbers of its chiral partner e_L^- and the properties of the vacuum (see Eq. (9); incidentally, $\overline{qq}$ pairs of the chiral vacuum condensate are found in the $^3P_0$ state).

CHARACTERISTIC SCALES AND MASSES

The complexity of the vacuum and the large size of the gauge group make for a complex picture.

Scales

Since the nature of confinement is as yet unclear, we shall assume the grand unification mass $M \sim 10^{14}$–10^{15} GeV and quark confinement radius $r_c \sim 10^{-13}$ cm as given. The characteristic scale of the model is the ''coherence length'' r_φ of quadruplets of fermions making up the fields $\varphi_0(\tilde{d},\ \tilde{d},\ \tilde{d},\ e^-)$ and $\varphi_0^+(d,\ d,\ d,\ e^+)$. The question of

the value of r_φ is related with the question of the sizes of the composite particles. All components of a quintet interact identically only at distances $r<M^{-1}$, so that the sizes r_q of the particles U, D, and E formed from them must be of the same order of magnitude, $r_q \sim M^{-1}$. However, this is at odds with the threshold ($E_0 \approx 200$ GeV) discovered in Ref. 1, above which an excess of jets with transverse energy $E_T > E_0$ was observed. Recently there have appeared reports[4] of an observation of excess events in deep inelastic e^+p scattering experiments with large momentum transfers $Q>120$ GeV (the $H1$ group) and $Q>190$ GeV (ZEUS group). It is obvious that these effects are possible only if structures with a scale $r_0^{-1} \sim 150$–200 GeV appear. The contradiction is removed if it is assumed that it was the effective sizes of the composite particles, $r_q^{\text{eff}} \equiv R_q \gg r_q$, that were observed. Quarks and leptons can perturb the vacuum in their vicinity (analogs: polarons, skyrmions), so that R_q could be of the order of the coherence length r_φ. Then experiments[1,4] indicate that $r_\varphi^{-1} \sim 150$–200 GeV.

This model can yield an estimate of the relative number of events with the participation of neutral ($e^+p \to e^+X$) and charged ($e^+p \to \tilde{\nu}X$) currents. Such processes can occur only on the ''coat'' surrounding the U, D, and E particles, i.e., on the fields φ_0, φ_0^+. A positron can be scattered by all four components of both Higgs fields (neutral currents), so that the cross section $\sigma_n \sim 2(3\sigma_{e^+\tilde{d}} + \sigma_{e^+e^-} + \sigma^Z) \sim (8/3)\sigma_{e^+e^-} + 2\sigma^Z$ (σ^Z is the cross section with participation of a Z^0 boson). Conversely, in the case of scattering with the participation of charged currents a positron can be scattered only by an electron of the φ_0 field, i.e., $\sigma_{\text{ch}} \sim \sigma^W$ and $\sigma_n/\sigma_{\text{ch}} \sim 3$–$4$. The $H1$ group observed 12 ''neutral'' events and 4 ''charged'' events, which is consistent with the estimate made. An excess of antiquarks should be expected in processes with charged currents. This can be interpreted as violation of baryon number conservation. Therefore, from the standpoint of the proposed model the experiments of Ref. 4 attest to the manifestation of a composite Higgs field φ_0 (''leptotriquarks'').

The coherence length of the second Higgs field Φ_b^a (see above) is much shorter. Since all subparticles enter in the nonzero vacuum average $\langle \Phi_{24} \rangle_0 \sim \langle \zeta^* \Lambda_{24} \zeta \rangle_0$ (Λ_{24} is proportional to the diagonal matrix (1, 1, 1,-3/2, -3/2)), such states are possible only in the region of unbroken $SU(5)$ symmetry, i.e., $r_\Phi \sim M^{-1}$. The Higgs field $\Phi'_{24} \sim \varphi^+ \Lambda_{24} \varphi$, composed of the fields φ_a^+ and φ^a, should also be kept in mind. Clearly $r_{\Phi'} \sim r_\varphi$.

Masses

The photon mass M_{ph} in a superconductor equals $(e^2 n_s/m_e)^{1/2}$, where n_s is the density of superconducting electrons and e and m_e are the electron charge and mass. It is significant that the electron density is not directly related with the electron coherence length ξ ($n_s \sim 10^{23}$ cm^{-3}, $\xi \sim 10^{-5}$ cm). If it is assumed by analogy to superconductivity that the masses of the $B_\mu^{\alpha i}(X_\mu, Y_\mu)$ bosons are of the order of

$$M_{X,Y} \sim \left(\frac{4\pi \alpha_{GUM} n}{m} \right)^{1/2}, \tag{16}$$

where n is the density of the φ_0 Higgs mesons in the vacuum condensate and m is their effective mass, then it is easy to see that they can exceed the mass M. Indeed, for $n \sim M^3$, $m \sim r_\varphi^{-1}$ we have

$$M_{X,Y} \sim (4\pi \alpha_{GUM} M/m)^{1/2} M > M. \tag{17}$$

This eliminates the proton lifetime problem. Exchange of subparticles $\tilde{d} \leftrightarrow e^-$ ($\tilde{d} \leftrightarrow \nu$) between the U and D quarks of the proton occurs via the exchange of X (Y) bosons between their $\tilde{d}$ and e^- (ν and $\tilde{d}$) components, i.e.,

$$\tau_p \sim \left(\frac{M_{X,Y}}{m_p}\right)^4 \frac{1}{\alpha_{GUM}^2 m_p} \sim \left(\frac{M}{m}\right)^2 10^{30} \text{ yr}. \tag{18}$$

The ratio M/m can be large ($M/m \gg 1$).

The quark masses are determined by diagonalizing the mass matrix, formed by the amplitudes of transitions of the type (10) and (15). The lepton masses are obtained similarly via processes of the type (9) and, for example, $E_R^- \to M_R^-$. These matrices of ano- and catoquarks make it possible to find the Cabbibo–Kobayashi–Maskawa matrix.

SOME PREDICTIONS

The model admits a comparatively simple experimental check. For example, in collider experiments with polarized beams, on account of the different structure of the left- and right-handed particles, it is sufficient to count jets with high transverse energies (as was done in Ref. 1). If N is the number of jets with transverse energies greater than a certain critical value above which the structured nature of the quarks and leptons begins to be manifested, then, for example, for scattering of polarized electrons by polarized electrons we have

$$N_{RR}:N_{RL}:N_{LL}=9:3:1, \tag{19}$$

where, for example, N_{RL} is the number of jets with energies above the threshold value in a collision of right- and left-polarized electrons. The figures given are related with the fact that a right-handed electron contains three subparticles and a left-handed electron is elementary. The analogous ratios for proton–proton beams are

$$N_{RR}:N_{RL}:N_{LL}=81:63:49 \tag{20}$$

and are likewise related with the number of subparticles. In a system with an infinite momentum we have

$$P_R(U_R(de^+\tilde{\nu})U_R(de^+\tilde{\nu})D_L(\tilde{d}\tilde{d}e^-)), \quad P_L(U_L(\tilde{d}\tilde{d}\nu)U_L(\tilde{d}\tilde{d}\nu)d_R),$$

i.e., the right-polarized proton contains nine subparticles and the left-polarized proton contains seven subparticles, whence follow relations (17). Conversely, since for antiprotons

$$\overline{P_R}(\tilde{U}_R(dd\tilde{\nu})\tilde{U}_R(dd\tilde{\nu})\tilde{d}_L), \quad \overline{P_L}(\tilde{U}_L(\tilde{d}e^-\nu)\tilde{U}_L(\tilde{d}e^-\nu)\tilde{D}_R(dde^+)),$$

in $\overline{P}P$ scattering we have

$$N_{LR}:N_{LL}:N_{RR}:N_{RL}=81:63:63:49. \tag{21}$$

Here the first index designates the polarization of the antiprotons. Relations (19)–(21) should hold only at very high energies, where the constants in all three interactions are approximately the same. At energies of the order of r_φ^{-1}, however, the lepton interactions can be neglected. Then, since P_R and P_L contain four and five, respectively, and $\overline{P_R}$ and

$\overline{P_L}$ contain five and four strongly interacting particles, at these beam energies the right-hand sides of relations (20) and (21) become, respectively, 16:20:25 and 16:20:20:25. It should be underscored that if the threshold energy E_0 in Ref. 1 was determined correctly, then the proposed check can in principle be made even on the Tevatron. Another attractive feature of the predictions (19)–(21) is that they do not depend on the details of the dynamics and they require neither knowledge of the structure functions nor laborious calculations.

Some other consequences of the model are as follows. The transition $\mu \to e\gamma(e\gamma\gamma)$ as a result of the annihilation $\tilde{d}\tilde{d}dd \to e\gamma(e\gamma\gamma)$ in M_R^- is predicted. Further, in processes with large momentum transfers $Q \gg r_q^{-1}$ a U_R quark behaves not as an $SU(2)$ singlet but rather as a pair of components of the isodoublet e^+ and $\tilde{\nu}$, i.e., for it the probabilities of weak processes with charged currents should be twice as high as the probabilities of the corresponding processes for left-handed quarks. At these energies an electron starts to interact strongly, since E_R^- contains only quarks. In collisions of electrons or positrons short-range forces arise as a result of exchange of a π^0 meson, for example. These forces are extremely weak. The probability w_π that a quark emits a π^0 meson is proportional to the probability of observing it in a volume of the order of the volume of E_R^-; taking $R_e^{-1} \sim 200$ GeV gives $\omega_\pi \sim (R_e/r_\pi)^3 \sim 10^{-9}$. The probability that a π^0 meson is absorbed by one of the constituent quarks of $E_R^-(ddd)$ is the same. The scattering cross section on account of such an exchange is of the order of $\sigma_\pi \sim 3^2 w_\pi^2 m_\pi^{-2} \sim 10^{-43}$ cm^2. This is also true of neutrinos, because the field ω contains quarks.

In closing, I wish to call attention to the fact that the technical problems associated with obtaining beams of polarized protons and antiprotons at ultrahigh energies have now been solved.[5]

I wish to thank the referee for some stimulating remarks.

[a)]e-mail: apver@onti.niif.spb.su

[1] F. Abe, H. Akimoto, A. Akopian *et al.* Phys. Rev. Lett. **77**, 438 (1996).
[2] L. V. Prokhorov, JETP Lett. **16**, 397 (1972).
[3] H. Georgi and S. L. Glashow, Phys. Rev. Lett. **32**, 438 (1974).
[4] H1 Collaboration, DESY Preprint No. 97-024; ZEUS Collaboration, DESY Preprint No. 97-025; Phys. Today **4**, 18 (1997).
[5] CERN Courier. **36**, No. 5, 6 (1996).

Translated by M. E. Alferieff

$Z\to b\bar{b}$ probability and asymmetry in a model of dynamical electroweak symmetry breaking

B. A. Arbuzov[a)] and M. Yu. Osipov
Institute for High Energy Physics, Russian Academy of Sciences, 142284 Protvino, Moscow Region, Russia

(Submitted 16 July 1997)
Pis'ma Zh. Éksp. Teor. Fiz. **66**, No. 5, 299–303 (10 September 1997)

The deviations from the Standard Model in the probability of $Z\to b\bar{b}$ decay and in the forward–backward asymmetry in the reaction $e^+e^-\to b\bar{b}$ are studied in the framework of the model of dynamical electroweak symmetry breaking, the essential feature of which is the existence of a triple anomalous W-boson vertex in a region of momenta restricted by a cutoff Λ. We obtain a set of equations for additional terms in the $Wb\bar{t}$ vertex and apply its solution to the process $Z\to b\bar{b}$. We show that it is possible to obtain a consistent description of both deviations, which is quite nontrivial because these effects are not simply correlated. The necessary value of the anomalous W interaction coupling, $\lambda=-0.22\pm0.01$, is consistent with existing bounds and leads to definite predictions, e.g., for pair W production in e^+e^- collisions at LEP200. © *1997 American Institute of Physics.* [S0021-3640(97)00317-4]

PACS numbers: 13.38.Dg, 11.30.Qc

It is well known that the Standard Model (SM) of the electroweak (EW) interaction is in very good shape in respect to experimental checks, the only dubious points consisting in two effects which both involve the $b\bar{b}$ final state. Namely, experiment gives for the probability ratio $R_b=0.2178\pm0.0011$ as compared to the SM value 0.2158 and for the forward–backward asymmetry $A_{FB}^b=0.0979\pm0.0023$ as compared to the SM value 0.1022.[1] The relative discrepancies are as follows:

$$\Delta_b=\frac{R_b(\text{exp})-R_b(\text{theor})}{R_b(\text{theor})}=0.009\pm0.005\,,$$

$$\Delta_{FB}=\frac{A_{FB}^b(\text{exp})-A_{FB}^b(\text{theor})}{A_{FB}^b(\text{theor})}=-0.042\pm0.023\,. \tag{1}$$

In the present note we consider whether one can explain these deviations as something other than purely statistical fluctuations. Note that two independent deviations of 1.8 standard deviations each have a rather small probability of being a statistical fluctuation. For the present purpose we consider the version of EW theory in which the symmetry breaking is due to a self-consistent appearance of an additional triple gauge boson vertex in the region of small momenta.[2,3] This vertex can be described by the following expres-

 © 1997 American Institute of Physics

sion in momentum space, which, according to the approach taken, acts in a region limited by an effective cutoff Λ which is of the order of magnitude of a few TeV:[4,5]

$$\Gamma^{abc}_{\mu\nu\rho}(p,q,k)=\epsilon^{abc}\frac{i\lambda g}{M_W^2}F(p^2,q^2,k^2)\Gamma_{\mu\nu\rho}(p,q,k),$$

$$\Gamma_{\mu\nu\rho}(p,q,k)=g_{\mu\nu}(p_\rho(qk)-q_\rho(pk))+g_{\nu\rho}(q_\mu(pk)-k_\mu(pq))$$
$$+g_{\rho\mu}(k_\nu(pq)-p_\nu(qk))+k_\mu p_\nu q_\rho-q_\mu k_\nu p_\rho. \qquad (2)$$

$$F(p^2,q^2,k^2)=\frac{\Lambda^6}{(\Lambda^2-p^2)(\Lambda^2-q^2)(\Lambda^2-k^2)}.$$

Note that this term, among others, is currently considered[6,7] in the phenomenological analysis of possible gauge boson interactions. Vertex (2) leads to the generation of masses for the W and Z,[2,3] with $|\lambda|$ being a few tenths of a TeV and Λ being of the order of a few TeV. The mass generation for the t quark in this approach is connected with the other self-consistent vertex, having a Lorentz–Dirac structure of the anomalous magnetic moment of the t quark:[3,4]

$$\Gamma^t_\mu(p,q,k)=\frac{ie\kappa}{2M_t}F(p^2,q^2,k^2)\sigma_{\mu\nu},k_\nu, \qquad (3)$$

where $F(p^2,q^2,k^2)$ is the same form factor as in vertex (2), and k_ν is the photon momentum. The corresponding solution gives κ to be around unity, and an experimental bound $|\kappa|\leqslant 1$ is derived from the t production data in Ref. 4.

Adding anomalous vertices (2), (3) to the usual ones, we formulate equations for another anomalous vertex for the $\overline{t}Wb$ interaction. Let us look for it in the form

$$\Gamma^{tb}_\rho(p,q,k)=\frac{ig}{2M_t}F_m(p^2,k^2)\sigma_{\rho\omega}k_\omega(\xi_+(1+\gamma_5)+\xi_-(1-\gamma_5)), \qquad (4)$$

where p and q are, respectively, the t-quark and b-quark momenta, k is the W momentum, and the form factor

$$F_m(p^2,k^2)=\frac{\Lambda^4}{(\Lambda^2-p^2)(\Lambda^2-k^2)}.$$

We assume that not only left-handed b quarks but possibly also right-handed ones take part in the interaction. Due to the gauge invariance there is, in addition to (4), a four-leg $\overline{t}bW^+W^0$ vertex

$$\Gamma^{tb}_{\mu\nu}(p,k_1,k_2)=\frac{ig^2}{2M_t}F(p,k_1^2,k_2^2)\sigma_{\mu\nu}(\xi_+(1+\gamma_5)+\xi_-(1-\gamma_5)); \qquad (5)$$

where μ and ν are, respectively, the indices of W^+ and W^0, and p, k_1, and k_2 are the momenta of the t quark and of the same bosons, respectively.

We consider equations for vertex (4) in the one-loop approximation. This means that we take the following equation (written in a schematic form):

$$\Gamma^{tb}=\Gamma_0^{tb}+(\Gamma_0(bbA)\Gamma^{tb}\Gamma(WWA))+(\Gamma_0(bbZ)\Gamma^{tb}\Gamma(WWZ))$$
$$+(\overline{\Gamma_0^{tb}}\Gamma^t\Gamma(WWA))+(\Gamma^{tb}\Gamma^t\Gamma_0(WWA))+(\Gamma^{tb}\Gamma^t\Gamma(WWA))$$
$$+(\Gamma^{tb}\Gamma_0(ttZ)\Gamma(WWZ))+(\Gamma^{tb}\Gamma_0(ttA)\Gamma(WWA))$$
$$+(\Gamma^{tb}(WA)\Gamma(WWA))+(\Gamma^{tb}(WZ)\Gamma(WWZ))+(\Gamma^{tb}(WA)\Gamma^t). \tag{6}$$

Here a subscript zero means the corresponding SM vertex and, e.g., $\Gamma(WWA)$ means vertex (2) for the interaction of two W bosons and a photon (factor $\sin\theta_W$). The symbol $\Gamma^{tb}(\ldots)$ means vertex (5) with the corresponding vector bosons. The new vertex

$$\overline{\Gamma_{0\alpha}^{tb}}=\frac{g}{2\sqrt{2}}\gamma_\alpha(\eta_+(1+\gamma_5)+\eta_-(1-\gamma_5)) \tag{7}$$

is introduced for the purpose of taking into account the contributions of loop diagrams to different matrix structures. We have of course the corresponding propagators between vertices and the usual momentum integration with a factor of $(2\pi)^{-4}$. All ten one-loop terms diverge quadratically if one neglects the form factors mentioned above. The integrations in loop diagrams (6) are performed with the use of Wick rotation in Euclidean momentum space. Taking the form factors into account, we obtain a finite result, which reads

$$\eta_+=1-\frac{\sqrt{2}}{8}\kappa K\xi_+\left(\frac{1}{4}+\frac{\lambda}{5\cos^2\theta_W}\right),\quad \eta_-=-\frac{\sqrt{2}}{8}\kappa K\xi_-\left(\frac{1}{4}+\frac{\lambda}{5\cos^2\theta_W}\right),$$
$$\xi_+=-\frac{\lambda C\kappa\eta_+}{24\sqrt{2}\,F_1}\quad \xi_-=\frac{\lambda CK\kappa^2}{192\,F_2}\xi_-\left(\frac{1}{4}+\frac{\lambda}{5\cos^2\theta_W}\right),$$
$$F_1=1-\lambda C\left(\frac{\kappa}{40}-\frac{7}{48\sin^2\theta_W}\right)\quad C=\frac{\alpha\Lambda^2}{\pi M_W^2}, \tag{8}$$
$$F_2=1-\lambda C\left(\frac{\kappa}{40}-\frac{1}{8\sin^2\theta_W}\right)\quad K=\frac{\alpha\Lambda^2}{\pi M_t^2}.$$

From set (8) one concludes that there can be two types of solutions. The first one could be called a trivial solution; that is, it corresponds to

$$\xi_-=0. \tag{9}$$

However a non-zero solution may also exist, provided that the following condition is fulfilled:

$$\frac{\lambda\kappa^2CK}{192F_2}\left(\frac{1}{4}+\frac{\lambda}{5\cos^2\theta_W}\right)=1. \tag{10}$$

This condition gives a relation among the parameters of the model. Namely, using formulas (8) and (10), we get

$$\lambda = 5\cos^2\theta_W\left(\frac{24}{\sin^2\theta_W} - \frac{24\,\kappa}{5} - \frac{\kappa^2 K}{4}\right)\frac{1-\sqrt{1+A}}{2\,\kappa^2 K}, \tag{11}$$

$$A = \frac{768\,\kappa^2 M_Z^2}{5M_t^2}\left(\frac{24}{\sin^2\theta_W} - \frac{24\,\kappa}{5} - \frac{\kappa^2 K}{4}\right)^{-2}, \quad \xi_+ = -\sqrt{2}\,\kappa\,\sin^2\theta_W .$$

Now we use the relations obtained to evaluate the vertex $Z\overline{b}b$. We have for this vertex the symbolic one-loop representation

$$\begin{aligned}\Gamma^b = {} & \Gamma_0^b + (\Gamma^{tb}\Gamma_0^t\Gamma^{tb}) + (\Gamma^{tb}\Gamma_0(WWZ)\Gamma^{tb}) \\ & + (\Gamma^{tb}\Gamma(WWZ)\Gamma^{tb}) + (\Gamma_0^{tb}\Gamma(WWZ)\Gamma^{tb}) \\ & + (\Gamma^{tb}\Gamma(WWZ)\Gamma_0^{tb}) + (\Gamma^{tb}(WZ)\Gamma^{tb}) + (\Gamma^{tb}\Gamma^{tb}(WZ)).\end{aligned} \tag{12}$$

Here the vertex Γ^b has the form

$$\Gamma_\rho^b = \frac{g}{2\cos\,\theta_W}(a\,\gamma_\rho + b\,\gamma_\rho\gamma_5 + c\,i\sigma_{\rho\mu}k_\mu). \tag{13}$$

Performing again the usual loop calculations, we have for the vertex

$$a = a_0 + a_1, \quad b = b_0 + b_1, \quad a_0 = -\frac{1}{2} + \frac{2}{3}\sin^2\theta_W, \quad b_0 = -\frac{1}{2},$$

$$a_1 = \frac{\xi_+^2 K}{4}\left(-\frac{1}{3} + \left(\frac{\sin^{-2}\theta_W}{4} - \frac{1}{3}\right)R^2 - \cot^2\theta_W(1+R^2) + \sin^{-2}\theta_W(1+R^2)\frac{\lambda}{5}\right),$$

$$b_1 = \frac{\xi_+^2 K}{4}\left(-\frac{1}{3} - \left(\frac{\sin^{-2}\theta_W}{4} - \frac{1}{3}\right)R^2 - \cot^2\theta_W(1-R^2) + \sin^{-2}\theta_W(1-R^2)\frac{\lambda}{5}\right),$$

$$c = \frac{\lambda K M_t}{2M_W^2}\cot^2\theta_W R\left(\frac{\xi_+^2}{5} - \frac{\xi_+}{3\sqrt{2}}\right), \quad R = \frac{\xi_-}{\xi_+}. \tag{14}$$

Using vertex expression (13) and results (14), we obtain the following asymmetries Δ_b and Δ_{FB}, which we define as the relative differences of our results and the SM calculations, to be compared with the experimental numbers (1):

$$\Delta_b = \frac{1}{a_0^2 + b_0^2}\left(2(a_0a_1 + b_0b_1) + a_1^2 + b_1^2 + \frac{M_Z^2}{2}c^2\right), \quad \Delta_{FB} = \frac{\xi_1 - \xi_2}{1+\xi_2},$$

$$\xi_1 = \frac{12(a_1b_0 + a_0b_1 + a_1b_1)}{3 - 4\sin^2\theta_W}, \tag{15}$$

$$\xi_2 = \frac{72(a_0a_1 + b_0b_1) + 36(a_1^2 + b_1^2) + 45c^2M_Z^2}{(3 - 4\sin^2\theta_W)^2 + 9}.$$

Let us compare results (15) with the data given in Eq. (1). Let us first take solution (9), i.e., $R = 0$. Then the signs of both deviations (1) are negative throughout the entire range

TABLE I. Δ_b (upper lines) and Δ_{FB} (lower lines) for different values of $|R|$ (rows) and ξ_+ (columns).

	-0.05	-0.045	-0.04	-0.035	-0.03
2.0	0.008	0.003	0.002	0.001	0.001
	-0.038	-0.031	-0.024	-0.018	-0.013
2.3	0.01	0.008	0.006	0.004	0.003
	-0.051	-0.041	-0.032	-0.024	-0.017
2.6	0.018	0.014	0.010	0.008	0.005
	-0.067	-0.053	-0.041	-0.031	-0.022
2.9	0.027	0.021	0.016	0.011	0.008
	-0.085	-0.067	-0.052	-0.039	-0.028
3.2	0.038	0.029	0.022	0.016	0.011
	-0.105	-0.083	-0.064	-0.048	-0.034

of variation of our parameters. For example, for $K=1.74$ (which corresponds to $\Lambda=4.5$ TeV;[4] this is the value that we shall use in what follows), $\lambda=0.5$, and $\xi_+=0.04$ we have

$$\Delta_b=-0.01\,; \quad \Delta_{FB}=-0.0007\,.$$

Taking different values of the parameters, we become convinced that there is no way to obtain a comparatively large Δ_{FB} and a positive Δ_b, as the data (1) indicate.

Let us now turn to the nontrivial solutions (10). According to (11), for admissible values of κ, viz., $-1<\kappa<1$ (Ref. 4), one has

$$-0.23<\lambda<-0.21. \tag{16}$$

These numbers are in no way inconsistent with the experimental bounds.[8,9] Relation (16) specifies λ to good accuracy. In addition to λ and K, which is already determined, we also have the parameters R and ξ_+. For the nontrivial solution $\xi_-\neq 0$ the ratio R is arbitrary. The parameter ξ_+ is connected with the effective anomalous magnetic moment κ of the t quark (10). Now we take $\lambda=-0.22$ and present in Table I the dependence of deviations (1) on $|R|(2.0<|R|<3.2)$ and $\xi_+(-0.05<\xi_+<-0.03)$.

We see that quite acceptable numbers are concentrated around the main diagonal of Table I. For example, for

$$|R|=2.45, \quad \xi_+=-0.043 \tag{17}$$

the numbers hit precisely the center values of (1). We conclude that for the nontrivial solution (10) it is possible to obtain agreement with both numbers (1). This result is by no means obvious — we recall that for the trivial solution agreement is impossible. The important qualitative feature of our result is the presence of a large contribution of right-handed b quarks to the anomalous vertex (see Eqs. (4) and (7)). This modified vertex gives a number of predictions. For example, the t-quark width now reads

$$\Gamma_t=\Gamma_0(1+\Delta), \tag{18}$$

$$\Gamma_0=\frac{g^2(M_t^2-M_W^2)^2(2M_W^2+M_t^2)}{64\pi M_t^3 M_W^2},$$

$$\Delta=-\frac{6\sqrt{2}M_W^2\xi_+}{2M_W^2+M_t^2}+\frac{K\beta\xi_+^2}{4\sin^2\theta_W}+\frac{2M_W^2(2M_t^2+M_W^2)\xi_+^2(1+R^2)}{M_t^2(2M_W^2+M_t^2)}$$

$$+\frac{3KM_W^2\beta\xi_+^3(1+R^2)}{2\sqrt{2}\sin^2\theta_W(2M_W^2+M_t^2)}+\frac{K^2\beta^2\xi_+^4(1+R^2)}{64\sin^4\theta_W}, \tag{19}$$

$$\beta=\left(\frac{1}{4}+\frac{\lambda}{5\cos^2\theta_W}\right).$$

Here Γ_0 is the SM value, and if we take the parameter values (17), we find from Eq. (19) that $\Delta=0.062$, i.e., more than a 6% effect is predicted for the t-quark width.

As to possible values for λ (16), this prediction could be checked at LEP200,[10] provided that the necessary integral luminosity is accumulated in the study of reaction $e^+ + e^- \to W^+ + W^-$.

This work is partially supported by the Russian Fund for Fundamental Research under Project 95-02-03704.

Note added in proof. The latest experimental bound $-0.31<\lambda<0.29$ (Ref. 11), which is consistent with our prediction (16), demonstrates that the experimental accuracy is approaching the necessary level.

[a)]e-mail: arbuzov@mx.ihep.su

[1] G. Altarelli, Preprint CERN-TH/96-265; hep-ph/9611239.
[2] B. A. Arbuzov, Phys. Lett. B **288**, 179 (1992).
[3] B. A. Arbuzov, in *Advanced Study Conference on: Heavy Flavours*, Pavia (Italy), Eds. G. Bellini *et al.*, Frontiers, Gif-sur-Yvette, 1994, p. 227.
[4] B. A. Arbuzov and S. A. Shichanin, JETP Lett. **60**, 79 (1994).
[5] B. A. Arbuzov, Phys. Lett. B **353**, 532 (1995).
[6] K. Hagiwara, R. D. Peccei, D. Zeppenfeld, and K. Hikasa, Nucl. Phys. B **282**, 253 (1987).
[7] K. Hagiwara, S. Ishihara, R. Szalapski, and D. Zeppenfeld, Phys. Rev. D **48**, 2182 (1993).
[8] F. Abe *et al.* (CDF Collab.), Phys. Rev. Lett. **74**, 1936 (1995).
[9] F. Abe *et al.* (CDF Collab.), Phys. Rev. Lett. **75**, 1017 (1995).
[10] G. L. Kane, J. Vidal, and C. P. Yuan, Phys. Rev. D **39**, 2617 (1989).
[11] S. Abachi *et al.* (D0 Collab.), Phys. Rev. Lett. **78**, 3634 (1997).

Published in English in the original Russian journal. Edited by Steve Torstveit.

Channeling in single-wall nanotubes: possible applications

L. A. Gevorgyan, K. A. Ispiryan,[a] and R. K. Ispiryan
Erevan Physical Institute, 375036 Erevan, Armenia

(Submitted 17 July 1997)
Pis'ma Zh. Éksp. Teor. Fiz. **66**, No. 5, 304–307 (10 September 1997)

The relevant potentials are calculated and used to investigate the trajectories and various characteristics of axial channeling of high-energy positively charged particles in the recently discovered single-wall nanotubes (SWNTs). The application of SWNTs in high-energy physics, specifically, in future colliders, is discussed, in view of the fact that the dechanneling length in SWNTs is much longer than in single crystals.
© *1997 American Institute of Physics.* [S0021-3640(97)00417-9]

PACS numbers: 61.85.+p, 61.46.+w, 61.48.+c

Fullerenes and nanotubes have already found wide applications in various fields of science and technology,[1,2] but as yet there have been no studies of their applications in high-energy physics, apart from the acceleration of C_{60} ions in small storage rings.[b)] We have calculated the potentials inside C_{60} and multiwall nanotubes in order to explain the relatively large component of the positron lifetime observed in C_{60} crystals[3] and to investigate channeling conditions in nanotubes. However, these results were never published, since the data obtained in Ref. 3 were not confirmed and nanotubes greater than tens of microns in length had not been synthesized.

The synthesis of a graphite SWNT of the type (10, 10) with diameter $2R=13.8\pm0.2$ Å and length exceeding 100 μm from the crystallographic planes of graphite was reported in 1996.[4] It was reported that 100–500 such SWNTs with metallic properties form ''ropes'' whose cross section is a triangular lattice with lattice constant $A_T=17$ Å (see Fig. 1, where the dashed circles represent SWNT sections). In Ref. 5 it was asserted that such SWNTs with kilometer lengths will be synthesized in the near future.

On basis of this as well as the fact that, because of the large radius, multiple-scattering in SWNTs is much weaker than in single crystals, in the present work we investigated channeling processes in SWNTs.

With allowance for the amplitude u_1 of the thermal vibrations, the potential produced at the point (x_k, y_k, z_k) inside a ''rope'' by N atoms located at the points (x_j, y_j, z_j), $j=1, 2, \ldots, N$, can be represented in the form

$$U(x_k,y_k,z_k)=\frac{Ze^2}{2}\sum_{j=1}^{N}\frac{1}{r_{jk}}\sum_{\mu=1}^{3}\alpha_\mu\exp(u_\mu^2)[\exp(-r_\mu)\mathrm{erf}(u_\mu-r_u)$$
$$-\exp(r_\mu)\mathrm{erf}(u_\mu+r_u)]. \quad (1)$$

 © 1997 American Institute of Physics

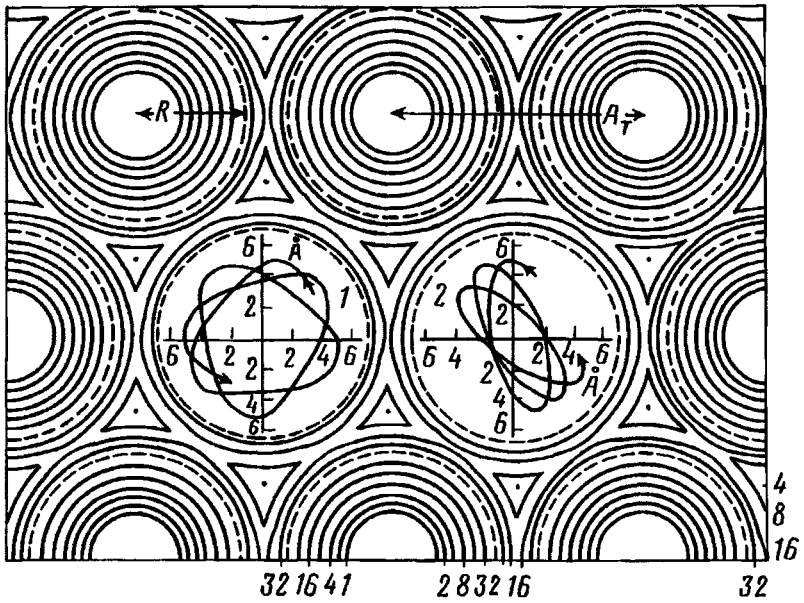

FIG. 1. SWNT lattice (dashed circles), lines of equipotential surfaces in electron volts (solid lines), and trajectories of protons with $\varepsilon_0 = 100$ GeV and $\psi_0 = \pi/2$, $r_0 = 4$ Å in the cases: *1*— $\theta_0 = 1.9$ μrad ($\delta = 0.9$) and *2* — $\theta_0 = 6.85$ μrad ($\delta = 0.55$).

Here Z is the nuclear charge, r_{jk} is the distance between the points (x_k, j_k, z_k) and (x_j, y_j, z_j),

$$u_\mu = \frac{u_1 \beta_\mu}{2^{1/2} R_{TF}}, \quad r_\mu = \frac{r_{jk} \beta_\mu}{R_{TF}}, \quad r_u = \frac{r_{jk}}{2^{1/2} u_1}, \tag{2}$$

α_μ(0.1, 0.55, 0.35) and β_μ (6.0, 1.2, 0.3) are constants in the Molière model of the atom, R_{TF} is the Thomas–Fermi screening radius, and erf(t) is the error function.

In the calculations of the potential of a SWNT performed with Eq. (1) and the parameters presented above, the summation over j was performed over the largest possible number of atoms of neighboring SWNTs making an appreciable contribution at a given point, and it was assumed that $R_{TF} = 0.26$ Å and $u_1 = 0.06$ Å. We note that there are no data on u_1 but, according to the calculations, the dependence on u_1 is weak. The results (see Fig. 1, where the lines of the equipotential surfaces are shown) show that if the points lying at a distance less than R_{TF} from the wall of a SWNT are excluded, then the potential inside the SWNT can be approximated by the expression $U(r) = U_0 r^6$, where U is measured in eV and r, the distance from the axis of the SWNT, is measured in Å. This approximation, which is poor for values of r at which the potential is negligible, is used in the following analytical investigation of the channeling of positive particles inside a SWNT. We note that the particle motion and emission processes within an entire ''rope'' consisting of a straightened SWNT and a curved SWNT can be investigated by numerical methods using Eq. (1).

Let a particle enter the SWNT at a point with the cylindrical coordinates $r_0, \varphi_0, z_0 = 0$ and momentum $q_0 = \varepsilon_{00}/c$, at a small angle θ_0 to the Z axis, which is also the axis of the SWNT, and at an angle α_0 to the X axis (see Fig. 1 in Ref. 6). Denoting $\psi_0 = \varphi_0 - \alpha_0$ and $m = \varepsilon_0/c^2$, where $\varepsilon_0 = (P_0^2c^2 + m_0^2c^4)^{1/2}$, we obtain the invariants of the transverse motion in such an axisymmetric field:[7] $M = \varepsilon_0 r_0 \theta_0 \sin\psi_0/c$ and $E = \varepsilon_0\theta_0^2/2 + U(r_0)$ (the longitudinal motion along the Z axis is uniform to a good approximation). A particle is channeled if $\delta = 32U_0M^6/27m^3E^4 \leqslant 1$, with a period

$$T = \frac{2K(k)}{(3q\lambda)^{1/2}}\left(\frac{2m^3}{U_0E^2}\right)^{1/6} \simeq \frac{\pi}{(3q\lambda)^{1/2}}\left(\frac{2m^3}{U_0E^2}\right)^{1/6}. \tag{3}$$

Here and below we employ the following notation (the dimensionless variable z is used instead of the radius r):

$$k^2 = \frac{1}{2}\left(1 - \frac{1}{q}\right), \quad q = \frac{(\eta^4 + 2\eta^2 + 9)^{1/2}}{3}, \quad \lambda = (1 + (1-\delta)^{1/2})^{1/3} + (1 - (1-\delta)^{1/2})^{1/3},$$

$$\eta = ((4 - 3\delta)^{1/2} - 1)^{1/2}, \quad r = \left(\frac{E}{2^{1/2}U_0}\right)^{1/6} \lambda^{1/4} z^{1/2}, \quad z_{\min,\max} = \frac{1 \mp \eta}{2}$$

and $K(k)$ is the complete elliptic integral of the first kind. Series expansions,[8] taking account of the fact that $k^2 \leqslant 0.067 \ll 1$, are used on the right-hand side of Eq. (3) as well as in Eq. (5) below.

The trajectory of the transverse motion and the rotation angle of the perihelion over one period will be[7,8]

$$\varphi = \varphi_0 + A[\Phi(z_0) - \Phi(z)], \quad \Delta\varphi = 2A[\Phi(z_{\min}) - \Phi(z_{\max})], \tag{4}$$

where

$$\Phi(z) = -\frac{\alpha_1}{\eta}F(\phi,k) + B\left[\Pi(\phi, -\beta^2, k) - C\frac{\tan^{-1}[\alpha \sin\phi/C]}{(1 - k^2\sin^2\phi)^{1/2}}\right]$$

$$\simeq -\frac{\alpha_1}{\eta}\phi + B\left[\frac{\tan^{-1}[(1+\beta^2)^{1/2}\tan\phi]}{(1+\beta^2)^{1/2}} - C\tan^{-1}[\alpha\sin\phi/C]\right], \tag{5}$$

$$A = \frac{\delta^{1/6}}{32^{1/2}\lambda}\frac{3(1+q) - \eta^2}{q^{1/2}}, \quad B = \frac{\alpha - \alpha_1}{\eta(1-\alpha^2)}, \quad C = \frac{\alpha}{(\beta^2 + k^2)^{1/2}},$$

$$\alpha = \frac{3q(1-\eta^2) - 3 - \eta^4}{4\eta}, \quad \alpha_1 = \frac{3(1-q) + \eta^2}{2\eta}, \quad \beta^2 = \frac{\alpha^2}{1-\alpha^2},$$

$$\cos\phi = \frac{(z_{\max} - z)(1 + 2z_{\min}^2)^{1/2} - (z - z_{\min})(1 + 2z_{\max}^2)^{1/2}}{(z_{\max} - z)(1 + 2z_{\min}^2)^{1/2} + (z - z_{\min})(1 + 2z_{\max}^2)^{1/2}},$$

$F(\phi,k)$ and $\Pi(\phi, -\beta^2, k)$ are elliptic integrals of the first and second kinds.

Analysis of the results obtained shows that by analogy to axial channeling of negative particles the following cases are possible in the case of the channeling of positive particles in SWNTs: a) for $\psi_0=0$ and $\theta_0=0$ ($\delta=0$, $\eta=1$) a particle trajectory will be a two-dimensional figure with a perpendicular trajectory consisting of a straight line segment; b) for $\psi_0=\pi/2$ and $\theta_0=\theta_{cr}=r_0^3(6U_0/\varepsilon_0)^{1/2}$ ($\delta=1$, $\eta=0$) the motion will be a helix with a circular projection. In all other cases the perpendicular motion will be ellipsoidal with rotation. The trajectories of protons with energy $\varepsilon_0=100$ GeV, which were calculated using Eq. (4) for some values of r_0, θ_0, and ψ_0, are shown inside the SWNT in Fig. 1.

Using the condition $\delta\leqslant 1$ and the methods of Ref. 6, the fraction of the channeled particles entering the SWNT can be calculated. However, this will not correspond to the real fraction for the following reason. As one can see from the figure, a large fraction of the particles in the beam can be channeled between neighboring SWNTs. On account of the complexity of the potential outside the SWNT, this can be taken into account only by numerical calculations. A rough estimate of the fraction of particles channeled in a rope of SWNTs gives $D=1-S/S_0=1-4.62\pi RR_{TF}/A_T^2=0.91$ (S is the area around the wall of a SWNT of width $2R_{TF}$, and S_0 is the area per SWNT), which can be compared with $D_P=1-2R_{TF}/d_P=0.7$–0.9 (d_P is the distance between neighboring planes) in the case of planar channeling.

Proceeding now to possible applications of SWNTs in high-energy physics, it should be noted that the prospects of greatest interest lie not in the formation of radiation by channeled particles but rather in relation to: 1) bending of particle trajectories without magnets for the purpose of extracting beams and constructing future colliders,[9,10] 2) particle acceleration in crystals,[11,12] 3) focusing of beams and increasing the luminosity of colliders,[13,14] and 4) channeling of heavy ions, including C_{60}. Of the many problems arising in the solution of these problems, two are fundamental, specifically, obtaining long channels and long dechanneling lengths, and will be solved with the aid of SWNTs. Indeed, specialists developing the technology for synthesizing SWNTs believe that, in contrast to crystals, the problem of obtaining long SWNTs is solvable. In any case, substantial theoretical and experimental progress in joining SWNTs even with different (n,m) has already been achieved (see Ref. 15 and the references cited therein). Without discussing the questions concerning the production of such clean SWNTs in the form of crystals and curving them, let us examine weak dechanneling in SWNTs.

As is well known, for low transverse energies multiple scattering and therefore dechanneling occur mainly on electrons inside a channel according to an exponential law with a dechanneling length $L_0\sim\Lambda\varepsilon_0$ and dechanneling constant $\Lambda\sim d_P^2$. In ordinary crystals $d_P\approx 1$–2 Å, $\Lambda\approx 1$–10 μm/MV. The measured values of L_0 in a Si single crystal are proportional to ε_0 and are of the order of 10 cm for $\varepsilon_0\approx 100$ GeV. The picture is more complicated in the case of curved crystals.[16,17] For SWNTs the distribution of the electrons must be taken into account more accurately, and a theory similar to that presented in Ref. 17 must be developed for axial channeling. Nonetheless, since R for SWNTs is an order of magnitude longer than d_P in crystals, and $\Lambda\sim d_P^2$, it can be expected that for $\varepsilon_0\geqslant 100$ GeV the dechanneling length will be greater than 1 m, even without accelerating fields.[12] The inevitable development of SWNT nanotechnology[4,15] will make the solution of the problems 1–4 mentioned above a reality.

[a)]e-mail: ispirian@vxl.yerphi.am
[b)]E. Uggerhoj, private communication.

[1] A. V. Eletskiĭ and B. M. Smirnov, Usp. Fiz. Nauk **163**, 33 (1993).
[2] M. S. Dresselhaus, G. Dresselhaus, and P. C. Eklund, *Science of Fullerenes and Carbon Nanotubes*, Academic Press, San Diego, 1996.
[3] J. Kristiak, K. Kristiak, and O. Sausa, Phys. Rev. B **50**, 2792 (1994).
[4] A. Thess, R. Lee, P. Nikolaev *et al.*, Science **273**, 483 (1996).
[5] B. Schwarzschild, Phys. Today **49**, No. 12, 19 (1996).
[6] S. M. Darbinian and K. A. Ispirian, Phys. Status Solidi B **96**, 835 (1979).
[7] L. D. Landau and E. M. Lifshitz, *Mechanics*, 2nd ed., Pergamon Press, New York, 1969 [Russian original, Nauka, Moscow, 1965].
[8] P. F. Byrd and M. D. Friedman, *Handbook of Elliptic Integrals for Engineers and Scientists*, Springer-Verlag, New York, 1971.
[9] E. N. Tsyganov, Preprints FNAL-TM-682; FNAL-TM-684 (1986)
[10] S. A. Bogacz, D. B. Cline, and D. A. Sanders, Nucl. Instrum. Methods B **119**, 199 (1996).
[11] T. Tajima and M. Cavenago, Phys. Rev. **59**, 140 (1987).
[12] Z. Huang, P. Chen, and R. D. Ruth, Phys. Rev. Lett. **74**, 1759 (1995); Nucl. Instrum. Methods B **119**, 192 (1996).
[13] M. A. Kumakhov, *Radiation from Channeled Particles in Crystals* [in Russian], Énergoatomizdat, Moscow, 1986.
[14] P. Chen and R. J. Noble, Preprint FERMILAB-Conf-96/441, SLAC-PUB-7402 (1996).
[15] M. Dresselhaus, Phys. World **9**, No. 5, 18 (1996).
[16] A. M. Taratin *et al.*, Phys. Status Solidi B **100**, 273 (1980); Nucl. Instrum. Methods B **58**, 103 (1991).
[17] J. A. Ellison, Nucl. Phys. B **206**, 205 (1982).

Translated by M. E. Alferieff

Corrections of order $O(\overline{\alpha\alpha_s})$ and $O(\overline{\alpha^2})$ to the $\overline{b}b$-decay width of the neutral Higgs boson

A. L. Kataev
Institute of Nuclear Studies, Russian Academy of Sciences, 117312 Moscow, Russia

(Submitted 25 July 1997)
Pis'ma Zh. Éksp. Teor. Fiz. **66**, No. 5, 308–311 (10 September 1997)

Analytical expressions are presented for contributions of order $O(\overline{\alpha\alpha_s})$ and $O(\overline{\alpha^2})$ to the $\overline{b\,b}$-decay width of the neutral Higgs boson of the standard model of electroweak interactions. The numerical value of the mixed QED and QCD correction of order $O(\overline{\alpha\alpha_s})$ is comparable to other computed terms in the perturbation series. © *1997 American Institute of Physics.* [S0021-3640(97)00517-3]

PACS numbers: 14.80.Bn, 12.20.Ds, 12.38.Bx

The study of the properties of the as yet unobserved Higgs boson of the standard model of electroweak interactions is an important problem in modern high-energy physics (see, for example, the reviews in Ref. 1). An experimental lower bound on the mass $M_H > 65$ GeV has been obtained on the LEP accelerator. Experiments searching for the H^0 boson, which could have a mass in the range 65 GeV $< M_H \leqslant 2M_W \approx 160$ GeV, are planned for the LEP2 and LHC accelerators. The main decay mode of such a scalar boson should be decay into a $\overline{b\,b}$ pair.

As a result of substantial efforts made by theorists, the effects of different QCD corrections to $\Gamma(H^0 \to \overline{b\,b})$ have been calculated and analyzed (see Refs. 2–11). The leading contributions of the electroweak interactions to this fundamental quantity were found in Ref. 12. The degree of accuracy which has now been achieved in theoretical calculations necessitates the analysis of a number of other contributions which *a priori* could equal in absolute magnitude the terms in the perturbation series for $\Gamma(H^0 \to \overline{b\,b})$ which have already been calculated.

Following the analogous calculations of the QED and QCD corrections to the hadronic decay width of a Z^0 boson,[13] we report in this letter analytical results for the coefficient of the term of order $O(\overline{\alpha\alpha_s})$ in the expression for $\Gamma(H^0 \to \overline{b\,b})$ (found in the study reported in Ref. 4 but thus far unpublished) and for a correction of order $O(\overline{\alpha^2})$ to the same quantity. The results will pertain to the $\overline{MS}$ scheme.

In the limit $M_H \geqslant 2m_b$ of interest here (where m_b is the pole mass of the b quark) the perturbation theory approximation for $\Gamma(H^0 \to \overline{b\,b})$ can be represented in the form

$$\Gamma(H^0 \to \overline{b\,b}) = \overline{\Gamma}_0^{(b)}[1 + \Delta\Gamma_1 \overline{a_s} + \Delta\Gamma_2 \overline{a_s^2} + \Delta\Gamma_3 \overline{a_s^3} + \ldots$$

 © 1997 American Institute of Physics

$$-6\frac{\overline{m_b^2}}{M_H^2}(1+\Delta\Gamma_1^{(m)}\overline{a_s}+\Delta\Gamma_2^{(m)}\overline{a_s^2}+\ldots)+\Delta_t+\Delta^{\mathrm{QED}}], \tag{1}$$

where $\overline{\Gamma_0^{(b)}}=(3\sqrt{2}/8\pi)G_F M_H \overline{m_b^2}$ and $\overline{m_b}=\overline{m_b}(M_H)$, $\overline{a_s}=\overline{\alpha_s}(M_H)/\pi$ are the running QCD parameters, normalized to the polar mass of the Higgs boson, in the $\overline{MS}$ scheme. The coefficients $\Delta\Gamma_1$ and $\Delta\Gamma_2$ are well known:[2,3]

$$\Delta\Gamma_1=\frac{17}{4}C_F\approx 5.667,$$

$$\Delta\Gamma_2=\left[\left(\frac{893}{4}-62\zeta(3)\right)C_A-(65-16\zeta(3))Tf+\left(\frac{691}{4}-36\zeta(3)\right)C_F\right]\frac{C_F}{16}$$
$$-\pi^2\left(\frac{11C_A-4Tf+18C_F}{48}\right)C_F\approx 29.147, \tag{2}$$

where $C_F=4/3$, $C_A=3$, $T=1/2$, $f=5$, and $\zeta(3)=1.202\ldots$. The value of the coefficient $\Delta\Gamma_1^{(m)}$ can be extracted from the computational results in Ref. 14

$$\Delta\Gamma_1^{(m)}=5C_F\approx 6.667. \tag{3}$$

The corrections $\Delta\Gamma_2^{(m)}$ and $\Delta\Gamma_3$ were calculated in Refs. 6 and 9, respectively. For the case of $f=5$ active quark flavors they have the numerical values

$$\Delta\Gamma_2^{(m)}\approx 14.621, \quad \Delta\Gamma_3\approx 41.758. \tag{4}$$

An expression, which is very convenient for phenomenological applications, for the contribution of a virtual t quark to $\Gamma(H^0\to\overline{b}\,b)$ was recently given in Ref. 11. It has the quite complicated form

$$\Delta_t=\overline{a_s^2}\left(3.111-0.667L_t-\frac{\overline{m_b^2}}{M_H^2}\left(-10+4L_t+\frac{4}{3}\ln(\overline{m_b^2}/M_H^2)\right)\right.$$
$$+\overline{a_s^3}(50.474-8.167L_t-1.278L_t^2)+\overline{a_s^2}\frac{M_H^2}{m_t^2}(0.241-0.070L_t)$$
$$\left.+X_t(1-4.913\overline{a_s}+\overline{a_s^2}(-72.117-20.945L_t))+\ldots,\right. \tag{5}$$

where $L_t=\ln(M_H^2/m_t^2)$, $X_t=G_F m_t^2/8\pi^2\sqrt{2}$, and m_t is the local polar mass of a t quark.

We shall now calculate the quantum-electrodynamic part Δ^{QED} in Eq. (1), defined as

$$\Delta^{\mathrm{QED}}=\left[\Delta\Gamma_{1,\mathrm{QED}}-6\frac{\overline{m_b^2}}{M_H^2}\Delta\Gamma_{1,\mathrm{QED}}^{(m)}\right]\frac{\overline{\alpha}}{\pi}+\Delta\Gamma_{2,\mathrm{QED}}\left(\frac{\overline{\alpha}}{\pi}\right)^2+\Delta\Gamma_{\mathrm{QED}\times\mathrm{QCD}}\frac{\overline{\alpha}}{\pi}\frac{\overline{\alpha_s}}{\pi}, \tag{6}$$

where $\overline{\alpha}=\overline{\alpha}(M_H)$ is the running QED coupling constant, normalized to the mass of the Higgs boson, in the $\overline{MS}$ scheme. The coefficients $\Delta\Gamma_{1,\mathrm{QED}}$, $\Delta\Gamma_{1,\mathrm{QED}}^{(m)}$, and $\Delta\Gamma_{2,\mathrm{QED}}$ can

be found from the analytical expressions (2) and (3) after the following substitutions are made: $C_A \to 0$, $C_F \to Q_b^2$, and $Tf \to (3\Sigma_{j=u}^{b} Q_j^2 + N)$, where $N=3$ is the number of leptons and Q_j are the charges of the corresponding quarks. The result is

$$\Delta\Gamma_{1,\mathrm{QED}} = \frac{17}{4} Q_b^2 \approx 0.472, \quad \Delta\Gamma_{1,\mathrm{QED}}^{(m)} = 5 Q_b^2 \approx 0.556, \tag{7}$$

$$\Delta\Gamma_{2,\mathrm{QED}} = \left(\frac{691}{64} - \frac{9}{4}\zeta(3) - \frac{3\pi^2}{8} \right) Q_b^4 - \left(\frac{65}{16} - \zeta(3) - \frac{\pi^2}{12} \right) \times Q_b^2 \left(3\sum_{j=u}^{b} Q_j^2 + 3 \right) \approx -1.455.$$

To calculate the values of the coefficient of the correction of order $O(\overline{\alpha\alpha_s})$ in Eq. (6), the following substitutions must be made in the analytical expression (2): $C_A \to 0$, $Tf \to 0$, and $C_F^2 \to 2C_F Q_b^2$, where the factor of 2 is a symmetry factor and $C_F = 4/3$. After these substitutions are made, we obtain the desired answer

$$\Delta\Gamma_{\mathrm{QED}\times\mathrm{QCD}} = \left(\frac{691}{24} - 6\zeta(3) - \pi^2 \right) Q_b^2 \approx 1.301. \tag{8}$$

An interesting question is the question of the numerical value of the contributions under study to $\Gamma(H^0 \to \overline{b}\,\overline{b})$. In discussing this question we shall confine our attention to the hypothetical case $M_H \sim M_Z \approx 91$ GeV, which will make it possible to simplify substantially the estimates made. The numerical value of the parameter $\overline{\alpha}(M_H)$ is virtually identical to the high-energy value of the invariant QED charge $\alpha_{\mathrm{inv}}(M_Z) \approx 1/129$, found in a number of works (see, for example, Ref. 15). The other parameters of the theory will be fixed as follows: $m_b \approx 4.62$ GeV, $m_t \approx 175$ GeV, $G_F \approx 1.166 \times 10^{-5}$ GeV^{-2}, $X_t \approx 3.2 \times 10^{-3}$, $\overline{m_b}(M_Z) \approx 2.8$ GeV (which corresponds to the central value of the results of the analysis of the DELPHI collaboration data for the LEP accelerator on the production of heavy quarks in three-jet events[16]), and $\alpha_s(M_Z) \approx 0.117$ (which corresponds to the central value for the running QCD coupling constant, recently obtained in an analysis of tevatron data for the structure function xF_3 of deep inelastic νN scattering[17]).

Substituting the input data, listed above, into formula (6) and taking account of the values of the coefficients (7) and (8), we obtain the following numerical estimates for the different terms in the perturbation series for Δ^{QED}:

$$\Delta^{\mathrm{QED}} = 1.16 \times 10^{-3} - 7.79 \times 10^{-6} - 8.86 \times 10^{-6} + 1.19 \times 10^{-4}. \tag{9}$$

In summary, the correction of order $O(\overline{\alpha\alpha_s})$ is an order of magnitude smaller than the four-loop correction $\Delta\Gamma_3 \overline{a_s^3}$ calculated in Ref. 9, which makes a contribution of $+2.6 \times 10^{-3}$ to $\Gamma(H^0 \to \overline{b}\,\overline{b})/\overline{\Gamma_0^{(b)}}$. However, it is important to take the order $O(\overline{\alpha\alpha_s})$ term into account systematically in the final expression for $\Gamma(H^0 \to \overline{b}\,\overline{b})$, since its total contribution to $\Gamma(H^0 \to \overline{b}\,\overline{b})/\overline{\Gamma_0^{(b)}}$ is comparable in order of magnitude to the previously computed contribution of order $O(\overline{a_s^2}\,\overline{m_b^2}/M_H^2)$ (Ref. 6) and the terms of order $O(\overline{a_s^2} M_H^2/m_t^2)$, $O(X_t \overline{a_s})$, and $O(X_t \overline{a_s^2})$ presented in Ref. 11, which in the case at hand have the numerical values -1.15×10^{-4} and 1.24×10^{-4}, -5.85×10^{-4}, and

-1.98×10^{-4}, respectively. We hope to take account of the corrections listed above in the SEEHIGGS computer code, the present capabilities of which have been demonstrated in graphical form in Ref. 18.

I wish to thank V. T. Kim for our collaboration, which started in 1992 during our joint tenure at CERN.

This work was performed as part of the scientific program of Projects 96-01-01860 and 96-02-18897 sponsored by the Russian Fund for Fundamental Research.

[1] B. A. Kniehl, Phys. Rep.**240**, 211 (1994). M. Spira, Preprint CERN-TH/97-68 (hep-ph/9705337).
[2] E. Braaten and J. P. Leveille, Phys. Rev. D **22**, 715 (1980); N. Sakai, Phys. Rev. D **22**, 2220 (1980); T. Inami and T. Kubota, Nucl. Phys. B **179**, 171 (1981); S. G. Gorishniĭ, A. L. Kataev, and S. A. Larin, Yad. Fiz. **40**, 517 (1984) [Sov. J. Nucl. Phys. **40**, 329 (1984)].
[3] S. G. Gorishny, A. L. Kataev, S. A. Larin, and L. R. Surguladze, Mod. Phys. Lett. A **5**, 2703 (1990); Phys. Rev. D **43**, 1633 (1991).
[4] A. L. Kataev and V. T. Kim, Report ENSLAPP-A-407/92 (1992) (hep-th/9304282).
[5] A. L. Kataev and V. T. Kim, Mod. Phys. Lett. A **9**, 1309 (1994).
[6] L. R. Surguladze, Phys. Lett. B **341**, 60 (1994).
[7] K. G. Chetyrkin and A. Kwiatkowski, Nucl. Phys. B **461**, 3 (1996).
[8] S. A. Larin, T. van Ritbergen, and J. A. M. Vermaseren, Phys. Lett. B **362**, 134 (1995).
[9] K. G. Chetyrkin, Phys. Lett. B **390**, 390 (1997).
[10] K. G. Chetyrkin, B. A. Kniehl, and M. Steinhauser, Phys. Rev. Lett. **78**, 594 (1997).
[11] K. G. Chetyrkin and M. Steinhauser, Preprint MPI/PhT/97-032 (hep-ph/9706462).
[12] D. Yu. Bardin, B. M. Vilenskiĭ, and P. Kh. Khristov, Yad. Fiz. **53**, 240 (1991) [Sov. J. Nucl. Phys. **53**, 152 (1991)]; B. A. Kniehl, Nucl. Phys. B **376**, 3 (1992); A. Dabelstein and W. Hollik, Z. Phys. C **53**, 507 (1992).
[13] A. L. Kataev, Phys. Lett. B **287**, 209 (1992).
[14] L. R. Surguladze and F. V. Tkachov, Nucl. Phys. B **331**, 35 (1990).
[15] R. B. Nevzorov, A. V. Novikov, and M. I. Vysotskiĭ, JETP Lett. **60**, 399 (1994); B. V. Geshkenbein and V. L. Morgunov, Phys. Lett. B **340**, 185 (1994); N. V. Krasnikov, Mod. Phys. Lett. A **9**, 2825 (1994).
[16] G. Rodrigo, A. Santamaria, and M. Bilenkii, Phys. Rev. Lett. **79**, 193 (1997).
[17] A. L. Kataev, A. V. Kotikov, G. Parente, and A. V. Sidorov, Preprint INR-947/97; JINR E2-97-194; US-FT/20-97 (hep-ph/9706534).
[18] A. L. Kataev and V. T. Kim, Preprint INR-918/96 (hep-ph/9603246); published in PNPI Research Report of 1994–1995; St. Petersburg, 1996.

Translated by M. E. Alferieff

Excitation of nuclei in a hot, dense plasma: feasibility of experiments with ^{201}Hg

A. V. Andreev, V. M. Gordienko, A. B. Savel'ev, and E. V. Tkalya[a)]
M. V. Lomonosov Moscow State University, 119899 Moscow, Russia

A. M. Dykhne
Troitsk Insitute of Innovational and Thermonuclear Studies

(Submitted 31 July 1997)
Pis'ma Zh. Éksp. Teor. Fiz. **66**, No. 5, 312–316 (10 September 1997)

It is shown that in a plasma produced on the surface of a sample consisting of a natural mixture of mercury isotopes, $\sim 10^4$–10^5 ^{201}Hg nuclei can be excited into the low-lying isomeric level $1/2^-$ (1.561 keV) by an ultrashort laser pulse with energy ≈ 1 J, duration ≈ 200 fs, and intensity $\approx 10^{16}$ W/cm^2 and the lifetime of the level can be determined. Possible mechanisms leading to the excitation of ^{201}Hg nuclei by photons and electrons in a dense, hot plasma are examined and the cross sections of the processes are estimated. Schemes for detecting the effect are proposed. © *1997 American Institute of Physics.* [S0021-3640(97)00617-8]

PACS numbers: 27.80.+w, 25.20.Dc, 25.30.Dh, 52.50.Jm

The results of the first and seemingly successful experiments[1] on the excitation of atomic nuclei in a hot plasma were published twenty years ago. The problem concerned the filling of the lowest-lying of the nuclear states known by the end of the 1970s, specifically, $1/2^+$ (76.8 eV, 25 min) in ^{235}U. The plasma was produced on the surface of a natural uranium sample containing 0.72% ^{235}U by pulsed CO_2 laser radiation (pulse energy 1 J, pulse duration 100 ns, intensity 10^{11} W/cm^2) and, according to estimates made by the authors, the electron density n_e was $\simeq 10^{12}$ cm^{-3} and the temperature T was equal to several tens of electron volts.

The theoretical calculations invoked to explain the experimental results of Ref. 1 were based on a model proposed in Ref. 2 for the process of excitation of nuclei in atomic transitions (known in the English-language literature as NEET, for nuclear excitation by electron transition). The errors made in Ref. 2 in estimating the NEET probability were indicated back in Ref. 3. The theory of NEET was developed in detail in Ref. 4, where, specifically, calculations were also performed for the $E3$ transition from the ground state to a low-lying isomeric level of ^{235}U. As a result, it was established that the NEET probability employed in Refs. 1 and 2 was least six orders of magnitude too high, and it cannot explain the observed yield of isomeric nuclei.

The experimental results of Ref. 1 have not been confirmed, either. In a similar experiment[5] performed by a group from the I. V. Kurchatov Institute of Atomic Energy, which was working with a target with 6% enrichment in ^{235}U, the parameters of the plasma of Ref. 1 were first reached and then exceeded. However, the isomer ^{235m}U was

 © 1997 American Institute of Physics

not detected. A positive result for ^{235}U was obtained only in 1990,[6] in an experiment in which the plasma was produced by an electron beam from the high-current TRITON pulsed accelerator and was later found[7] to have no bearing on the excitation of the low-lying level of ^{235}U. The isomers ^{235m}U ($1/2^+$, 76.8 eV, 25 min) were produced in inelastic scattering of 500-keV electrons in a beam by ^{235}U nuclei via low-lying states of ^{235}U with energies ranging from 50 to 415 keV followed by filling of the isomeric level $1/2^+$ (76.8 eV, 25 min).[7]

At present there are no other experimental data on the excitation of nuclei in plasmas. Meanwhile, the problem is of considerable interest in connection with the following: first, investigations of the properties of low-lying isomers of nuclei (some characteristics of the first excited levels are still unknown for a number of long-lived and even stable nuclides); second, studies of the various processes lying at the interface between nuclear physics and plasma physics (examples — self-maintained γ-emission wave in a plasma with isomeric nuclei[8,9] or multiphoton excitation of nuclei[10]); and, third, a dense high-temperature plasma can be used for producing a population inversion in a system of nuclei for a γ-ray laser. Here both nuclei with a low-lying level, near 10 keV, as well as nuclei in which a short-lived level lies near a high-lying isomeric level are suitable.[8,9,11] Finally, nuclei with the indicated characteristic features in their spectra can be used for plasma diagnostics in ranges of the parameters where the traditional diagnostic methods do not work (for example, high temperatures and solid-state densities[8,9,11–13]).

The key to solving these problems is the production of excited nuclei in plasmas. In our view ^{235}U is not the optimal choice for the first experiments. The high multipolarity of the isomeric transition negates the advantages associated with the relatively low energy of the isomeric state. At present there are no special difficulties in obtaining, with the aid of ultrashort laser pulses, a hot surface plasma with a temperature of several hundreds of electron volts and a solid-state electron density.[14,15] Different schemes for excitation of nuclear transitions and stimulation of nuclear reactions in a laser plasma with an intensity of up to $I_L \simeq 10^{19}$–10^{20} W/cm^2 on target have also been studied in Refs. 16–18. It should be noted that exceedingly expensive laser systems are required in order to obtain such intensities, which greatly limits the range of possible applications. At the same time, it has been established that when a solid target is exposed to subpicosecond laser pulses with $I_L \simeq 10^{16}$–10^{17} W/cm^2 a hot, highly ionized plasma with an electron temperature $\simeq 1$ keV, a solid-state density of nuclei and electrons, and a high x-ray emission intensity is produced. For this reason, a nuclide with an isomeric transition energy of the order of 1 keV and minimum multipolarity should be chosen as the nucleus for excitation.

We shall consider in this context the nucleus ^{201}Hg. Its first excited level $1/2^-$ (1.561 keV), whose lifetime is unknown,[19] is coupled to the $3/2^-$ (0.0) ground state by $M1$ and $E2$ transitions. For preliminary calculations of the most likely values of the excitation cross sections we shall take the data given in Ref. 20 for the reduced probability of the main $M1$ transition: $B_{W.u.}(M1;1/2^- \rightarrow 3/2^-) \simeq 0.24$–$0.024$ Weisskopf units. This estimate was obtained by comparing the properties of similar $M1$ transitions in neighboring odd-A nuclei. It was also shown there that the contribution of the $E2$ transition can be neglected over a very wide range of attenuation factors for $M1$ and $E2$ transitions.

The main decay channel of the isomer ^{201m}Hg($1/2^-$, 1.561 keV) is internal electron conversion. The conversion factor α_{M1} can be easily calculated[20] and equals $\sim 2.1\times 10^4$. Correspondingly, the lifetime $T_{1/2}^{\rm is}$ of the excited nuclei most likely falls in the range 1–10 ns. Electron conversion at a level of approximately 74% occurs on the atomic $4S_{1/2}$ (or N_I) subshell. Therefore it is possible to detect the characteristic $N_I N_{II}$ and $N_I N_{III}$ x-rays from mercury with energy near 123 and 230 eV.

Let us estimate the cross section for the excitation of mercury nuclei by photons and electrons in a plasma by direct photoexcitation (σ_γ), inelastic scattering of electrons by nuclei ($\sigma_{ee'}$), and inverse internal electron conversion ($\sigma_{\rm IIEC}$). We start with the first-order process — photoexcitation of nuclei by plasma radiation with a photon energy distribution $n(\omega)$ whose characteristic width is much greater than the total width of the nuclear state $\Gamma_{N*}^{\rm tot}=\ln 2/T_{1/2}^{\rm is}\simeq 4\times 10^{-7}$–$4\times 10^{-8}$ eV. The cross section has the form

$$\sigma_\gamma(\omega)=\frac{\lambda^2}{4}\Gamma_N^{\rm rad}(\omega;{\rm gr}\to{\rm is})\,\delta(\omega_N-\omega),$$

where $\lambda=2\pi/\omega$, ω_N is the energy of a nuclear transition (the system of units is $\hbar=c=1$), and $\Gamma_N^{\rm rad}(\omega_N;{\rm gr}\to{\rm is})\simeq 2\times 10^{-11}$–$2\times 10^{-12}$ eV is the radiation width of the nuclear transition from the ground state $|{\rm gr}\rangle$ into the isomeric state $|{\rm is}\rangle$. For a plasma with a Planckian photon energy distribution

$$n(\omega)=\frac{2}{\pi}\frac{\omega^2}{e^{\omega/T}-1}$$

it is easy to estimate the excitation efficiency ζ as the ratio of the number N^* of nuclei excited over the lifetime τ of the plasma to the number N of nuclei in the interaction region

$$\zeta_\gamma\simeq\tau\xi\int_0^\infty n(\omega)\sigma_\gamma(\omega)\,d\omega\simeq 10^{-8}-10^{-9}.$$

Here $\xi=13.18\%$ is the amount of isotopes with atomic number $A=201$ in a natural mixture of mercury isotopes. For the laser plasma obtained in the experiments of Ref. 21 $T\approx 500-800$ eV and $\tau\approx 1-5$ ps. If the photon spectrum is strongly nonequilibrium, then large deviations from the estimate presented above are possible. Specifically, the fraction of photons with energies in the range 1–2 keV in the spectrum of a HgTe plasma[21] ($I_L\approx 10^{16}$ W/cm^2, $\tau\approx 200$ fs, $\lambda_L=600$ nm) is approximately two orders of magnitude higher. Correspondingly, ζ_γ can be expected to take on values $\simeq 10^{-6}$–10^{-7}.

The cross section of the IIEC process on an empty atomic shell $|i\rangle$ can be calculated, to within a statistical factor taking account of the different spins of the initial and final states, from the formula

$$\sigma_{\rm IIEC}(E_e;|i\rangle)\simeq\frac{\lambda_e^2}{4}\Gamma_{N*}^{\rm conv}(\omega_N;|i\rangle)\,\delta(\omega_N-(E_e-E_{|i\rangle})),$$

where λ_e is the wavelength of an electron with energy E_e in the continuous spectrum and $E_{|i\rangle}$ is the binding energy in the $|i\rangle$ shell ($E_{|i\rangle}<0$) and $\Gamma_N^{\rm conv}(\omega_N;|i\rangle)$ is the conversion probability for the indicated shell. Calculations show that the conversion width $\Gamma_{N*}^{\rm conv}$,

which in our case is practically identical to the total width $\Gamma_{N*}^{\mathrm{tot}}$ of the nuclear level, is ''distributed'' over the atomic shells approximately as follows: $4S_{1/2}$ — 74%, $4P_{1/2}$ — 8%, $5S_{1/2}$ — 15%, $5P_{1/2}$ — 1.5%. In the plasma of the experimental setup of Ref. 21 the average electron density n_e was equal to $\simeq 10^{25}$ cm^{-3} and the degree of ionization z reached ≈ 30. In the case of a Maxwellian electron energy distribution $dn_e(E_e)/dE_e = n_e f(E_e)$, where the function $f(E_e)$ has the form

$$f(E_e) = \frac{2}{\sqrt{\pi}} \sqrt{\frac{E_e}{T}} e^{-E_e/T} \frac{1}{T},$$

the excitation efficiency in the IIEC process

$$\zeta_{\mathrm{IIEC}}(|i\rangle) \simeq \tau \xi n_e \int_0^\infty f(E_e) \sigma_{\mathrm{IIEC}}(E_e; |i\rangle) v_e dE_e,$$

is approximately equal to $3\times 10^{-6} - 3\times 10^{-7}$ for a transition to the $4S_{1/2}$ subshell and $3\times 10^{-7} - 3\times 10^{-8}$ for a transition to the $5S_{1/2}$ subshell. (We note that in our plasma the IIEC process to the $4F_{1/2}$ subshell evidently will not occur because the degree of ionization of the plasma is too low.)

In contrast to the mechanisms considered above, excitation in inelastic scattering of plasma electrons by nuclei is a nonresonant process. All electrons in the spectrum whose energies are higher than the nuclear transition energy participate in this process. To determine the cross section, the self-consistent field of the nucleus and the electronic shell of ions with different degrees of ionization were calculated by the Hartree–Fock–Slater method. The relativistic wave functions of the scattered electrons were found in this field. The cross section for ^{201}Hg is virtually independent of the degree of ionization and falls off from $\sigma_{e,e'} \approx 1.4\times 10^{-29}$ cm^2 with incident electron energy $E_e = 1.6$ keV to $\approx 4.7\times 10^{-30}$ cm^2 for $E_e = 5.1$ keV and further to $\approx 2.6\times 10^{-30}$ cm^2 for $E_e = 9.6$ keV. Averaging over a Maxwellian distribution with $T = 800$ eV gave for the reaction rate $\langle \sigma_{e,e'} v_e \rangle \simeq 0.8\times 10^{-20}$ cm^3/s. Estimating the excitation efficiency as $\zeta_{e,e'} \simeq n_e \tau \langle \sigma_{e,e'} v_e \rangle \xi$ gives the range $\zeta_{e,e'} \simeq 2\times 10^{-8} - 2\times 10^{-9}$.

It should be noted that the unsteady nature of the processes in a femtosecond plasma will strongly influence the ratio of the efficiencies of different excitation channels. At the same time, comparing all excitation mechanisms shows that an efficiency $\zeta \simeq 10^{-7}$ can be counted on. In the plasma of Ref. 21 the number of atoms reaches $N \simeq 10^{11} - 10^{12}$. Therefore $N^* \simeq 10^4 - 10^5$ isomeric nuclei ^{201m}Hg($1/2^-$, 1.561 keV) can be excited by an ≈ 1 J laser pulse. Since the lifetime of isomers should be two to three orders of magnitude longer than that of the plasma, the conversion x-rays will be detected without a background. Also, keeping in mind the reserved margin of one order of magnitude in the efficiency (the range for ζ_γ under the experimental conditions of Ref. 21 should be $10^{-6} - 10^{-7}$), it can be concluded that the observation of the excitation of low-lying isomers in plasmas in the near future is entirely realistic.

We thank N. I. Koroteev for helpful discussions.

This work was supported by the Russian Fund for Fundamental Research (Grants Nos. 96-02-16200a and 97-02-17013a), a Grant from the State Scientific–Technical Program ''Physics of quantum and wave processes,'' and Grant No. 96-15-96481 from the Leading Scientific Schools.

[a)]e-mail: tkalya@p5-lnr.msu.su

---

[1] Y. Izawa and C. Yamanaka, Phys. Lett. B **88**, 59 (1979).
[2] M. Morita, Prog. Theor. Phys. **49** 1574 (1973).
[3] D. P. Grechukhin and A. A. Soldatov, Preprint IAÉ-2706 [in Russian], Institute of Atomic Energy, Moscow, 1976.
[4] E. V. Tkalya, Zh. Éksp. Teor. Fiz. **102**, 379 (1992) [Sov. Phys. JETP **75**, 200 (1992)].
[5] R. V. Arutyunyan, V. Yu. Baranov, L. A. Bol'shov *et al.*, *Proceedings of the International Symposium on Short Wavelength Lasers and Their Applications*, USSR, Samarkand, 1990, Nova Science Publishers, Inc., New York, 1991, p. 127.
[6] R. V. Arutyunyan, L. A. Bol'shov, V. D. Vikharev *et al.*, Yad. Fiz. **53**, 36 (1991) [Sov. J. Nucl. Phys. **53**, 23 (1991)].
[7] E. V. Tkalya, JETP Lett. **53**, 463 (1991).
[8] R. V. Arutyunyan, L. A. Bol'shov, and E. V. Tkalya, Dokl. Akad. Nauk SSSR **299**, 99 (1988) [Sov. Phys. Dokl. **23**, 207 (1988)].
[9] R. V. Arutyunyan, L. A. Bol'shov, V. F. Strizhov, and E. V. Tkalya, Kvant. Élektron. **17**, 496 (1990) [Sov. J. Quantum Electron. **20**, 430 (1990)].
[10] E. V. Tkalya, Dokl. Akad. Nauk SSSR **318**, 1158 (1991) [Sov. Phys. Dokl. **36**, 467 (1991)].
[11] A. V. Andreev, Vestn. Mosk. Univ. Fiz. Astron. **35**, 28 (1994).
[12] R. V. Arutyunyan, L. A. Bol'shov, and E. V. Tkalya, JETP Lett. **46**, 446 (1987).
[13] A. V. Andreev, V. M. Gordienko, and A. B. Savel'ev, Preprint No. 1/1997 [in Russian], Department of Physics, Moscow State University.
[14] B. Luther-Davis, E. G. Gamaliĭ, Y. Wang *et al.*, Kvantovaya Élektron. (Moscow) **19**, 317 (1992) [Sov. J. Quantum Electron. **22**, 317 (1992)].
[15] V. T. Platonenko, Laser Phys. **2**, 852 (1992).
[16] P. Gibbon and R. Forster, Plasma Phys. Controlled Fusion **38**, 769 (1996).
[17] A. B. Borovskiĭ and A. L. Galkin, *Laser Physics: X-Ray Lasers, Ultrashort Pulses, Powerful Laser Systems* [in Russian], Izd. AT, Moscow, 1996.
[18] M. Yu. Romanovsky, in *Dynamik Evolution, Strukturen. Nichtlinear Dynamik und Statistik komplexer Strukturen*, edited by J. Freund, Verlag Dr. Koster, Berlin, 1996, p. 136.
[19] M. R. Scmorac, Nucl. Data Sheets **49**, 733 (1986).
[20] V. F. Strizhov and E. V. Tkalya, Dokl. Akad. Nauk SSSR **325**, 284 (1992) [Sov. Phys. Dokl. **37**, 359 (1992)].
[21] A. B. Savel'ev, A. V. Andreev, V. M. Gordienko and P. M. Mikheev, *Abstracts of Ultrafast Processes in Spectroscopy 97*, Estonia, Tartu, 1997.

Translated by M. E. Alferieff

Observation of the penetration of subbarrier ultracold neutrons through beryllium foils and coatings

V. E. Varlamov, V. V. Nesvizhevskiĭ, A. P. Serebrov,[a)] R. R. Tal'daev, and A. G. Kharitonov
B. P. Konstantinov Institute of Nuclear Physics, Russian Academy of Sciences, 188350 Gatchina, Russia

P. Geltenbort
Institute Max von Laue — Paul Langevin, 38042, Grenoble, France

M. Pendlebury
University of Sussex, Brighton BN1 9QH, UK

A. V. Strelkov and V. N. Shvetsov
Joint Institute of Nuclear Research, 141980 Dubna, Russia

K. Schreckenbach
Technische Universität München, D-85747 Garching, Germany

(Submitted 5 August 1997)
Pis'ma Zh. Éksp. Teor. Fiz. **66**, No. 5, 317–322 (10 September 1997)

The subbarrier passage of ultracold neutrons through beryllium foils and coatings with a probability much higher than that of tunneling is observed. This effect may be responsible for the so-called anomalous loss of ultracold neutrons. © *1997 American Institute of Physics.* [S0021-3640(97)00717-2]

PACS numbers: 28.20.−v

INTRODUCTION

A basic property of ultracold neutrons (UCNs) is their capability of undergoing total internal reflection from a surface and therefore being confined in closed material traps. Immediately after the discovery of UCNs,[1,2] attempts were made to obtain the theoretically predicted long storage times of UCNs in traps.

However, starting in 1968, investigations with UCNs raised a series of problems with no obvious solutions. The chief one is the inadequate storage time of UCNs in traps. This phenomenon was observed in the first experiments on storage of UCNs.[3,4] In 1978 additional losses of UCNs in the walls of a trap were found. These losses were due to heating of UCNs by hydrogen impurities in the surface.[5,6] However, high hydrogen densities were required to explain the observed losses. This problem became more obvious in 1990 in experiments performed in Gatchina on measuring the neutron lifetime[7] and in a subsequent careful investigation of beryllium, one of the best wall materials for UCN traps. The UCN losses in beryllium traps were found to be two orders of magnitude higher than the theoretical estimates based on the neutron trapping data and were equal to 3×10^{-5} (per collision) at temperatures of 10–15 K. Furthermore, the observed losses were virtually temperature-independent below 80 K. At the same time, the probability of

heating could be strongly temperature-dependent, which is at variance with the observations reported in Ref. 7. A subsequent careful analysis of the trap surfaces did not show the presence of any contaminants with a high trapping cross section. The phenomenon was characterized as an anomalous loss of UCNs.[8]

Several other unexplained experiments with UCNs were recently performed: observation of selective intensification of trapping of UCNs by some materials,[9] enhanced heating of UCNs by the surface of a beryllium foil,[10] and others.

If we assume that there exists a process whereby UCNs penetrate into a material, we could possibly understand most of the existing phenomena. We shall not attempt to discuss in this letter the possible theoretical basis for such penetration. Separate attempts have been made to explain the anomalous UCN losses.[11,12] The idea that is being most actively discussed is UCN localization in the medium, followed by diffusion of the neutrons.[13]

In this letter we discuss a number of experimental facts concerning the penetration of subbarrier UCNs through beryllium foils and coatings. Since the energy of the UCNs which had penetrated through the foil was not measured accurately in this experiment, we cannot prove that the penetration of UCNs beneath a barrier was observed. A more precise statement would be that penetration of subbarrier UCNs was observed in the experiment.

MEASUREMENT OF THE PENETRATION OF SUBBARRIER UCNs THROUGH BERYLLIUM FOILS AND COATINGS

The first experimental indication of the penetration of subbarrier UCNs through 0.3–0.5 μm thick beryllium coatings (prepared by magneton sputtering) was obtained in Refs. 7 and 8. The trap was fabricated from aluminum and coated with beryllium. The total UCN losses in the energy range $E_0 \sim 0-0.7$ m were measured in the experiment. Here the UCN energy is expressed in terms of the height h of the step in the earth's gravitational field using the expression $E_0 = mgh$. The maximum energy of the UCNs $E_{\max} = 0.7$ m in this experiment (''KOVSh'') was higher than the critical energy of the aluminum substrate $E_{\mathrm{Al}} = 0.52$ m. The experimental apparatus consisted of a gravitational differential total UCN loss spectrometer. A detailed description of the method used to measure the energy dependence of the total losses can be found in Ref. 7. An increase in losses in the energy range $E > E_{\mathrm{Al}}$ and also a sharp change in the loss factor at the energy E_{Al} could mean that the UCNs penetrated into the beryllium and then into the aluminum. The observed penetration probability was equal to $\sim 10^{-3}$ per collision, which is much higher than the probability of tunneling through such a beryllium layer. However, the quality of the coating was not carefully analyzed at the time and therefore the results were attributed to poor quality of the coatings.

To check the subbarrier UCN penetration hypothesis, special investigations were performed first with a 150-μm thick vacuum-tight beryllium foil and beryllium coatings on an aluminum foil (Gatchina, 1991–1993) and then with a 56-μm thick vacuum-tight beryllium foil (Grenoble, 1997). The arrangement of our Grenoble apparatus is shown in Fig. 1. The same method was used in the experiments performed in Gatchina (1991–1993). The idea of the measurements is as follows: When the storage volume *3* is filled

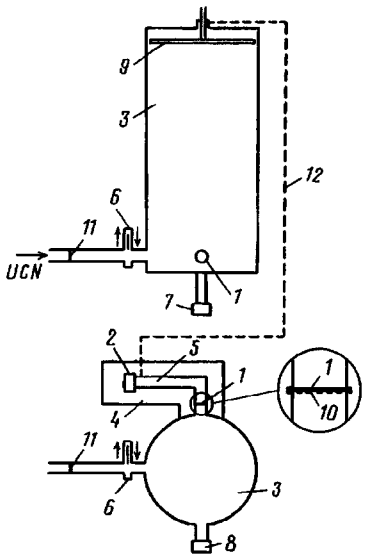

FIG. 1. Diagram of the apparatus in the ILL reactor in Grenoble for studying subbarrier penetration through a beryllium foil: *1* — 56-μm beryllium foil, *2* — UCN detector (''DUNya''), *3* — UCN storage vessel (gravitational spectrometer), *4* — neutron shielding of the detector, *5* — bent neutron guide, *6* — UCN valve, *7* and *8* — UCN and above-barrier neutron monitor detectors, respectively; *9* — polyethylene absorber, *10* — stainless steel support grating, *11* — separating aluminum foil, *12* — tube for evacuating the bent neutron guide.

with UCNs, the UCN detector *2* will detect only the background present in the laboratory and the neutrons penetrating through the foil 1. To eliminate spurious effects, neutrons with energy $E>E_{\mathrm{Be}}=2.35$ m (critical energy for beryllium) must be removed from the storage volume. This was accomplished by two methods: 1) preliminary preparation of a spectrum in a closed trap in which the critical velocity for the walls is much lower than that for beryllium, and 2) subsequent analysis of the time dependence of the intensity of the UCNs that have passed through.

The measurement procedure consisted of the following (Fig. 1): A gas of UCNs flowed through the valve *6* and filled the storage volume *3*, after which the valve was closed. The flux of suprabarrier neutrons with $E>E_{\mathrm{Be}}$ would decrease over several seconds to a very low value because the suprabarrier (for beryllium) neutrons are lost in the polyethylene absorber *9* and also in the walls of the stainless-steel storage volume (critical energy $E_{SS}\sim 1.9$ m).

The preliminary storage volume was filled in 100 s and the UCN valve *6* was closed for 210 s. The total cycle required 310 s.

A decisive conclusion concerning the penetration of subbarrier UCNs will be based on the measurements performed with a vacuum-tight beryllium foil. For this reason, these measurements will be described in detail below, and the results obtained with beryllium coatings will only be listed.

A vacuum-tight beryllium foil *1* (Fig. 1) was prepared from drop-forged beryllium

by rolling to a thickness of 56 μm. The foil covered the entire transverse cross section, 9 cm in diameter, of the neutron guide *5* connecting the storage volume and the UCN detector *2*. A stainless steel grating *10* was installed in order to prevent air pressure from damaging the foil. The foil area not screened by the grating was equal to 48 cm^2. A vertical cylinder 0.6 m in diameter and 2 m high was used as the storage volume *3*. The storage vessel and the neutron guides were made of polished stainless steel. The neutrons were transported from a Steyerl turbine to the storage volume along a neutron guide with an aluminum separating foil *11*. The neutron guide could be closed with the valve *6*. The UCN flux at the level of the beryllium foil was equal to 500 neutrons $\cdot$ $s^{-1}\cdot$ cm^{-2}. The spectrometer contained a polyethylene absorber *9* placed at a height of 1.8 m; this absorber ensured the appropriate upper cutoff of the UCN spectrum at $E_{\max}\sim 1.8$ m. The aluminum separating foil *11* in the entrance neutron guide gives a lower limit of the spectrum $E_{\min}\sim 0.52$ m. The UCN detector (Fig. 1; 10 torr ^{3}He and 900 torr Ar, 100-μm aluminum window *2* with an area of 60 cm^2) was placed at the other end of a neutron guide of length ~ 75 cm along the axis, which had a 90° bend. In this arrangement the detector does not ''see'' the beryllium foil directly, so that the background formed by the neutrons scattered inelastically in foil *1* is greatly reduced..

The beryllium foil provided vacuum-tight separation of the storage volume, at a pressure $(1–2)\times 10^{-4}$ mbar and the volume of the bent neutron guide. Sealing the beryllium foil eliminated leakage of UCNs by-passing the foil.

The neutron shield *4* of the UCN detector consisted of a 1-cm thickness of borated rubber and a 16-cm thickness of borated polyethylene.

Figure 2 shows the time dependence of the UCN count measured by the detector *2*. The UCN flux penetrating th rough the beryllium foil was found to be $(1.16\pm 0.20)\times 10^{-2}$ s^{-1} for the energy range $E_0\sim 0.52–1.8$ m. Taking account of the UCN flux incident on the foil, the probability that UCNs penetrate through the foil was equal to $(5.0\pm 1.0)\times 10^{-7}$ per collision. The statistical reliability of a measurement was equal to ~ 6 standard deviations.

The probability of penetration of subbarrier UCNs was calculated by fitting the function

$$\alpha_1+\alpha_2\ \exp(-t/\tau_{\rm st}), \tag{1}$$

to the experimental data, where α_1 and α_2 are free parameters that correspond to the background and flux of penetrating neutrons and $\tau_{\rm st}$ is the storage time in the spectrometer and was extracted from measurements with a monitor detector *7*. Only the data obtained after the 120th second, when the flux of above-limit neutrons became small, were used in the analysis.

The signal/noise ratio was 15. This was achieved with a high UCN flux in the ILL reactor and a very low background neutron flux in the experimental chamber of the reactor in Grenoble and by using the low-background ''DUNya'' UCN detector with differential tuning of the discriminator to a narrow peak corresponding to a neutron-detection signal and 4π neutron shielding of the detector. In the experiment the temporal and amplitude spectra of the detector pulses were detected simultaneously. This made it possible to perform subsequently an analysis of the data by varying the amplitude dis-

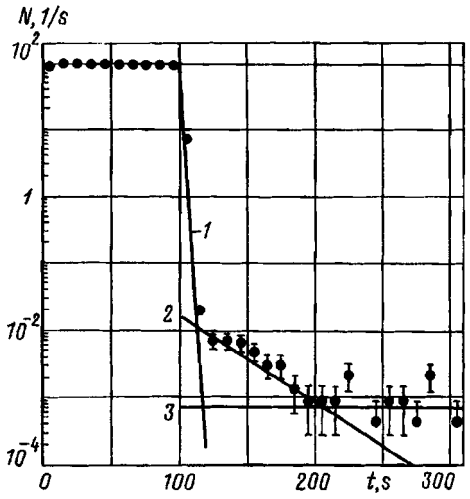

FIG. 2. UCN detection rate versus time, discrimination for the peak $Q=0.764$ MeV: *1* — Computed dependence of the above-limit neutron flux versus time; *2* — subbarrier-neutron flux measured by a monitor detector and normalized to the penetration flux of UCNs; *3* — background level. 0–100 sec — filling of the spectrometer. The detector count was due to above-limit neutrons with a short storage time; 100–120 s — sharp decrease in the counting rate after the input valve is closed; 120–310 s — the penetrating UCN flux decreases simultaneously with the UCN flux in the spectrometer all the way down to the level of the constant background.

crimination level. It is interesting to compare, for example, the results for two different discrimination levels: one within the narrow peak due to the reaction $n+{}^3\mathrm{He}\rightarrow t+p$, $Q=0.764$ MeV and another with a much wider range of amplitudes with lower limit $E=0.15$ MeV. The results for these two cases are compared in Table I.

Almost all the detected events were found in the amplitude window corresponding to the peak $Q=0.764$ MeV. This means that the observed effect is caused by the neutrons and not by stray pickup, which would show a wide amplitude distribution. The background of the shielded detector in a window corresponding to the peak of the reaction with the reactor shut down was equal to $(5.8\pm0.9)\times10^{-4}$ s^{-1}. This background is not due to neutrons, because there is no sharp peak near $Q=0.764$ MeV. This is the limit for the detector employed.

TABLE I. Comparison of two variants of the amplitude discrimination of the UCN detector signal.

	UCN detection rate, s^{-1}	
	tuning to the $Q=0.764$ MeV window	tuning to the range $E>0.15$ MeV
Background	$(7.4\pm1.8)\times10^{-4}$	$(2.6\pm0.3)\times10^{-3}$
Penetration	$(1.16\pm0.2)\times10^{-2}$	$(1.20\pm0.22)\times10^{-2}$

TABLE II. Supra- and subbarrier neutron fluxes versus air pressure in the neutron guide connecting the beryllium foil and the UCN detector.

Air pressure in neutron guide, mbar	Suprabarrier neutron flux, s^{-1}	Subbarrier neutron flux, s^{-1}
0	(123.5 ± 1.0)	$(1.16\pm0.20)\times10^{-2}$
210	(35.4 ± 0.4)	$(0.25\pm0.15)\times10^{-2}$

Heating of UCNs to the thermal-neutron energy range on the spectrometer walls could produce a spurious effect if the detector shielding is too thin. However, the measurements showed that the counting rate by a completely unshielded UCN detector did not change in time, while the UCN density in the spectrometer changed by several orders of magnitude.

The fact that the detected neutrons are not thermal can also be checked by measuring the dependence of the counting rate of the detector on the air pressure in the neutron guide *5* (Fig. 1). It can be estimated that air pressure of 210 mbar decreases the counting rate by approximately a factor of 4.5 for UCNs and above-limit neutrons. But thermal neutrons would not be affected by the presence of air in the neutron guide. This was also confirmed by an experiment whose result is presented in Table II.

Thus the UCN detection rate of the detector, which has the same time dependence as the UCN density in the spectrometer, is definitely due to the UCNs which have reached the detector along the neutron guide. At present we do not see any explanation for this effect other than the penetration of subbarrier UCNs.

In Gatchina measurements of the penetration of UCNs through beryllium coatings on aluminum foils were also performed. These measurements do not make it possible to draw a conclusion concerning the penetration of subbarrier UCNs, because there could be small but numerous defects in the coatings that were not found by optical means. But these data can be used to obtain a more complete picture of the phenomenon. All samples with a 0.07–0.8 μm thick coating showed penetration of UCNs with probability 2×10^{-4}–3×10^{-3} (see Fig. 3). An examination of the surface of a coating in an optical microscope with 700$\times$ magnification showed that the fraction of the surface with defects does not exceed 10^{-4}. Penetration of UCNs through a 100-μm aluminum foil with a bilateral 0.5-μm beryllium coating was not observed. This experiment makes it possible to gauge the time dependence of the suprabarrier neutron flux because the penetration of subbarrier neutrons through such a specimen is very weak, while the suprabarrier neutron flux remains almost unchanged. A foil with a gauged opening was used to measure the absolute value and time-dependence of the UCN flux in the storage volume.

ANALYSIS OF EXPERIMENTAL RESULTS

It is helpful to compare the probability of the observed penetration with the probability of tunneling under a Be potential barrier. This comparison (Fig. 3) shows that

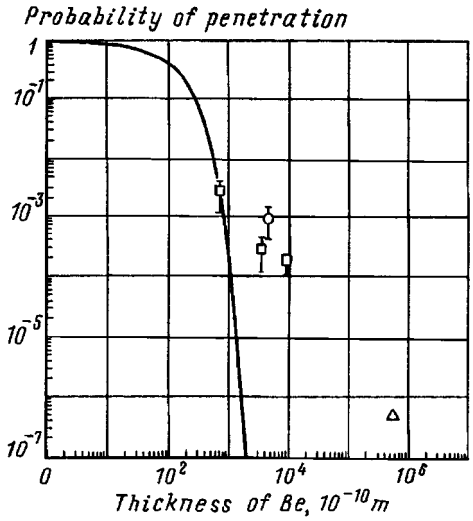

FIG. 3. Comparison of the probability of tunneling through a Fermi potential with experimental data on subbarrier UCN penetration through beryllium foils and coatings. Solid line — estimate of the tunneling effect averaged over the UCN spectrum; △ — measurements in Grenoble with a 56-μm beryllium foil; □ — measurements in Gatchina with coatings on an aluminum foil; ○ — UCN penetration estimated from neutron lifetime measurements.[7]

there is an additional penetration of UCNs through the beryllium foils and coatings. It becomes important at a thickness of 0.1 μm, when tunneling starts to decrease relatively rapidly with increasing thickness. The use of vacuum-tight beryllium foils shows that the problem does not reduce to one of the quality of the coating technology and indicates that this phenomenon occurs for some other reason.

CONCLUSIONS

The penetration of subbarrier neutrons through beryllium foils and coatings has been observed experimentally. The penetration probability for a 56-μm vacuum-tight beryllium foil was found to be $(5\pm1)\times10^{-7}$ per collision. This value is many orders of magnitude greater than the quantum-mechanical tunneling for this thickness. The observed effect is very likely of the same nature as the anomalous loss of UCNs during storage in traps. To confirm that the observed effect is in fact subbarrier penetration, in future investigations it is most important to make quite accurate measurements of the energy of the neutrons that penetrate through the foil.

The experiment was performed with the support of the Russian Fund for Fundamental Research (Grant No. 92-02-18663) and INTAS (Grant No. 93-0298). We are grateful to N. V. Borovikova for preparing the samples, to S. Neumaier for assisting during the experiment in Grenoble, and to all of our colleagues for helpful discussions and interest in this work.

[a)]e-mail: serebrov@lnpi.spb.su

[1] V. I. Lushchikov, Yu. N. Pokotilovskiĭ, A. V. Strelkov *et al.*, JETP Lett. **9**, 23 (1969).
[2] A. Steyerl, Phys. Lett. **29**, 33 (1969).
[3] L. V. Groshev, V. N. Dvoretsky, A. M. Demidov *et al.*, Phys. Lett. **34**, 293 (1971).
[4] A. I. Egorov, V. M. Lobashev, V. A. Nazarenko *et al.*, Yad. Fiz. **19**, 300 (1974) [Sov. J. Nucl. Phys. **19**, 147 (1974)].
[5] A. V. Strelkov and M. Hetzelt, Zh. Éksp. Teor. Fiz. **74**, 23 (1978) [Sov. Phys. JETP **47**, 11 (1978)].
[6] A. D. Stoica, A. V. Strelkov, and M. Hetzelt, Z. Phys. B **29**, 349 (1978).
[7] V. P. Alfimenkov, V. E. Varlamov, A. V. Vasil'ev *et al.*, JETP Lett. **52**, 373 (1990).
[8] V. P. Alfimenkov, V. V. Nesvizhevskiĭ, A. P. Serebrov *et al.*, JETP Lett. **55**, 84 (1992).
[9] S. S. Arzumanov, L. N. Bondarenko, E. I. Korobkina *et al.*, JETP Lett. **65**, 1 (1997).
[10] A. V. Strelkov, G. N. Nekhaev, V. N. Shvetsov *et al.*, ILL Research Report 3-14-52, Grenoble, 1997.
[11] V. K. Ignatovich and M. Utsuro, Phys. Lett. A **225**, 195 (1997).
[12] A. I. Frank and V. G. Nosov, Phys. At. Nucl. **58**, 453 (1995).
[13] A. P. Serebrov, *International Seminar on the Interaction of Neutrons with Nuclei*, Dubna, May 13–17, 1997.

Translated by M. E. Alferieff

Extension of the Sommerfeld diffraction integral to the case of extremely short optical pulses

V. A. Aleshkevich and V. K. Peterson[a)]
M. V. Lomonosov Moscow State University, 119899 Moscow, Russia

(Submitted 24 July 1997)
Pis'ma Zh. Éksp. Teor. Fiz. **66**, No. 5, 323–326 (10 September 1997)

The Sommerfeld diffraction theory is extended to the case of extremely short pulses. It is shown that a simple qualitative analysis and a quantitative solution of a wide class of diffraction problems are possible for pulses with durations of the order of the period of the light oscillations and an arbitrary initial distribution of the light field. © *1997 American Institute of Physics.* [S0021-3640(97)00817-7]

PACS numbers: 42.25.Fx, 61.10.−i

Substantial progress in the generation of pulses of extremely short duration has been made in the last few years. This is due mainly to improvement of the technique for the mode locking of titanium–sapphire lasers, which are capable of generating pulses with durations down to 7.5 fs at a wavelength of 800 nm, by in-cavity compensation of frequency modulation with the aid of dispersive elements.[1] Extracavity fiber-optic compression makes it possible to decrease the pulse duration further down to 5 fs.[2] According to estimates in Ref. 2, a figure of 4 fs is entirely realistic.

In many problems involving the application of ultrashort pulses, such as the pumping of x-ray lasers, the generation of shock waves in hot, dense plasmas, the formation of optical solitons, the control of light by light, and others, the spatiotemporal structure of the radiation must be carefully monitored. One of the fundamental physical reasons leading to a large transformation of this structure is intercoupled diffraction conversion of the frequency and angular spectra.

Femtosecond optical pulses contain only several oscillations of the electromagnetic field. It is completely obvious that to describe their propagation in linear and especially nonlinear media the slowly-varying-amplitude approximation becomes inapplicable. The strongly nonstationary diffraction effects arising during the propagation of such bunches of the electromagnetic field were discussed earlier in Ref. 3. In Ref. 4 the specific problem of diffraction of a Gaussian pulse in free space was solved and the relationship of the pulse to the spatial and temporal characteristics were traced on the basis of a spectral approach in the paraxial approximation. The dynamics of the interaction of extremely short pulses with two-level atoms was analyzed in Ref. 5 on the basis of the Maxwell–Bloch equations without taking diffraction into account.

Our objective in the present letter is to extend the Sommerfeld stationary theory of diffraction, which is a powerful and universal tool for analyzing diffraction phenomena of any nature, to the highly nonstationary cases of extremely short pulses. No additional restrictions will be imposed on the initial spatiotemporal distribution of the wave field.

Generalized diffraction integral. As is well known, the diffraction of a monochromatic wave by a flat screen is described by the Sommerfeld integral:

$$E(x,y,z)=2\int\int E(x',y',0)\frac{\partial G}{\partial z'}|_{z'=0}dx'dy', \tag{1}$$

where the Green's function $G(R)=\exp(ikR)/4\pi R$, and $R=\sqrt{(x-x')^2+(y-y')^2+(z-z')^2}$ is the length of the segment connecting the point of integration with the coordinates (x',y',z') on the flat screen and the point of observation (x,y,z). If the field of the monochromatic wave is written in the form $E(x,y,z,t)=E(x,y,z)\exp(-i\omega t)$ and it is assumed that $kR\gg 1$, $k=\omega/c$, then

$$\frac{\partial G}{\partial z'}|_{z'=0}\approx ik\frac{\partial R}{\partial z'}\frac{\exp(ikR)}{4\pi R}=-ik\frac{z}{R}\frac{\exp(ikR)}{4\pi R}. \tag{2}$$

Using expression (1) and summing over all frequencies, we obtain the following expression for the diffracted electric field:

$$E(x,y,z,t)=\frac{\partial}{\partial t}\int\int\int E(x',y',0,\omega)\exp(-i\omega t)\frac{2z}{cR}\frac{\exp(i\omega R/c)}{4\pi R}dx'dy'd\omega. \tag{3}$$

Introducing the notation $t'=t-R/c$ and using the inverse Fourier transform we obtain

$$E(x,y,z,t)=\frac{\partial}{\partial t'}\int\int\int E(x',y',0,t'')\frac{z}{2\pi cR^2}\delta(t''-t')dt''dx'dy'. \tag{4}$$

Performing the integration in Eq. (4) over t'', we arrive at a formula describing the diffraction of an arbitrary electromagnetic disturbance,

$$E(x,y,z,t)=\frac{1}{2\pi c}\int\int\frac{\partial}{\partial t}E(x',y',0,\ t-R/c)\frac{\cos\vartheta}{R}dx'dy', \tag{5}$$

where $\cos\vartheta=z/R$ is the cosine of the angle between the direction to the observation point and the normal to the plane of the screen. The diffraction integral (5) is a generalization of the Sommerfeld diffraction integral and is applicable for an arbitrary electromagnetic disturbance which is diffracted by a flat screen. We shall employ the diffraction integral obtained above to analyze the diffraction of an extremely short pulse with a duration of the order of one period of the light oscillations.

Diffraction by a circular opening. Let an electromagnetic pulse with duration τ_0 be incident in a direction along the normal on an opaque screen with a circular opening of radius r_0. If the electric field $E_0(t)$ in the incident pulse does not depend on the transverse coordinates x' and y', then the field on the axis of the opening can be easily calculated from expression (5), taking into account the fact that $dx'dy'=2\pi d\rho=2\pi RdR$:

$$E(0,0,z,t)=\frac{1}{2\pi c}\int_z^{\sqrt{z^2+r_0^2}}\frac{\partial}{\partial t}E_0\left(t-\frac{R}{c}\right)\frac{\cos\vartheta}{R}2\pi RdR. \tag{6}$$

Setting $\cos\vartheta\approx 1$ and noting that $\partial/\partial t=-c\partial/\partial R$, we write expression (6) in the form

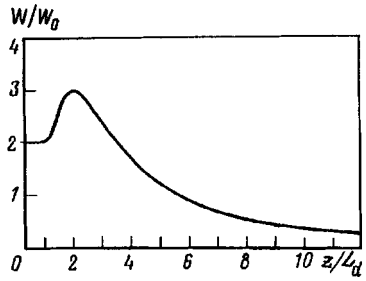

FIG. 1. Variation of the energy density with distance z in the case of the diffraction of a pulse consisting of one period of the electromagnetic oscillations.

$$E(0,0,z,t)=-\int_z^{\sqrt{z^2+r_0^2}}\frac{\partial}{\partial R}E_0(t-R/c)dR=E_0(t-z/c)-E_0(t-\sqrt{z^2+r_0^2}/c). \quad (7)$$

Therefore the diffraction of a short pulse results in the appearance of two heteropolar pulses on the axis of the opening which are identical to the incident pulse but are separated by a time interval $\Delta t=r_0^2/2zc$ $(z\gg r_0)$. It is obvious that on the axis of the opening the field, being a superposition of the fields of two heteropolar pulses, will depend on the ratio of the time delay Δt and the pulse duration τ_0. In the near field $\Delta t>\tau_0$ or $z<Ld=r_0^2/2c\tau_0$ the heteropolar pulses do not overlap, and the energy density

$$W=\int E^2(0,0,z,t)dt=2\int E_0^2(t)dt$$

is two times higher than in the incident pulse $W_0=\int E_0^2(t)dt$. In the far field $\Delta t<\tau_0$ or $z>L_d$ one has

$$E(0,0,z,t)=E_0(t-z/c)-E_0(t-\sqrt{z^2+r_0^2}/c)\approx\frac{\partial E_0}{\partial t}(t-z/c)\frac{r_0^2}{2zc}, \quad (8)$$

and the increasing overlap of the pulses results in a weakening of the diffracted field with increasing distance z, the shape of the diffracted pulse being determined by the derivative of the initial time dependence. If the incident pulse consists of one period of the electromagnetic oscillations, $E_0(t)=E_0\sin(2\pi t/\tau_0)$ for $0\leqslant t\leqslant\tau_0$ and $E_0(t)=0$ for $t<0$ and $t>\tau_0$, then the energy distribution along the z axis has the form displayed in Fig. 1.

For small z the energy density on the axis is constant and equals twice the energy density in the incident pulse. At the distance z_M where $\Delta t=r_0^2/2z_Mc=\tau_0/2$ $(z_M=2L_d)$, summing the pulses even triples the energy density. At distances $z>3.5L_d$ one has $W\propto z^{-2}$. The energy density W as a function of the transverse coordinate ρ is shown in Fig. 2. For $z<L_d$ there exists a ring, which is most pronounced at distances of the order of $0.3L_d$ and gradually vanishes as $z\to L_d$. For $z\gg L_d$ the form of $W(\rho)$ is nearly Gaussian, with an e^{-1} width of the distribution which can be approximated to a high degree of accuracy by the expression $r_0(z)=r_0\sqrt{1+(z/5L_d)^2}$.

Diffraction of a pulse with a Gaussian transverse amplitude distribution. Now let $E(x',y',0,t)=\exp[-(x'^2+y'^2)/r_0^2]E_0(t)$ in the incident pulse, which pulse once again con-

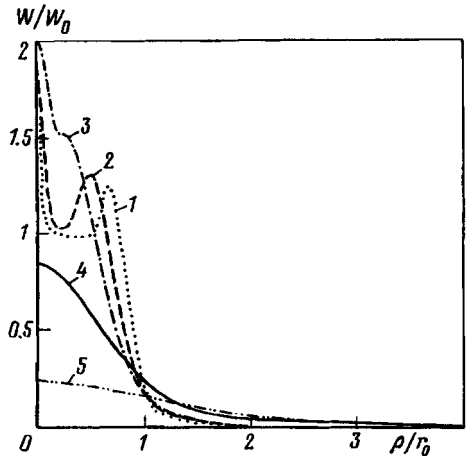

FIG. 2. Energy density versus the transverse transverse coordinate ρ for $z/L_d=0.3$ (*1*), 0.6 (*2*), 1.2 (*3*), 6.0 (*4*), and 12 (*5*).

sists of a single period of the electromagnetic oscillations. The characteristic temporal shape of the diffracted pulse is shown in Fig. 3. We note that at a sufficiently large distance $z>L_d$ the initial sine curve transforms on the axis of the beam into a cosine curve, i.e., there is a tendency for the curve to transform into its derivative. However, the retardation effects at the periphery of the beam are more complicated.

The energy density as a function of the transverse coordinate remains Gaussian at all distances. Here the radius $r_0(z)=r_0\sqrt{1+(z/L_d)^2}$ (where $L_d=\pi r_0^2/c\tau_0$) increases with

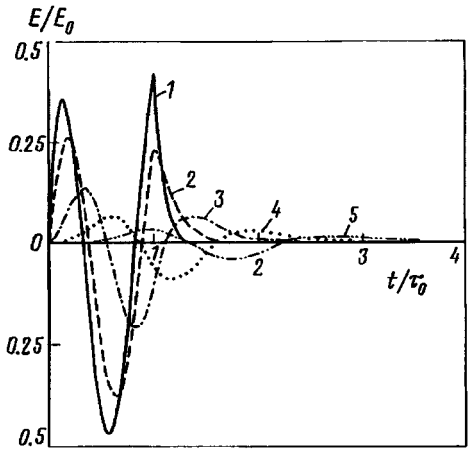

FIG. 3. Temporal behavior of a diffracted short pulse with a Gaussian transverse distribution of the field amplitude at distances $z=2L_d$ and different distance from the axis z: $\rho/r_0=0$ (*1*), 1.0 (*2*), 2.0 (*3*), 3.0 (*4*), and 5.0 (*5*).

distance just as in the case of the diffraction of a beam of monochromatic radiation with $\lambda = c\tau_0$.

In closing, we note that the approach developed above for describing nonstationary diffraction makes it possible to perform a simple qualitative analysis of wave fields of any nature and can be extended to the case of dispersive nonlinear media.

[a)]Deceased

[1] L. Xu, Ch. Spielman, F. Krausz, and R. Szipocs, Opt. Lett. **21**, 1259 (1996).
[2] A. Baltuska, Z. Wei, M. S. Phenichnicov, and D. A. Wiersma, Opt. Lett. **22**, 269 (1997).
[3] É. M. Belenov and A. V. Nazarkin, JETP Lett. **53**, 200 (1991).
[4] Z. Wang, Z. Zhang, Z. Xu, and Q. Lin, IEEE J. Quantum Electron. **33**, 566 (1997).
[5] É. M. Belenov, A. V. Nazarkin, and V. A. Ushchipovskiĭ, Zh. Éksp. Teor. Fiz. **100,** 762 (1991) [Sov. Phys. JETP **73**, 422 (1991)].

Translated by M. E. Alferieff

Pulsed magnetooptic compression of cold atoms

V. I. Balykin

Institute of Spectroscopy, Russian Academy of Sciences, 142092 Troitsk, Moscow Region, Russia; Institute for Laser Science, University of Electro-Communications Chofugaoka, Chofushi, Tokyo 182, Japan

(Submitted 6 August 1997)
Pis'ma Zh. Éksp. Teor. Fiz. **66**, No. 5, 327–331 (10 September 1997)

A method is proposed for increasing the density of cold atoms. The method is based on pulsed laser irradiation of the atoms in a nonuniform magnetic field. The interaction conditions under which the velocity of an atom is damped to a value that depends only on the magnitude of the magnetic field and the position of the atom at the moment it is irradiated by the laser field are found. The atom completely loses all memory of its initial coordinates and velocity. In a three-dimensional interaction geometry an irradiated atomic ensemble transforms into an ensemble contracting toward the origin. The basic physical processes accompanying the compression of atoms are studied. © *1997 American Institute of Physics.* [S0021-3640(97)00917-1]

PACS numbers: 32.80.Pj, 85.70.Sq

Efficient methods of laser cooling and trapping of free atoms, making it possible to obtain a temperature of the localized atoms in the range 10^{-6} and lower, have been developed during the last ten years.[1,2] One of the most striking accomplishments in this field is the observation of Bose–Einstein condensation of free weakly interacting atoms.[3]

As a rule, one of the most important parameters in all investigations with cold localized atoms is the density of the atoms. The now standard method for obtaining a high density of atoms is, first, to cool the free atoms to a temperature equal to several degrees Kelvin and then to localize the atoms in a magnetooptical trap (MOT), where the atoms are further cooled to temperatures $\sim 10^{-4}$–10^{-5} K. The maximum density of atoms achievable in this process is $\sim 10^{10}$–10^{11} cm^{-3}. A fundamental limit on the maximum density of atoms arises from the very nature of a magnetooptic trap: At a high density of atoms in a MOT the scattered laser photons are again absorbed by atoms, giving rise to an effective force that pushes the atoms apart and limits their density.[4] A large increase in the density of atoms has been achieved by the so-called ''dark'' MOT technique, in which the atoms that have been localized are optically pumped into a sublevel of the hyperfine structure, where the atoms are out of resonance with the main laser field localizing the atoms. The method has been successfully used to localize Na atoms,[5] but there are substantial difficulties in applying the method to other elements.[6] The increase in density in the process of cooling atoms in a magnetic trap by the ''evaporative cooling'' method[7] results in a substantial decrease in the total number of localized atoms.

In the present letter we propose a new method for increasing the density of cold

 © 1997 American Institute of Physics

atoms. In this method the total number of atoms remains practically unchanged. The crux of the method is as follows. The initial ensemble consists of atoms localized in a MOT. The case of an optical transition in an atom between a state with total angular momentum $J_g=0$ and an excited state with $J_e=1$ is studied. The MOT is formed by three mutually perpendicular circularly polarized $(\sigma_+-\sigma_-)$ laser standing waves propagating along the $\mathbf{e}_1$, $\mathbf{e}_2$, and $\mathbf{e}_3$ axes of the coordinate system, and a spatially nonuniform quadrupole magnetic field[8]

$$\mathbf{B}(\mathbf{r})=B_0[\mathbf{e}_1(x/a)+\mathbf{e}_2(y/a)-2\mathbf{e}_3(z/a)], \tag{1}$$

where B_0 is the amplitude of the magnetic field and a is the characteristic spatial scale of the magnetic field. At a certain moment in time the laser field localizing the atoms is switched off, and the atoms freely expand away from the center of the trap in a time t_p. The expansion time t_p should be, first, sufficient for the density of atoms to decrease substantially as compared with the initial density and, second, the optical density of the atoms after expansion should be much less than 1. The maximum expansion time is required to satisfy the condition $t_p \ll a/\langle v\rangle$, where $\langle v\rangle$ is the average initial velocity of the atoms in the MOT. After undergoing free expansion the atoms are irradiated with a short (duration t_i) laser pulse, initially used to confine the atoms in the MOT. A force due to the light pressure acts on the atoms during the time t_i of the compressing laser pulse. In the one-dimensional case (considered here in order to simplify the physical picture) and with a weak saturation of the atomic transition this force has the form

$$F_x=F_{\sigma_+}+F_{\sigma_-}=\hbar k\gamma\left[\frac{\omega_{xR}^2/2}{\delta_+^2+\omega_{xR}^2/2+\gamma^2}-\frac{\omega_{xR}^2/2}{\delta_-^2+\omega_{xR}^2/2+\gamma^2}\right], \tag{2}$$

where ω_{xR} is the Rabi frequency, 2γ is the homogeneous width of the atomic transition,

$$\delta_\pm=\left(\omega-\omega_0\pm\mathbf{k}v_x\pm\frac{\mu B(r)}{\hbar}\right) \tag{3}$$

are the detunings of the laser frequencies ω from the frequency ω_0 of the atomic transition in a nonuniform magnetic field $B(r)$, $\mathbf{k}$ is the wave vector, v_x is the velocity of the atom, μ is the magnetic moment of the atom, and η is Planck's constant. Assuming that the magnetic field is a linear function of the distance to the center of the trap, the force acting on an atom along the x axis equals

$$F_x=-\beta_x v_x-\omega_{0x}^2 x, \tag{4}$$

where

$$\beta_x=\frac{4v_r\mathbf{k}(\omega_{xR}^2/\gamma)(\delta/\gamma)}{[1+(\delta/\gamma)^2]^2}, \tag{5}$$

$$\omega_{0x}^2=\frac{4v_r b(\omega_{xR}^2/\gamma)(\delta/\gamma)}{[1+(\delta/\gamma)^2]^2}, \tag{6}$$

$$b=\mu_B(dB/dx), \tag{7}$$

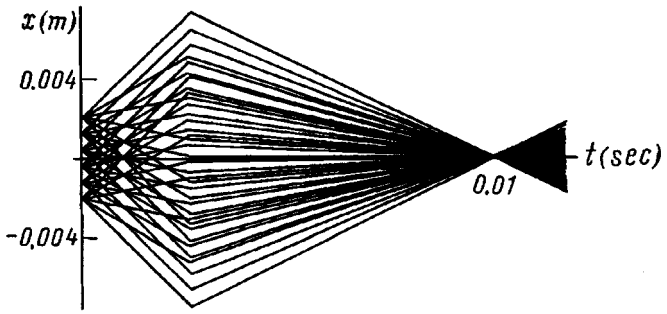

FIG. 1. One-dimensional compression of the atoms.

μ_B is the Bohr magneton, v_r is the recoil velocity of the atom, and $\delta=\omega-\omega_0$. It follows from Eqs. (4)–(7) that the behavior of an atom in the laser–magnetic field is described well by a damped oscillator with a damping constant β_x and oscillation frequency ω_{0x}.

When the interaction time of the atom and the laser field is short $t\approx(5-10)\beta^{-1}$, the displacement of the atom is very small. Then the change in the velocity of the atom is

$$v_x=-(\omega_{0x}^2/\beta_x)x_0+[(\omega_{0x}^2/\beta_x)x_0+v_{0x}]e^{-2\beta_x t}, \tag{8}$$

where x_0 and v_{0x} are the coordinate and velocity of the atom at the instant it is irradiated by the laser pulse. One can see from Eq. (8) that if the interaction time is greater than the decay constant $t\geqslant\beta_x$, the velocity of the atom is damped to the value

$$v_B=-(\omega_{0x}^2/\beta_x)x_0=-(b/k)x_0, \tag{9}$$

which is determined only by the magnitude of the magnetic field and the coordinate of the atom. The velocity of the atom is damped to a value that depends only on the magnitude of the magnetic field. Therefore, after the atom interacts with the laser pulse the direction of motion of the atom reverses and the speed depends only on the gradient of the magnetic field and coordinate of the atom. The return time of the atoms to the coordinate origin is $t_E=x_0/v_B=b/k$ and is the same for all atoms. An atom loses all memory of its initial coordinates and velocity in the initial MOT.

Figure 1 displays the dynamics of such a one-dimensional compression of the atoms. The initial position of the atoms is plotted along the vertical axis and the time of motion of the atom is plotted along the horizontal axis. The curves in the figure represent the free expansion of the atoms, a sharp change in their velocity under the action of a short laser pulse, and further compression of the atoms. The trajectories of the atoms were calculated for the exact expression of the force due to light pressure under the assumption that the gradient of the magnetic field is constant. The initial variance of the atom velocities is

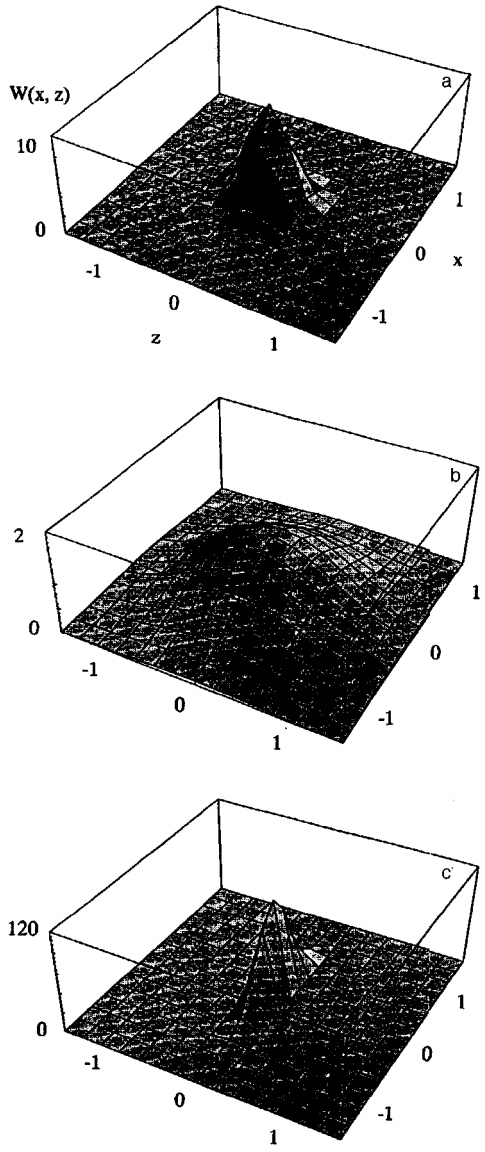

FIG. 2. Three-dimensional compression of the atoms. The spatial distributions $W(x,z)$ of the atoms in the (x,z) plane are shown. a — Initial distribution, b — distribution at the end of the free expansion of the atoms, and c — distribution at the end of the compression of the atoms.

$\delta v = 200$ cm/s, the duration of free expansion is $t_p = 2.5$ ms, the pulse duration is $t_i = 50$ μs, $(dB/dx) = 10$ G/s, $\omega_R = 0.5\gamma$, and $\delta = -2\gamma$.

When atoms are irradiated by a three-dimensional laser field, the freely expanding cloud of atoms is converted into a contracting cloud. After a certain period of time, all

atoms, irrespective of their coordinates and velocities, collect at the origin.

Let us now discuss the main physical processes that could destroy the ideal compression of the atoms. 1) The spatial nonuniformity of the laser fields during the irradiation of atoms by light is very small, since the decay constant β and the frequency ω_0 depend identically on the intensity of the laser field. 2) The force due to the light pressure is by nature a diffusion force, as a result of which there is a variance $\delta v = \sqrt{2Dt} \approx \sqrt{0.3 v_r v_B}$ of the atom velocities around the average value v_B, where D is the velocity diffusion coefficient and v_r is the recoil velocity of an atom. Accordingly, the radius of the atomic ensemble at the end of the compression of the atoms is finite. From the standpoint of pulsed compression, heavy atoms with a low recoil momentum are most promising. 3) Since the magnetic field (1) in a MOT is fundamentally anisotropic, the force, the coefficient of friction, and the diffusion coefficient are likewise anisotropic. This has the effect that the compression time along the x and y axes is two times longer than along the z axis and, accordingly, the atomic cloud is compressed into an ellipsoid of finite length and width along the z axis. The anisotropy of compression can easily be compensated by irradiating the atoms with a laser pulse along the z axis with a delay with respect to the pulses along the x and y axes equal to the compression time of the atoms along the x and y axes. 4) The MOT is formed by laser beams with $\sigma_{\pm}$ polarizations, which enable pumping of atoms into a sublevel with the largest value of m_F — the components of the ground-state magnetic moment of the atom. Incomplete pumping of the atoms into this sublevel (in the case $J_g \neq 0$) results in an additional spreading of the atoms in space.

Figure 2 shows the evolution of the spatial distributions of sodium atoms calculated by the Monte Carlo method. Figure 2a shows the spatial distribution of the atoms before they undergo free expansion; Fig. 2b shows the spatial distribution at the time of irradiation by the light pulse; and, Fig. 2c shows the distribution at the moment of maximum compression of the atoms. It was assumed that the magnetic field has a spatial dependence of the form (1), and the anisotropy of the coefficient of friction and the pulsed diffusion coefficient of the atoms were taken into account.[9] The initial distribution was chosen to be Gaussian with radius 0.3 cm and average velocity of the atoms equal to 150 cm/s. The free-expansion time $t = 5$ ms, the pulse duration is 50 μs, the saturation parameter of an atomic transition $G = 1$, and $dB/dx = 50$ G/cm. One can see that the spatial distribution of the atoms is broadened during the first stage of free expansion (Fig. 2b). The laser pulse transforms the free expansion of the atoms into a compression, which is manifested in Fig. 2c as a decrease in the diameter of the distribution and an increase in the density of the atoms. The maximum density of the atoms at the center of the compressed distribution is 15 times higher than the density of the initial distribution. The density of the atoms at the center can be increased even more (by an order of magnitude), as noted earlier, by delayed irradiation of the atoms along the x axis. The main process that limits the maximum density of the atoms during compression is momentum diffusion.

In closing, I wish to thank K. Shimizu and F. Shimizu for a helpful discussion of the results.

[1] *Laser Cooling and Trapping of Atoms*, Special Issue edited by S. Chu and C. Wieman, J. Opt. Soc. Am. **6** (1989).
[2] *Optics and Interferometry with Atoms*, Special Issue edited by J. Mlynek, V. Balykin, and P. Meystre, Appl. Phys. B **54,** (1992).
[3] M. H. Anderson, J. R. Ensher, M. R. Matthers *et al.*, Science **269**, 198 (1995).
[4] D. W. Seiko, T. G. Walker, and C. E. Wieman, J. Opt. Soc. Am. B **8**, 946 (1991).
[5] W. Ketterle, K. B. Davis, M. A. Joffe *et al.*, Phys. Rev. Lett. **70**, 2253 (1993).
[6] C. G. Townsend, N. H. Edwards, K. P. Zetie *et al.*, Phys. Rev. A **52**, 1423 (1995).
[7] K. B. Davis, M.-O. Mewes, M. A. Joffe *et al.*, Phys. Rev. Lett. **74**, 5202 (1995).
[8] E. Raab, M. Prentiss, A. Cable *et al.*, Phys. Rev. Lett. **59**, 2631 (1987).
[9] M. Gaida and J. Mostowski, Phys. Rev. **49,** 4864 (1994).

Translated by M. E. Alferieff

Superfluidity of indirect magnetoexcitons in coupled quantum wells

Yu. E. Lozovik,[a] O. L. Berman, and V. G. Tsvetus
Institute of Spectroscopy, 142092 Troitsk, Moscow District, Russia

(Submitted 22 July 1997)
Pis'ma Zh. Éksp. Teor. Fiz. **66**, No. 5, 332–337 (10 September 1997)

The temperature T_c of the Kosterlitz–Thouless transition to a superfluid state for a system of magnetoexcitons with spatially separated electrons e and holes h in coupled quantum wells is obtained as a function of magnetic field H and interlayer separation D. It is found that T_c *decreases* as a function of H and D at fixed exciton density n_{ex} as a result of an increase in the exciton magnetic mass. The highest Kosterlitz–Thouless transition temperature as a function of H *increases* (at small D) on account of an increase in the maximum magnetoexciton density n_{ex} versus magnetic field, where n_{ex} is determined by a competition between the magnetoexciton energy and the sum of the activation energies of incompressible Laughlin fluids of electrons and holes.
© *1997 American Institute of Physics.* [S0021-3640(97)01017-7]

PACS numbers: 71.35.Ji, 47.37.+q, 85.30.Vw

Systems of excitons with spatially separated electrons e and holes h (indirect excitons) in coupled or double quantum wells (CQWs) in magnetic fields H are now under intensive experimental investigation.[1–3] They are of interest, in particular, in connection with the possibility of superfluidity of indirect excitons or e–h pairs, which would manifest itself in the CQWs as persistent electrical currents in each well,[4] and also in connection with curious quasi-Josephson phenomena.[5] In high magnetic fields two-dimensional (2D) excitons exist in a substantially wider temperature region, as the exciton binding energies increase with increasing magnetic field.[6,7] In addition, 2D e–h systems in high fields H are of interest because of the existence, under some conditions, of unique exact solutions of the many-body problem and nontrivial kinetic properties.[8–10]

Attempts at experimental investigation of magnetoexciton superfluidity in CQWs[1] make it essential to study the magnetic-field dependence of the temperature of the phase transition to the superfluid state in systems of indirect excitons and to analyze the density of the superfluid component. This is the subject of this paper. It will be shown below that increasing the magnetic field at a fixed magnetoexciton density leads to a *lowering* of the Kosterlitz–Thouless transition temperature T_c on account of the increase of the exciton magnetic mass as a function of H. But it turns out that the highest possible Kosterlitz–Thouless transition temperature *increases* with increasing H (at small D) due to the rise in the maximum density of magnetoexcitons *versus* H.

To estimate the superfluid density let us start by obtaining the spectrum of collective excitations of a system of indirect magnetoexcitons.

 © 1997 American Institute of Physics

For an isolated magnetoexciton there exists a conserved quantity[11] (the exciton magnetic momentum $\mathbf{P}$) connected with the invariance of the system under a simultaneous translation of e and h and a gauge transformation (see Refs. 7 and 12). Here $\hat{\mathbf{P}}=-i\nabla_{\mathbf{R}}-(e/2)[\mathbf{H},\mathbf{r}]$, where $\mathbf{R}=\frac{1}{2}(\mathbf{r_e}+\mathbf{r_h})$ are the coordinates of the center of mass, $\mathbf{r}=\mathbf{r_e}-\mathbf{r_h}$ are the internal exciton coordinates, and the cylindrical gauge for the vector potential is used: $\mathbf{A_{e,h}}=\frac{1}{2}[\mathbf{H},\mathbf{r_{e,h}}]$ $(c=\hbar=1)$.

The dispersion relation $\varepsilon(P)$ for an isolated magnetoexciton at small $\mathbf{P}$ is a quadratic function: $\varepsilon(P)\approx(P^2/2m_H)$, where m_H is the effective magnetic mass, which depends on H and the distance D between e layers and h layers (see Ref. 7). For the magnetoexciton ground state $m_H>0$.

The quadratic dispersion relation holds for small P at arbitrary H and follows from the fact that $P=0$ is an extremal point of the dispersion relation $\varepsilon(P)$. The last statement may be proved by taking into account the regularity of the Hamiltonian $H_{\mathbf{P}}$ as function of the parameter $\mathbf{P}$ at $\mathbf{P}=0$ and also the invariance of $H_{\mathbf{P}}$ under simultaneous rotation of $\mathbf{r}$ and $\mathbf{P}$ in the plane of the CQW[12] ($H_{\mathbf{P}}$ is the effective Hamiltonian for eigenfunctions of $\mathbf{P}$).[6,7,11]

For high magnetic fields $r_H\ll a_0^*$ and at $D\sim r_H$ the quadratic dispersion relation is valid at $P\ll 1/r_H$, but for $D\gg r_H$ it holds over a wider region: $P\ll(1/r_H)(D/r_H)$ ($a_0^*=1/2\mu e^2$ is the radius of a 2D exciton at $H=0$; $\mu=m_e m_h/(m_e+m_h)$; $m_{e,h}$ are the effective masses of e and h; $r_H=(1/eH)^{1/2}$ is the magnetic length).

Using the quadratic dispersion relation for magnetoexcitons, one has at any H an expression for the magnetoexciton velocity analogous to that for the ordinary momentum, $\dot{\mathbf{R}}=\partial\varepsilon/\partial\mathbf{P}=\mathbf{P}/m_H$, and the following expression for the mass current of an isolated magnetoexciton:

$$\mathbf{J}(\mathbf{P})=\frac{M}{m_H}\mathbf{P}, \tag{1}$$

where $M=m_e+m_h$.

The indirect magnetoexcitons interact as parallel dipoles if D is larger than the mean distance between an electron and hole along the quantum wells, $D\gg\langle\mathbf{r}\rangle$. But in high fields H one has $\langle\mathbf{r}\rangle\approx Pr_H^2$ (Refs. 6 and 7). Typical values of the magnetic momentum P for dilute magnetoexciton systems obey the inequality $P\ll\sqrt{n_{ex}}$ (due to the ''large'' logarithm $\ln(n_{ex})$ — see below). So the inequality $D\gg\langle\mathbf{r}\rangle$ is valid at $D\gg\sqrt{n_{ex}}r_H^2$.

The distinction between excitons and bosons is due to exchange effects.[13] But these effects for indirect excitons with spatially separated e and h in a dilute system $n_{ex}a^2(H,D)\ll 1$ are suppressed on account of the barrier associated with the dipole–dipole repulsion of the excitons[14] (e.g., in high fields H the small parameter is

$$\exp[-(2m_H)^{5/6}e^{5/3}D^{2/3}n_{ex}^{-1/12}\ln^{1/3}(1/8\pi n_{ex}m_H^2e^4D^4)];$$

$a(D,H)$ is the magnetoexciton radius along the quantum wells). Therefore exchange effects are negligible and the system under consideration can be treated by the diagram technique for a boson system.

For a dilute 2D magnetoexciton system (at $n_{ex}a^2(D,H)\ll 1$) summation of the ladder diagrams is adequate. But in contrast with a 2D system without a magnetic field,[15] some problems arise due to nonseparation of the relative motion of e and h and the exciton center-of-mass motion.[6,7,11] So the Green functions depend on both the external coordinates $\mathbf{R},\mathbf{R}'$ and the internal coordinates $\mathbf{r},\mathbf{r}'$. It is convenient to treat the problem in the representation of the eigenfunctions $|nm\mathbf{P}\rangle$ of the Hamiltonian and magnetic momentum of an isolated magnetoexciton.

In high magnetic fields, when the typical interexciton interaction $D^2n_{ex}^{-3/2}\ll\hbar\omega_c$ (where $\omega_c=eH/\mu$ is the cyclotron energy, and $\mu=m_em_h/(m_e+m_h)$), one can ignore transitions between Landau levels and consider only the states on the lowest Landau level $m=n=0$. Since r has a typical value of r_H and $P\ll 1/r_H$, the equation for the vertex Γ in the ladder approximation for a dilute magnetoexciton system ($n_{ex}a^2(H,D)\ll 1$) in the $n,m,\mathbf{P}$ representation turns out to be analogous to that for a 2D boson system without a magnetic field, but with the magnetoexciton magnetic mass m_H (which depends on H and D) instead of the exciton mass ($m=m_e+m_h$):

$$\Gamma(p,q;L)=U_F(\mathbf{p}-\mathbf{q})+\int\frac{d\mathbf{l}}{(2\pi)^2}\frac{U_F(\mathbf{p}-\mathbf{l})\Gamma(l,q;L)}{\kappa^2/m_H+\Omega-L^2/4m_H-l^2/m_H+i\delta},$$

$$\mu=\kappa^2/2m_H=n_{ex}\Gamma=n_{ex}\Gamma(0,0,0). \tag{2}$$

Here μ is the chemical potential of the system (L is the sum and $2p$ the difference of the initial magnetic momenta of a pair of excitons, and $2q$ is the difference of the final magnetic momenta), and $U_F(\mathbf{P})$ is the Fourier transform of the potential energy $U(\mathbf{R_1}-\mathbf{R_2})=e^2D^2/|\mathbf{R_1}-\mathbf{R_2}|^3$.

At small magnetic momenta P the spectrum of collective excitations is $E(P)=c_s(H,D)P$, with the sound velocity $c_s=\sqrt{\mu/m_H}$.

A simple (analytical) solution for the chemical potential $\mu=\mu(H,D)$ can be obtained from Eq. (2), e.g., at $r_H\ll D\ll(r_H^4/n_{ex}^{1/2})^{1/5}$:

$$\mu=\kappa^2/2m_H=8\pi n_{ex}/2m_H\ln(1/8\pi n_{ex}m_H^2e^4D^4).$$

So at fixed n_{ex} and in high magnetic fields the sound velocity in the magnetoexciton system (due to $m_H=m_H(H,D)$) falls off approximately as $H^{-1/2}$ at $D\ll r_H$ and as H^{-2} at $D\gg r_H$.

The temperature T_c of the Kosterlitz–Thouless transition[16] to the superfluid state in a 2D magnetoexciton system is determined by the equation $T_c=0.5\pi\hbar^2n_s(T_c)/k_Bm_H$, where $n_s(T)$ is the superfluid density of the magnetoexciton system as a function of the temperature T, magnetic field H, and interlayer distance D, and k_B is Boltzmann's constant.

The function $n_s(T)$ can be found from the relation $n_s=n_{ex}-n_n$ (n_{ex} is the total density, n_n is the normal-component density). We determine the normal-component density by the usual procedure (see, e.g., Ref. 17). Suppose that the magnetoexciton system moves with a velocity u. At $T\neq 0$ dissipating quasiparticles will appear in this system. Since their density is small at low T, one can assume that the gas of quasiparticles is an ideal Bose gas.

To calculate the superfluid-component density we start by finding the total current of quasiparticles in a frame in which the superfluid component is at rest. Using Eq. (1), we can see that the total current of the system is proportional to the total momentum, with a coefficient that depends on n_n. As a result, we have for the superfluid density

$$n_s = n_{ex} - n_n = n_{ex} - \frac{3\zeta(3)}{2\pi}\frac{T^3}{c_s^4 m_H}. \tag{3}$$

Substituting the superfluid-component density n_s from Eq. (3) into the equation above for the Kosterlitz–Thouless temperature, we obtain:

$$T_c = \left[\left(1+\sqrt{\frac{16}{(6\cdot 0.45)^3\pi^4}\left(\frac{m_H T_c^0}{n_{ex}}\right)^3+1}\right)^{1/3} + \left(1-\sqrt{\frac{16}{(6\cdot 0.45)^3\pi^4}\left(\frac{m_H T_c^0}{n_{ex}}\right)^3+1}\right)^{1/3}\right]\frac{T_c^0}{(4\pi)^{1/3}}. \tag{4}$$

Here T_c^0 is an auxiliary quantity equal to the temperature T_c^0 at which the superfluid density vanishes in the mean field approximation, i.e., $n_s(T_c^0)=0$:

$$T_c^0 = \left(\frac{2\pi n_{ex} c_s^4 m_H}{3\zeta(3)}\right)^{1/3}. \tag{5}$$

In high magnetic fields the Kosterlitz–Thouless temperature is

$$T_c \approx \frac{T_c^0}{(4\pi)^{1/3}} \approx \left(\frac{32}{3\zeta(3)\ln^2(1/8\pi n_{ex} m_H^2 D^4)}\right)^{1/3}\frac{\pi n_{ex}}{m_H}. \tag{6}$$

In high fields H at small $\mathbf{P}$ the effective magnetic mass of an exciton on the lowest Landau level ($n=0$) and with quantum number $m=0$ is given by $m_H = 2^{3/2}/e^2 r_H\sqrt{\pi}$ at $D \ll r_H$ and by $m_H \approx D^3/e^2 r_H^4$ at $D \gg r_H$. At large D, i.e., for $D \gg a_0^*$ in weak fields ($r_H \gg a_0^*$) or for $D \gg r_H$ in high fields ($r_H \ll a_0^*$), one has $m_H = M + H^2 D^3/c^2$ (Refs. 7 and 12.

According to Eqs. (4) and (5) the temperature of the onset of superfluidity due to the Kosterlitz–Thouless transition at a fixed magnetoexciton density decreases as a function of magnetic field due to the increase in m_H as a function of H and D, while T_c decreases as $H^{-1/2}$ at $D \ll r_H$ or as H^{-2} at $D \gg r_H$, and n_s is a slowly decreasing function of D. The dependence of T_c on H is shown in Fig. 1.

From Eqs. (4) and (5) one can see that the Kosterlitz–Thouless temperature of a dilute magnetoexciton system is proportional to the magnetoexciton density n_{ex}. At high magnetic fields the symmetry $\nu \to 1-\nu$, $e \leftrightarrow h$ obtains at the Landau level. Thus unoccupied states on Landau levels for spatially separated electrons and holes can bind to ''antiexcitons,'' and superfluidity of antiexcitons may also take place at $1-\nu \ll 1$. The Kosterlitz–Thouless temperature for superfluidity of antiexcitons as a function of H and D is symmetrical to that for excitons. The top Kosterlitz–Thouless temperature at high magnetic fields corresponds to the ''maximum'' density $n_{\max}$ of magnetoexcitons at the Landau level $n_{\max} = \nu_{\max} 1/4\pi r_H^2 \sim H$, where $\nu_{\max}(D)$ is the maximum filling of the Lan-

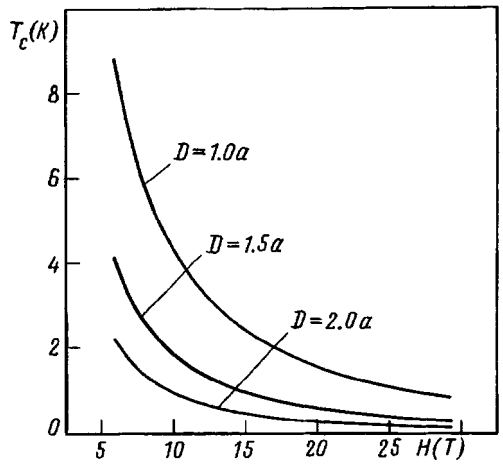

FIG. 1. The Kosterlitz–Thouless transition temperature T_c as a function of the magnetic field H for different interwell separations D (for GaAs structures).

dau level for magnetoexcitons (for antiexcitons the corresponding critical value is $1-\nu_{\max}(D)$), which obeys $\nu_{\max}(D)\leqslant 1/2$ (it is also possible to have an excitonic phase of the BCS type, originating from e–h pairing of composite fermions at $\nu=1/2$; Ref. 12). The excitonic phase is stable at $D<D_{\rm cr}(H)$ when the magnetoexciton energy $E_{\rm exc}(D,H)$ (calculated in Ref. 7) is larger than the sum of the activation energies $E_L=ke^2/\epsilon r_H$ for incompressible Laughlin fluids of electrons or holes; $k=0.06$ for $\nu=\frac{1}{3}$, etc.[18] (cf. Ref. 9). Since $k\ll 1$, the critical value $D_{\rm cr}\gg r_H$. In this case one has

$$E_{\rm exc}=\frac{e^2}{\epsilon D}\left(1-\frac{r_H^2}{D^2}\right)$$

for a magnetoexciton with quantum numbers $n=m=0$. As a result we have $D_{\rm cr}=r_H(1/2k-2k)$. This estimate is correct for small ν when the interaction between magnetoexcitons is small in comparison with the magnetoexciton energy $E_{\rm exc}$. For greater ν it gives an upper bound on $D_{\rm cr}$. The coefficient k in the activation energy E_L may be represented as $k=k_0\sqrt{\nu}$. So from the relation between $D_{\rm cr}$ and r_H one has

$$\nu_{\rm cr}=\frac{1}{k_0^2}\frac{r_H^2}{D^2}\left(1-\frac{r_H^2}{8D^2}\right).$$

Hence, the maximum Kosterlitz–Thouless temperature at which superfluidity appears in the system is $T_c^{\max}\sim n^{\max}(H,D)/m_H\sim\sqrt{H}$ at $D\leqslant r_H$ or $T_c^{\max}\sim H^{-1}$ at $D\gg r_H$ in high magnetic fields. It is of interest to compare this fact with experimental results on magnetoexciton systems. Note that if, at a given density of e and h and a given magnetic field H, several Landau levels are filled (but the high-field limit $r_H\ll a_0^*$ obtains), the superfluid phase can exist for magnetoexcitons on the highest nonfilled Landau level.

We have shown that at fixed exciton density n_{ex} the Kosterlitz–Thouless temperature T_c for the onset of superfluidity of magnetoexcitons decreases as a function of magnetic field as $H^{-1/2}$ (at $D \sim r_H$). But the maximum T_c (corresponding to the maximum magnetoexciton densities) *increases* with H in high magnetic fields as $T_c^{\max}(H,D) \sim \sqrt{H}$ (at $D \sim r_H$). This fact needs to be compared in detail with the results of experimental studies of the collective properties of magnetoexcitons. The excitonic phase is more stable than the Laughlin states of electrons and holes (with negligible $e-h$ correlations) at a given Landau filling ν if $D < D_{\rm cr} = r_H(1/2k - 2k)$, where k is the coefficient in the Laughlin activation energy. Below the Kosterlitz–Thouless temperature one may observe the appearance of persistent currents in separate quantum wells. The interlayer resistance due to the drag of electrons and holes can also be a sensitive indicator of the transition to the superfluid and other phases of the $e-h$ system.[12]

Yu. E. L. is grateful to participants of the ''Nanostructures '97'' for interesting discussions of the results. This work is supported by the Russian Fund for Fundamental Research, Programs ''Physics of Solid Nanostructures'' and ''Surface atomic structure.'' O. L. B. was supported by the Program ''Soros PhD students.''

[a)]e-mail: lozovik@isan.troitsk.ru

[1] L. V. Butov, A. Zrenner, G. Abstreiter, G. Bohm, and G. Weimann, Phys. Rev. Lett. **73**, 304 (1994).
[2] U. Sivan, P. M. Solomon, and H. Strikman, Phys. Rev. Lett. **68**, 1196 (1992).
[3] M. Bayer, V. B. Timofeev, F. Faller, T. Gutbrod, and A. Forchel, Phys. Rev. B **54**, 8799 (1996).
[4] Yu. E. Lozovik and V. I. Yudson, JETP Lett. **22**, 26 (1975); Zh. Éksp. Teor. Fiz. **71**, 738 (1976) [Sov. Phys. JETP **44**, 389 (1976)]; Solid State Commun. **18**, 628 (1976); Solid State Commun. **21**, 211 (1977); Yu. E. Lozovik, *Proceedings of the First All-Union Conference on Dielectric Electronics* [in Russian], Tashkent, 1973.
[5] A. V. Klyuchnik and Yu. E. Lozovik, Zh. Éksp. Teor. Fiz., **76**, 670 (1979) [Sov. Phys. JETP **49**, 335 (1979)]; J. Low Temp. Phys. **38**, 761 (1980); J. Phys. C **11**, L483, (1978); I. O. Kulik and S. I. Shevchenko, Solid State Commun. **21**, 409 (1977); Yu. E. Lozovik and V. I. Yudson, Solid State Commun. **22**, 117 (1977); Yu. E. Lozovik and A. V. Poushnov, Phys. Lett. A **228**, 399 (1997).
[6] I. V. Lerner, Yu. E. Lozovik, Zh. Éksp. Teor. Fiz. **78**, 1167 (1980) [Sov. Phys. JETP **51**, 588 (1980)].
[7] Yu. E. Lozovik and A. M. Ruvinsky, Phys. Lett. A **227**, 271, (1997); Zh. Éksp. Teor. Fiz. (1997) (in press).
[8] I. V. Lerner and Yu. E. Lozovik, Zh. Éksp. Teor. Fiz. **80**, 1488 (1981) [Sov. Phys. JETP **53**, 763 (1981)]; A. B. Dzyubenko and Yu. E. Lozovik, Fiz. Tverd. Tela (Leningrad) **25**, 1519 (1983) [Sov. Phys. Solid State **25**, 874 (1983)]; Fiz. Tverd. Tela (Leningrad) **26**, 1540 (1984) [Sov. Phys. Solid State **26**, 938 (1984)]; J. Phys. A **24**, 415 (1991); D. Paquet, T. M. Rice, and K. Ueda, Phys. Rev. B **32**, 5208 (1985); A. H. MacDonald and E. H. Rezayi, Phys. Rev. B **42**, 3224 (1990); D. S. Chemla, J. B. Stark and W. H. Knox, in *Ultrafast Phenomena VIII*, edited by J.-L. Martin *et al.*, Springer-Verlag, 1993, p. 21; G. Finkelstein, H. Strikman, and I. Bar-Joseph (in press).
[9] D. Yoshioka and A. H. MacDonald, J. Phys. Soc. Jpn. **59**, 4211 (1990).
[10] S. M. Dikman and S. V. Iordanskii, JETP **63**, 50 (1996).
[11] L. P. Gorkov and I. E. Dzyaloshinsky, Zh. Éksp. Teor. Fiz. **53**, 717 (1967) [Sov. Phys. JETP **26**, 449 (1968)].
[12] Yu. E. Lozovik, *Report on Adriatico Conference on Low-Dimensional Electron Systems*, Trieste, 1996; Physica E (in press).
[13] L. V. Keldysh and A. N. Kozlov, Zh. Éksp. Teor. Fiz. **54**, 978 (1968) [Sov. Phys. JETP **27**, 521 (1968)].
[14] Yu. E. Lozovik and O. L. Berman, Zh. Éksp. Teor. Fiz. **111**, 1879, (1997) [JETP **84**, 1027 (1997)].
[15] Yu. E. Lozovik, and V. I. Yudson, Physica A **93**, 493 (1978).
[16] J. M. Kosterlitz and D. J. Thouless, J. Phys. C **6**, 1181 (1973); D. R. Nelson and J. M. Kosterlitz, Phys. Rev. Lett. **39**, 1201 (1977); Zh. Éksp. Teor. **47**, 1427 (1964) [Sov. Phys. JETP **20**, 961 (1964)].

[17] A. A. Abrikosov, L. P. Gor'kov, and I. E. Dzyaloshinskiĭ, *Methods of Quantum Field Theory in Statistical Physics*, Prentice-Hall, Englewood Cliffs, N. J. (1963) [Russ. original, Fizmatgiz, Moscow (1962)].
[18] R. E. Prange and S. M. Girvin (Eds.), *The Quantum Hall Effect*, Springer-Verlag, New York (1987).

Published in English in the original Russian journal. Edited by Steve Torstveit.

Observation of ferrobielastic switching in langasite crystals under a uniaxial static pressure

G. D. Mansfel'd[a)]
Institute of Radio Engineering and Electronics, Russian Academy of Sciences, 103907 Moscow, Russia

J. J. Boy
Ecole Nationale Superieure de Mecanique et des Microtechniques, Besancon, France

(Submitted 23 July 1997)
Pis'ma Zh. Éksp. Teor. Fiz. **66**, No. 5, 338–340 (10 September 1997)

Ferrobielastic switching is observed by measuring the change in the frequency of a compound acoustic cavity made from a langasite ($La_3Ga_5SiO_{14}$) single crystal, under uniaxial pressure. The effect is detected from the jump in the cavity frequency at the point of switching. In quartz the measured value of the pressure at the point of switching is found to be much higher, 740 MPa. © *1997 American Institute of Physics.* [S0021-3640(97)01117-1]

PACS numbers: 62.20.Dc, 61.66.−f

According to Ref. 1, ferrobielastic switching stimulated by a uniaxial static pressure in certain specially chosen directions can occur in class 32 crystals, which are ferrobielastics. This transition of a sample as a whole into a twinned state has been observed repeatedly in quartz single crystals by optical[2] and, recently, acoustic[3] methods. The switching effect has also been observed in gallium orthophosphate crystals.[4] This letter reports the observation of switching in a langasite ($La_3Ga_5SiO_{14}$) single crystal.

The choice of the direction of application of the pressure giving rise to the ferroelastic switching is based on energy considerations: The energy of the crystal lattice after the transition to a twinned state should be less than in the initial phase. In accordance with Ref. 5, the change ΔG in the Gibbs function at a transition into the twinned phase should be negative for directions of application of the pressure which are favorable for the appearance of a switching effect. It can be shown that for X-cut plates of class 32 crystals

$$\Delta G = 2S_{1123}P^2F(\theta), \tag{1}$$

where the function $F(\theta)$ depends on the angle between the Z axis of the crystal and the direction Z' along which a mechanical stress P is applied:

$$F(\theta) = -2\sin 2\theta \sin^2\theta. \tag{2}$$

Positive values of $F(\theta)$ are shown in polar coordinates in Fig. 1a. Since the elastic compliance S_{1123} is negative for the langasite crystal, negative values of ΔG are possible only near angles of $+135°$ and $-45°$.

In the present work we employed an acoustic method, which we developed earlier and applied in Ref. 3, to study the effect of uniaxial pressure on the elastic properties of

 © 1997 American Institute of Physics

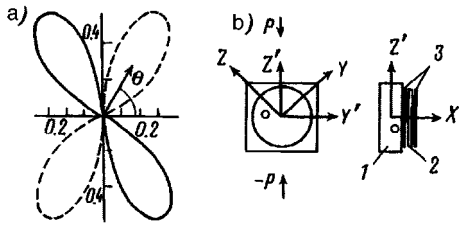

FIG. 1. a — Favorable angles of pressure application to produce a transition of a X-cut specimen to a twinned phase, solid curves — langasite, dashed curves — quartz. b — Experimental configuration for observing ferrobielastic switching in langasite: *1* — langasite single crystal — X-cut plate, *2* — ZnO film, *3* — electrodes.

a crystal and to observe the ferrobielastic switching effect. The experimental specimens of langasite were X-cut plates with optically polished, parallel faces (the nonparallelism was $<8''$) and were used as parts of compound acoustic cavities. Zinc oxide piezoelectric transducers were applied to one of these surfaces. A uniaxial pressure, in accordance with Eq. (1) and Fig. 1a, was applied at an angle of $-45°$ in the direction of the Z axis, as shown in Fig. 1b. All end faces of the samples were also optically polished and were strictly perpendicular with respect to the faces. The compound cavity is a multifrequency cavity; resonance always occurs when an integral number of half waves fits within the thickness of the structure. For a 3 mm thick langasite plate and a 8 μm thick ZnO film, a grid of resonance frequencies was observed from 100 to 600 MHz. The change in each resonance frequency under uniaxial pressure is uniquely related with the change in the so-called ''natural'' velocity of sound,[6] which should change abruptly upon ferrobielastic switching.[4]

In our experiment the resonance peaks were detected with a NR4396 microwave circuit analyzer simultaneously at two neighboring resonance frequencies — 419.824 MHz and 420.761 MHz. The average data from the measurements of the relative pressure-induced changes in frequency are presented in Fig. 2. The changes occurring in the resonance frequencies under uniaxial pressure were negative and monotonic functions

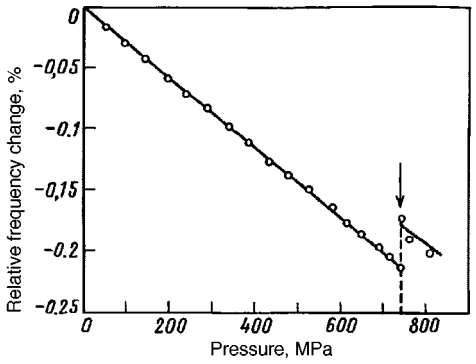

FIG. 2. Relative change in the frequency of a compound acoustic cavity versus applied pressure. The arrow marks the point of switching.

of the pressure. One can see that this character of the pressure dependence of the frequency change remains up to approximately 740 MPa. At a pressure of 740 MPa the measured resonance frequencies increase abruptly. As the pressure increases further, the resonance frequencies once again decrease monotonically (right up to pressures corresponding to onset of fracture of the sample).

It is interesting to compare these data with the results of investigations of a similar phenomenon in quartz.[4] For a X-cut plate and a pressure of the order of 500 MPa the resonance frequency undergoes a jump due to ferrobielastic switching, when in most of the sample (or in the entire sample) the crystal lattice passes into the twinned phase. Apparently a switching effect occurs in our case also. However, the sign of the frequency change in the case of quartz is different, and the initial change in frequency with pressure is positive. Furthermore, according to Eq. (1), to observe switching in quartz the mechanical stress must be applied at an angle of 45° with respect to the Z axis, as follows from Fig. 1a, where the dashed line shows the computational results for quartz. These differences in the direction of application of pressure and the character of the pressure-induced change in frequency are in accord with the theory of Ref. 6, specifically, they are due to the fact that the signs of the coefficient S_{1123} in quartz and langasite are different. The frequency change observed in langasite at the point of switching is itself much smaller. It should be noted that switching is much more difficult to observe in langasite than in quartz. The langasite available to us is more brittle than quartz, and the switching occurs at high pressures. For this reason, most specimens fractured mechanically even before the onset of switching.

In summary, in the present study we have obtained experimental data attesting to the fact that ferrobielastic switching can be stimulated in langasite single crystals by uniaxial pressure.

We are grateful of Academician Yu. V. Gulyaev and Professor R. Besson for their attention to this work.

This work was supported in part by Grant No. 96-02-17480 from the Russian Fund for Fundamental Research.

[a)]e-mail: mans@mail.cplire.ru

---

[1] K. Aizu, J. Phys. Soc. Jpn. **34**, 121 (1973).
[2] R. E. Newnham and L. E. Cross, Ferroelectrics **10**, 269 (1976).
[3] G. D. Mansfel'd, R. Besson, and P. Guzzo, Fiz. Tverd. Tela (St. Petersburg) **39**, 290 (1997) [Phys. Solid State **39**, 254 (1997)].
[4] G. D. Mansfeld, J. J. Boy, P. Guzzo, and O. V. Zvereva, Ultrasonics, Ferroelectrics, and Frequency Control **44**, 722 (1997).
[5] W. P. Mason, *Crystal Physics of Interaction Processes*, Academic Press, New York, 1966.
[6] V. E. Lyamov, *Polarization Effects and Anisotropy of Wave Interaction in Crystals* [in Russian], Moscow State University Press, New York, 1983.

Translated by M. E. Alferieff

Influence of magnetic impurities on the heat capacity of nuclear spins

A. M. Dyugaev and Yu. N. Ovchinnikov
Max-Planck-Institute for Physics of Complex Systems, D-01187 Dresden, Germany; L. D. Landau Institute of Theoretical Physics, Russian Academy of Sciences, 117940 Moscow, Russia

P. Fulde
Max-Planck-Institute for Physics of Complex Systems, D-01187 Dresden, Germany

(Submitted 3 July 1997; resubmitted 28 July 1997)
Pis'ma Zh. Éksp. Teor. Fiz. **66**, No. 5, 341–345 (10 September 1997)

It is found that over a wide range of temperatures and magnetic fields even a small concentration of magnetic impurities in a sample leads to a T^{-1} temperature dependence of the nuclear heat capacity. This effect is due to nuclear spin polarization by the magnetic impurities. The parameter that controls the theory turns out not to be the impurity concentration $n_{\rm imp}$ but instead the quantity $n_{\rm imp}\mu_e/\mu_n$, where μ_e and μ_n are the magnetic moments of an electron and a nucleus, respectively. The ratio of μ_e and μ_n is of order of 10^3. © *1997 American Institute of Physics.* [S0021-3640(97)01217-6]

PACS numbers: 65.40.+g, 75.40.Cx, 75.30.Hx, 75.25.+z

During the last years nuclear spin ordering has been observed in a considerable number of solids (see Ref. 1 for a review). This is due to impressive progress in cooling nuclear spin systems — temperatures as low as $T\sim 10^{-9}$ K have been attained. The ordering temperatures of the nuclear spin systems are as small as 58 nK for Cu and 0.56 nK for Ag (Refs. 2 and 3). The Curie temperature for $AuIn_2$ is 35 μK. In this system an interplay between nuclear magnetism and superconductivity has been observed.[4]

At such low temperatures all the degrees of freedom of the solid except for the nuclear spins are frozen. The temperature dependence of the resistivity is therefore due to conduction electron–nuclear spin interactions.[5] In Ref. 6 it was demonstrated that the nuclear spin susceptibility depends on the impurity concentration and that the heat capacity in low external magnetic fields does not obey a Schottky law. Instead, it is closer to a $1/T$ behavior. This seems to hold for a number of compounds.[6]

The aim of this paper is to show that magnetic impurities can give the main contribution to the heat capacity at low temperatures even if their concentration is very low. In the following we want to give a simple physical argument to justify that statement before we present a more quantitative theory.

Consider for simplicity a system in which the magnetic interaction between nuclear spins as well as between an impurity and the nuclear spins is of the dipolar form

 © 1997 American Institute of Physics

$$V_{1,2}=\frac{\boldsymbol{\mu}_1\cdot\boldsymbol{\mu}_2 r^2-3(\boldsymbol{\mu}_1\mathbf{r})(\boldsymbol{\mu}_2\mathbf{r})}{r^5}. \tag{1}$$

Here $\boldsymbol{\mu}_{1,2}=\mu_{1,2}\mathbf{S}_{1,2}$, where $\boldsymbol{\mu}_{1,2}$ and $\mathbf{S}_{1,2}$ are the magnetic moment and spin operators of two particles 1,2 separated by a distance $\mathbf{r}$. The temperature of the nuclear spin ordering is accordingly of order $T_{cn}\simeq\mu_n^2/a^3$, where a is the distance between neighboring nuclei. Note that the density of sites, i.e., nuclei, is $n_n\simeq a^{-3}$.

The crucial point is that the interaction between the impurity spin and a nuclear spin is much larger than the one between nuclear spins since the magnetic moment $\mu_{\rm imp}$ is much larger than the one of the nuclei μ_n, i.e., $\mu_{\rm imp}/\mu_n\simeq 10^3$. Therefore, around each impurity there is a volume of size $a^3\mu_{\rm imp}/\mu_n$ in which the impurity–nuclei interaction exceeds the one among the nuclei. Consequently, if the impurity concentration $n_{\rm imp}$ exceeds $\mu_n/\mu_{\rm imp}$ the different regions with dominating impurity–nuclei interaction overlap and influence each other. We shall consider here the clean limit, i.e., concentrations $c_{\rm imp}<\mu_n/\mu_{\rm imp}$. In that case it suffices to consider a single impurity. The calculated contribution to the heat capacity then has merely to be multiplied by $n_{\rm imp}$. Furthermore, we shall assume that the impurity spin is kept fixed by an applied magnetic field H_0, i.e., $\mu_{\rm imp}H_0\gg T_e$, where T_e denotes the temperature of the electron system. For $T_e\simeq 10^{-4}$ K this requires a magnetic field of order 1 G. In $AuIn_2$ (Ref. 4) the electron–nuclei interaction is sufficiently strong that the nuclear temperature T and the electron temperature T_e coincide. The effective field $\mathbf{H}$ acting on a nucleus consists then of the external field $\mathbf{H}_0$ and the field set up by the impurity, i.e.,

$$\mathbf{H}=\mathbf{H}_0+\mathbf{H}_1, \tag{2}$$

$$\mathbf{H}_1(\mathbf{r}_n)=\frac{3(\boldsymbol{\mu}_{\rm imp}\cdot\mathbf{r})\mathbf{r}/r^2-\boldsymbol{\mu}_{\rm imp}}{r^3}. \tag{3}$$

Here $\mathbf{r}=\mathbf{r}_n-\mathbf{r}_{\rm imp}$ is the distance between nucleus and impurity. The interaction Hamiltonian is $H_{\rm int}=-(\boldsymbol{\mu}_n\cdot\mathbf{H})$. The partition function Z_n of a nuclear spin is

$$Z_n=\frac{\sin h(\chi(2S+1))}{\sin h(\chi)},\quad \chi=\frac{\mu_n H(r_n)}{2T}, \tag{4}$$

where S is the spin of the nucleus.

The specific heat contribution follows from $C_n=-T(\partial^2 F_n/\partial T^2)$ where $F_n=-T\ln Z_n$. Here we have set Boltzmann's constant $k_B=1$. This gives

$$C_n=\chi^2\left(\frac{1}{\sin h^2\chi}-\frac{(2S+1)^2}{\sin h^2(\chi(2S+1))}\right). \tag{5}$$

The average value of the specific heat $\overline{C_n}$ is a sum over $\mathbf{r}_n$ multiplied by the impurity concentration. Furthermore, it is advantageous to subtract the specific heat $C_n^{(0)}$ of the pure material

$$\overline{C_n}-C_n^{(0)}=n_{\rm imp}\sum_{\mathbf{r}_n}\left(C_n(H(\mathbf{r}_n))-C_n^{(0}(H_0)\right). \tag{6}$$

When $C_n^{(0)}$ is expanded in powers of $\mu_n H_0/T$, we obtain to leading order in the external field

$$C_n^0 = n_n \left(\frac{\mu_n H_0}{T} \right)^2 \frac{S(S+1)}{3}, \tag{7}$$

where n_n is the concentration of nuclei.

In order that a high-temperature expansion of this type does also hold for the nuclei close to the impurity the condition $T \gg \mu_{\rm imp}\mu_n/a^3$ must be fulfilled. The square of the effective field is

$$H^2(\mathbf{r}) = H_0^2 + \frac{3(\boldsymbol{\mu}_{\rm imp}\cdot\mathbf{r})^2 + \boldsymbol{\mu}_{\rm imp}^2 r^2}{r^8} + \frac{2}{r^5}(3(\mathbf{r}\cdot\mathbf{H}_0)(\boldsymbol{\mu}_{\rm imp}\cdot\mathbf{r}) - (\boldsymbol{\mu}_{\rm imp}\cdot\mathbf{H}_0)r^2). \tag{8}$$

From Eqs. (6)–(8) the following expression is obtained for the specific heat in the high-temperature regime,

$$\overline{C_n} - C_n^{(0)} = n_{\rm imp} \frac{\mu_n^2}{T^2} \frac{S(S+1)}{3} \sum_{\mathbf{r}_n} \frac{3(\boldsymbol{\mu}_{\rm imp}\cdot\mathbf{r})^2 + \boldsymbol{\mu}_{\rm imp}^2 r^2}{r^8}. \tag{9}$$

The sum converges very rapidly. For fields less than

$$H_{00} = \frac{\mu_{\rm imp}}{a^3} (n_{\rm imp})^{1/2} \tag{10}$$

the main contribution to the specific heat comes from nuclei close to the magnetic impurity.

Consider next the range in T and H_0 defined by the inequalities

$$\mu H_0 \ll T, \tag{11}$$

$$\frac{\mu_n \mu_{\rm imp}}{a^3} \gg T \gg T_{cn} = \frac{\mu_n^2}{a^3}. \tag{12}$$

In that region the main contribution to the specific heat comes from nuclei at large distance from the impurity, i.e., $r \gg a$. For them one does not need to take into account the spin–spin interaction between nuclei (see Eq. (11)), and one can also convert the summation over $\mathbf{r}_n$ into an integral of the form $n_n \int d^3\mathbf{r} \ldots$. From Eq. (6) in this case we obtain

$$\overline{C_n} - C_n^{(0)} = n_{\rm imp} \frac{4\pi n_n \mu_{\rm imp}\mu_n S}{3T} \left(1 + \frac{1}{2\cdot 3^{1/2}} \ln(2+3^{1/2}) \right). \tag{13}$$

By comparing Eqs. (7) and (13) one notices that for fields

$$H_0 < \left(\frac{\mu_{\rm imp} T n_{\rm imp}}{\mu_n} \right)^{1/2} \tag{14}$$

the main contribution to the specific heat of the nuclear spin system comes from the interaction with magnetic impurities. The temperature dependence of this contribution is

T^{-1} rather then T^{-2}. A dependence of this kind has indeed been observed[6] for $AuIn_2$. We suggest that it is due to the impurity effect discussed here. However, for a quantitative comparison one must take into account that the main contribution to the specific heat comes from the In nuclei which have spin $S=9/2$. The electric field gradient due to the impurity leads to a quadrupolar splitting of the spin levels. Being proportional to r^{-3} the electric field gradient leads also to a T^{-1} temperature dependence of the specific heat. For metals such as Ag, with nuclear spin $S=1/2$ (Ref. 2), a quadrupole splitting of course does not occur.

We want to point out that a T^{-1} contribution results also from the nuclear spin–impurity spin RKKY-type of interaction

$$V_R=-\frac{\boldsymbol{\mu}_n\cdot\boldsymbol{\mu}_{\rm imp}}{r^3}\kappa f(2p_F r);\quad f(x)=\cos(x)-\frac{\sin(x)}{x}. \tag{15}$$

Here κ is a parameter proportional to the spin–spin Fermi contact interaction.[7] This interaction is proportional to the charge of the nucleus.[8] For a light nucleus $\kappa\ll 1$, while for a heavy one $\kappa\gg 1$. Therefore in a metal the spin–spin interactions between the nucleus of an impurity and the nuclei of the host contain two contributions given by Eqs. (1) and (15). As pointed out before, we shall consider here only the universal dipole–dipole interaction (1), which is the same in metals and insulators.

Next we consider the case of a strong magnetic field $\mu_n H_0\gg T$. In this regime the heat capacity is exponentially small (see Eq. (5)). The main contribution to it originates from nuclei for which the effective field $H(\mathbf{r})$ is of order T/μ_n. From Eq. (8) we find

$$H^2=\left(\frac{\mu_{\rm imp}}{r^3}-H_0\right)^2+\frac{3\mu_{\rm imp}}{r^3}\left(\frac{\mu_{\rm imp}}{r^3}+2H_0\right)\frac{(\mathbf{H}_0\cdot\mathbf{r})}{H_0 r}. \tag{16}$$

One notices that $H(\mathbf{r})$ is zero along a circle of radius $r_0=(\mu_{\rm imp}/H_0)^{1/3}$ around the impurity in a plane perpendicular to $\mathbf{H}_0$. The nuclei contributing most to the specific heat are within a torus whose axis is given by the circle of radius r_0. If $\delta r=r-r_0, z=(\mathbf{H}_0\cdot\mathbf{r})/H_0 r$ then $(z^2+(\delta r/r_0)^2)^{1/2}$ denotes the ''distance'' from this axis, and we find for the effective field

$$H^2=9H_0^2(z^2+(\delta r/r_0)^2). \tag{17}$$

With the help of Eqs. (5) and (17) we obtain

$$\overline{C_n}-C_n^{(0)}=\frac{16\pi^2T^2\mu_{\rm imp}n_n n_{\rm imp}}{9H_0^3\mu_n^2}\left(1-\frac{1}{(2S+1)^2}\right)I_1, \tag{18}$$

where

$$I_1=\int_0^\infty \frac{dx\ x^3}{\sin\ h^2 x}=\frac{3}{2}\zeta(3), \tag{19}$$

and $\zeta(x)$ is the Riemann zeta function.

Replacing the sum over $\mathbf{r}_n$ by an integral $n_n\int d^3\mathbf{r}$ is justified only if many nuclei lie within a radius $\delta r/r_0\simeq z\simeq T/\mu_n H_0$ of the torus. This restriction leads to the requirement

$$\frac{T^2\mu_{\rm imp}\mu_n n_n}{(\mu_n H_0)^3}\gg 1 \tag{20}$$

in order for Eq. (18) to hold. Together with the starting assumption ($\mu_n H_0 \gg T$) this implies the condition

$$T\ll\mu_n H_0\ll(T^2\mu_{\rm imp}\mu_n n_n)^{1/3} \tag{21}$$

on the applied field H_0.

Next we deal with the case when the impurity spins are frozen in a glassy state. Then Eqs. (5) and (6) must be averaged over all directions of the external field $\mathbf{H}_0$. As stated before, the main contribution to the nuclear heat capacity comes from nuclei in an effective field $H\simeq T/\mu_n$. As a result we obtain

$$\overline{C_n}-C_n^{(0)}=\frac{32\pi T^3\mu_{\rm imp}n_n n_{\rm imp}}{3H_0^4\mu_n^3}\left(1+\frac{1}{2\sqrt{3}}\ \ln(2+\sqrt{3})\right)\left(1-\frac{1}{(2S+1)^3}\right)I_2, \tag{22}$$

where

$$I_2=\int_0^\infty \frac{dx\ x^4}{\sin\ h^2 x}=\frac{\pi^4}{30}. \tag{23}$$

The restriction (21) for H_0 is changed accordingly to

$$T\ll\mu_n H_0\ll(T^3\mu_{\rm imp}\mu_n n_n)^{1/4}. \tag{24}$$

The required range of strong magnetic fields has not yet been studied experimentally, although in Ref. 6 the region $\mu_n H_0\leqslant T$ was investigated. For metals in the clean limit the nuclear spin contribution to the heat capacity has a maximum near $\mu_n H_0\sim T$, the position of which is only weakly dependent on the magnetic impurity concentration $n_{\rm imp}$, provided $n_{\rm imp}\mu_{\rm imp}/\mu_n\ll n_n$. We expect that in the strong-field regime $\mu_n H_0\gg T$ the heat capacity has a power-law behavior given by Eqs. (18) and (22). For pure samples an exponential temperature dependence is obtained (see Eq. (5)).

In summary, we have shown that in a wide region of temperature and magnetic fields the main contribution to the nuclear specific heat results from their interaction with small amounts of magnetic impurities which are present in most of the systems.

Two of us (Yu. N. O. and A. M. D.) wish to acknowledge die Max-Planck-Gesellschaft zur Förderung der Wissenschaften and Max-Planck-Institut für Physik komplexer Systeme for the hospitality during the period of doing this work. The research of Yu. N. Ovchinnikov was supported by the CRDF Grant RP1-194 and by the Naval Research Lab Contract 00173-97-P-3488. The research of A. M. Dyugaev was supported by the INTAS-RFBR Grant 95-553.

[1] A. S. Oja and O. V. Lounasmaa, Rev. Mod. Phys. **69**, 1 (997).
[2] M. T. Huiku and M. T. Loponen, Phys. Rev. Lett. **49**, 1288 (1982).
[3] P. J. Hakonen, S. Yin, and O. V. Lounasmaa, Phys. Rev. Lett. **64**, 2707 (1990).
[4] S. Rehmann, T. Herrmannsdörfer, and F. Pobell, Phys. Rev. Lett. **78**, 1122 (1997).
[5] A. M. Dyugaev, I. D. Vagner, and P. Wyder, JETP Lett. **64**, 207 (1996).
[6] T. Herrmannsdörfer and F. Pobell, J. Low Temp. Phys. **100**, 253 (1995).

[7] J. Winter, *Magnetic Resonance in Metals*, Clarendon Press, Oxford, 1971.
[8] L. D. Landau and E. M. Lifshitz, *Quantum Mechanics*, Reed Educational and Professional Publishing, 1980.

Published in English in the original Russian journal. Edited by Steve Torstveit.

Observation of the amplification of spin-wave envelope solitons in ferromagnetic films by parallel magnetic pumping

B. A. Kalinikos,[a] N. G. Kovshikov, and M. P. Kostylev
St. Petersburg Electrical Engineering University, 197376 St. Petersburg, Russia

P. Kabos and C. E. Patton
Colorado State University, Fort Collins, Colorado, USA

(Submitted 31 July 1997)
Pis'ma Zh. Éksp. Teor. Fiz. **66**, No. 5, 346–350 (10 September 1997)

The propagation of envelope solitons of microwave-frequency spin waves in a spatially periodic field oriented parallel to the magnetic pump has been investigated experimentally. In a pulsed pumping regime with amplitude much greater than the threshold for parametric excitation of spin systems, amplification of spin-wave envelope solitons exceeding their natural damping was obtained. © *1997 American Institute of Physics.* [S0021-3640(97)01317-0]

PACS numbers: 42.65.Tg, 42.65.Yj, 75.70.Ak, 75.30.Ds, 75.40.Gb.

In recent years envelope solitons of both strongly (dipole-exchange) and weakly (dipole) dispersive microwave-frequency spin waves (SWs) propagating in ferromagnetic films (FFs) have been observed and investigated in a series of experiments (see, for example, Refs. 1–6 and the literature cited therein). Specifically, it has been established that magnetic dissipation greatly limits the lifetime and therefore the propagation path length of solitons. Even in the case of high-quality single-crystal yttrium iron garnet (YIG) films, which exhibit record low losses, the single-soliton path length does not exceed 1 cm (Ref. 6). To increase the lifetime of spin-wave solitons, it is necessary to find a method for compensating their natural damping.

It is known theoretically that the damping of spin waves can be compensated by three- and four-wave nonlinear interactions realized under conditions of parallel and transverse parametric pumping. Experimental investigations have shown that the intensification of linear spin waves in YIG films can be accomplished with parallel pumping.[7,8] The use of local longitudinal pumping to compensate damping of spin-wave envelope solitons was recently reported.[9] The maximum gain achieved in Ref. 9 was equal to 0.7 dB. Our objective in the present work was to study the propagation of spin-wave envelope solitons in a spatially periodic parallel magnetic pump field for the purpose of obtaining efficient amplification of solitons.

Theoretical investigations of the parametric intensification of spin-wave envelope solitons[10] show that of the possible types of spin-wave solitons in ferromagnetic films intensification is most easily accomplished in the case of the so-called backward volume spin waves (BVSWs). These waves propagate in the direction of a constant magnetic field in tangentially magnetized films and exhibit negative dispersion in the long-

wavelength region of the spectrum. As was shown earlier,[11] both theoretically and experimentally, long BVSWs possess a low parametric excitation threshold h_{th}, which makes their parametric regeneration a comparatively easy matter. Furthermore, on account of the characteristic dispersive and nonlinear properties of BVSWs, it is comparatively easy to produce envelope solitons of these waves.[3,4,6] This is the reason why in the present work the parametric amplification experiments were performed with BVSW solitons.

Specimens in the form of narrow film strips 2 mm wide (spin-wave ''waveguides'') were used for the experiments. These waveguides were cut from single-crystal YIG films with thickness $L=5.2$ μm, grown on a gadolinium–gallium garnet substrate with (111) orientation. Launching and receiving of the spin waves were accomplished with the standard construction,[1,6] using 50-μm wide short-circuited launching and receiving microstrip antennas whose length was equal to the width of the film waveguide. The distance between the antennas was equal to 6.1 mm. Two types of periodic microstrip structures were used to produce the microwave field parallel to the magnetic pump: in-phase (''grating'') and antiphase (''meander''). The grating structure has a period of 0.3 mm and consists of seven 0.1-mm wide elements. The meander structure has a period of 0.3 mm and consists of eleven 0.1-mm wide elements. Each pumping structure was placed alternately between the antennas. The distance from the input antenna to the edge of the first element of the structure was chosen to be 3 mm, which ensured the formation of a single envelope soliton when the wave packet approached the edge of the structure. (A discussion of the production of BVSW solitons can be found in Ref. 6.)

A pulsed pumping regime was used to obtain efficient amplification of the solitons. In this technique, the pump pulse was applied at the moment when the spin-wave soliton approached the edge of the pump structure. According to theory,[10] when the soliton and pump pulses are superposed in this manner, amplification can be effected in a nonstationary regime in which, even at large supercritical pumping $h/h_{\text{th}} \gg 1$, the parametric excitation of parasitic (thermal) spin waves has still not developed.

We shall now discuss the experimental data obtained using the grating microstrip structure as the pump element. In the absence of a pump field, the soliton excitation and propagation regime was similar to that described in detail in Ref. 6. The experiments were performed at the signal carrier frequency $f_s = 4669$ MHz, which was 50 MHz lower than the frequency of the homogeneous ferromagnetic resonance of the experimental film specimen. The computed value of the carrier wave vector was $k_s = 110$ rad/cm. The pump frequency f_p was varied in the region of twice the signal frequency. The best soliton amplification regime was obtained for $f_p/2 - f_s = 5$ MHz.

The experiments were performed in two stages. The power threshold P_{th} of the parametric instability of the spin system was measured at the first stage under practically stationary excitation conditions. For this, long (more than 50 μs) microwave pulses were applied to the microstrip pump structure. The threshold was fixed according to the appearance of parametrically generated BVSWs at the output antenna at frequency $f_p/2$. The amplification of linear spin-wave pulses and spin-wave solitons with simultaneous application of f_s and f_p was investigated at the second stage. In so doing, the pump power was chosen to be close to and higher than the threshold value P_{th}.

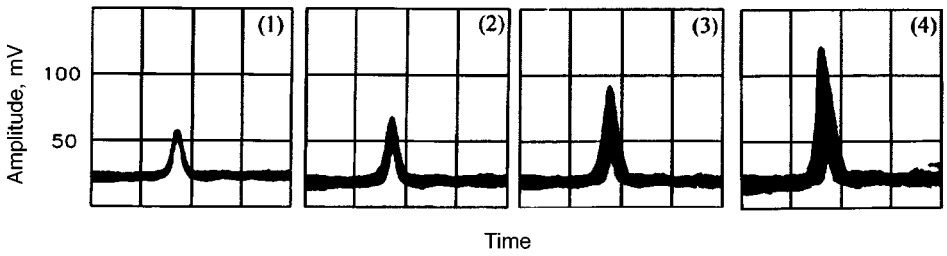

FIG. 1. Oscillograms of the envelope of a pulsed signal at the output antenna. The oscillograms were obtained for different pump powers: 1 — $P_p/P_{th}=2.5$, 2 — $P_p/P_{th}=128$, 3 — $P_p/P_{th}=155$, 4 — $P_p/P_{th}=251$.

Characteristic oscillograms illustrating the amplification of an BVSW envelope soliton are displayed in Fig. 1. The oscillograms were obtained with the following parameters: pump pulse duration — 100 ns, input signal pulse duration — 26 ns, soliton duration — 14 ns. The measured soliton delay time was equal to 237 ns, which gives a soliton velocity of 2.57×10^6 cm/s. This soliton velocity is close to the theoretically computed value of the group velocity of the carrier wave, equal to 2.4×10^6 cm/s.

It is clear from the oscillograms that the amplitude of the soliton increases with the pump power P_p, i.e., the soliton is amplified. We also note that the envelope of the amplified soliton pulses appears to be smeared in amplitude. This phenomenon is probably due to the asynchronicity of the signal and pump phases.

Figure 2 shows curves of the gain $G=f(P/P_{th})$ measured in the soliton regime and a regime which is linear in the input signal. We call attention to the fact that the gain for the linear pulse with the same pump powers P_p is much larger than the soliton gain.

The maximum soliton gain was equal to about 6 dB. The same gain was obtained using the meander pump structure.

Attempts to increase G by increasing P_p resulted in a change in the shape of the output pulse. Apparently, this corresponded to the onset of a transition into a two-soliton

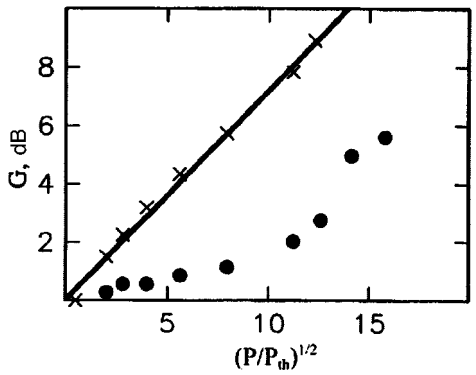

FIG. 2. Gain of linear spin-wave pulses (×) and spin-wave solitons (●) versus the normalized pump power. The solid line shows the computational result obtained from the numerical data.

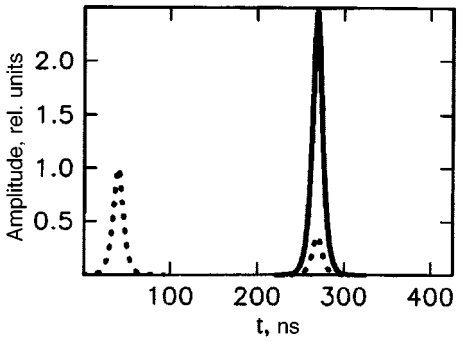

FIG. 3. Results of numerical simulation of the propagation of a spin-wave pulse in a YIG film. The dotted lines show the profiles of the input and output spin-wave pulses in the absence of a pump and the solid line shows the same profiles in the presence of a pump. The following parameters were used in the simulation: group velocity — 2.57×10^6 cm/s, input pulse duration — 14 ns, dissipation parameter — $\Delta H=0.25$ Oe, supercriticality — $(P_p/P_{\text{th}})^{1/2}=20$.

regime (according to the type described in Ref. 4). This last remark is tentative and requires a detailed experimental study. According to a theory in which the thresholds of the one- and many-soliton regimes are determined neglecting dissipation (see, for example, Ref. 12), the maximum gain in the one-soliton regime cannot exceed 9.6 dB.

A theory that would completely explain the experiments performed has not yet been developed. We performed a numerical simulation in order to determine the main features of the parametric amplification of the BVSW pulses by longitudinal-pump pulses. As the initial equations, we employed the evolutionary equations presented in Ref. 10. Two cases were simulated in order to clarify the physics of the process: co- and counterpropagation of the signal and idler waves. It was found that the experimental results obtained with linear-wave pulses find a good theoretical explanation when the signal and idler wave pulses propagate in the same direction. An example of the numerical results is shown in Fig. 3. For the numerical simulation, the profile of the signal wave was taken in the form $\text{sech}[a(t-t_0)]$. We underscore the fact that all other parameters were taken to be the same as in the experiment. The dotted lines in Fig. 3 show the profiles of the input and output signal pulses in the absence of a pump; the solid line shows the profile of the amplified spin-wave pulse. As is clear from the figure, the theoretical gain is greater than the natural damping of the spin-wave pulse.

The gain $G=f(P_p/P_{\text{th}})$ calculated from the numerical data is shown in Fig. 2 (solid line). It is easy to see that the experimental data are in good agreement with the calculations.

The codirectionality of the propagation of the signal and idler waves makes it possible to interpret their interaction in a pump field as a parametric process of the form $k_s+k_i=k_p$, where k_i and k_p are the wave numbers of the idler and pump waves. The latter relation gives $k_p=220$ rad/cm. This value of k_p gives $l=2\pi/k_p\cong0.029$ cm. These considerations were used to choose the period of the pump structures employed in the experiments.

A detailed description of the experimental results will be published later.

This work was sponsored by the Russian Fund for Fundamental Research (Project No. 96-02-19515).

[a)]e-mail: borisk@borisk.usr.etu.spb.ru

---

[1] B. A. Kalinikos, N. G. Kovshikov, and A. N. Slavin, Zh. Éksp. Teor. Fiz. **94**, 159 (1988) [Sov. Phys. JETP **67**, 303 (1988)].
[2] B. A. Kalinikos, N. G. Kovshikov, and A. N. Slavin, Phys. Rev. B **42**, 8658 (1990).
[3] M. Chen, M. A. Tsankov, J. M. Nash, and C. E. Patton, Phys. Rev. B **49**, 12773 (1994).
[4] J. M. Nash, C. E. Patton, and P. Kabos, Phys. Rev. B **51**, 15079 (1995).
[5] R. Marcelli and P. De Gasperis, IEEE Trans. Magn. **30**, 26 (1994).
[6] N. G. Kovshikov, B. A. Kalinikos, C. E. Patton *et al.*, Phys. Rev. B **544**, 15210 (1996).
[7] B. A. Kalinikos, M. K. Kovaleva, and N. G. Kovshikov, Izobreteniya Otkrytiya **26**, 225 (1988).
[8] G. A. Melkov and S. V. Sholom, Zh. Tekh. Fiz. **60**(8), 118 (1990) [Sov. Phys. Tech. Phys. **35**, 943 (1990)].
[9] A. V. Bagada, G. A. Melkov, A. A. Serga, and A. N. Slavin, in *Abstract Booklet of 41st Conf. on Magnetism and Magnetic Materials*, Atlanta, Georgia USA, November 12–15, 1996, p. 162.
[10] B. A. Kalinikos and M. P. Kostylev, *Digests of International Magnetics Conference*, New Orleans, Louisiana, 1997, p. AD-10.
[11] B. A. Kalinikos, N. G. Kovshikov, and N. V. Kozhus', Fiz. Tverd. Tela (Leningrad) **27**, 2794 (1985) [Sov. Phys. Solid State **27**, 1681 (1985)].
[12] S. P. Novikov, S. V. Manakov, L. P. Pitaevskiĭ, and V. E. Zakharov, *Theory of Solitons: The Inverse Scattering Method*, Consultants Bureau, New York, 1984 [Russian original, Nauka, Moscow, 1980].

Translated by M. E. Alferieff

Giant blue shift of photoluminescence in strongly excited type-II ZnSe/BeTe superlattices

S. V. Zaĭtsev, V. D. Kulakovskiĭ, A. A. Maksimov,[a] D. A. Pronin, and I. I. Tartakovskiĭ

Institute of Solid-State Physics, Russian Academy of Sciences, 142432 Chernogolovka, Moscow Region, Russia

N. A. Gippius

Institute of General Physics, Russian Academy of Sciences, 117942 Moscow, Russia

M. Th. Litz, F. Fisher, A. Waag, D. R. Yakovlev,[b] W. Ossau, and G. Landwehr

Physikalisches Institut der Universität Würzburg Am Hubland, 97074 Würzburg, Germany

(Submitted 5 August 1997)
Pis'ma Zh. Éksp. Teor. Fiz. **66**, No. 5, 351–356 (10 September 1997)

A giant blue shift (≈ 0.5 eV) and a large decrease in the emission time of a spectral band corresponding to radiative recombination of spatially separated electrons and holes are observed in ZnSe/BeTe superlattices at high laser excitation levels. On the basis of numerical calculations, the observed defects are attributed to band bending arising in type-II structures at high carrier density. © *1997 American Institute of Physics.* [S0021-3640(97)01417-5]

PACS numbers: 78.55.Et, 78.66.Hf

In contrast to quasi-two-dimensional type-I semiconductor structures, in type-II structures the energy minima for electrons and holes lie in different layers. Spatially separated electron and hole layers are easily realized in such systems, which greatly influences their optical properties.[1–3] ZnSe/BeTe superlattices are comparatively new objects which are extremely interesting both for fundamental research and because they have promising potential applications in different applied fields.[4] The case of a type-II system with a high localizing potential for electrons in the ZnSe layer (>2.0 eV) and for holes (≈ 0.9 eV), whose energy minimum lies in the BeTe layer, is realized in these structures. Such deep potential wells for electrons and holes make it possible to realize in photoexcited lattices an electron–hole system with separated layers of electrons and holes with density exceeding 10^{14} cm^{-2}. The electric fields induced by such dense electron–hole layers in turn should strongly modify the energy structure of the superlattice and therefore the energy of interband optical transitions. In a weakly-excited superlattice, direct (in space) optical transitions corresponding to radiative recombination of photoexcited electrons and holes in the ZnSe layer lie at energies near 2.8 eV. Indirect (in space) optical transitions, however, corresponding to radiative recombination of photoexcited electrons in the ZnSe layer and holes in the BeTe layer fall into the spectral range <2.0 eV.[5]

In the present letter we report on an investigation of a spectral reorganization of

 © 1997 American Institute of Physics

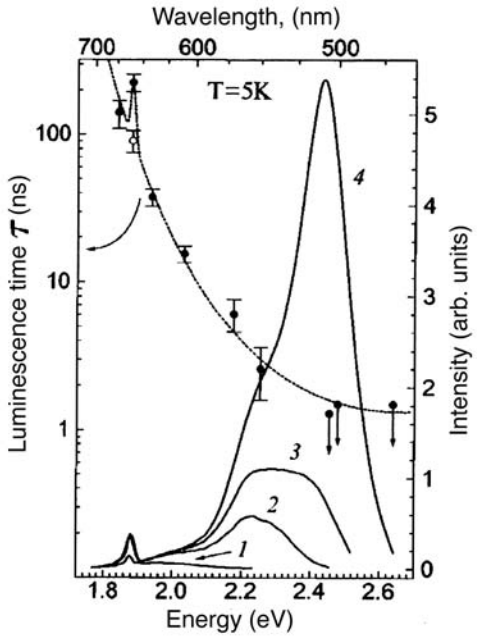

FIG. 1. Time-integrated photoluminescence spectra of a ZnSe/BeTe superlattice with different laser pump densities: *1* — 40, *2* — 160, *3* — 460, *4* — 1000 kW/cm^2 $=P_{\max}$. The dots show the spectral dependence of the emission time τ at $P_{\max}$. The measured values $\tau<1.5$ ns can serve as an estimate of the upper limit on the emission time (see text). The open circle was obtained at $T=40$ K.

radiative recombination in the region of spatially indirect transitions at high photoexcited carrier densities. The experimental samples were grown by molecular-beam epitaxy on (001) GaAs substrates and consisted of a superlattice containing 60 periods of alternating 7.2 nm and 4.0 nm thick ZnSe and BeTe layers, respectively. The samples were placed in helium vapors in an optical thermostat with the temperature regulable over the range $T=4.5-300$ K.

Photoluminescence was excited with a pulsed N_2 laser (pulse duration ~ 0.5 ns, pulse power 100 kW, pulse repetition frequency 50 Hz). The $\lambda=337.1$ nm ($\hbar\omega=3.678$ eV) radiation of this laser is absorbed only in the ZnSe layers, since the band gap in BeTe $E_g\simeq 4.2$ eV.[5] The laser excitation density P at the surface of the sample was varied by means of calibrated filters. The photoluminescence spectra were recorded with a MDR-23 spectrometer equipped with an optical multichannel analyzer and a fast 18ÉLU-FM photomultiplier; this enabled us to obtain time-integrated emission spectra and to record the luminescence pulses in different fixed spectral intervals with a temporal resolution of ~ 1.2 ns.

Figure 1 displays the photoluminescence spectra of a ZnSe/BeTe superlattice with different laser excitation levels. At low excitation levels (curve *1*) the spectrum consists of two bands: a relatively intense band with a maximum near $\hbar\omega\simeq 1.88$ eV and a wide band with a short-wavelength limit in the region $\hbar\omega\approx 2.05$ eV. The intensity of the

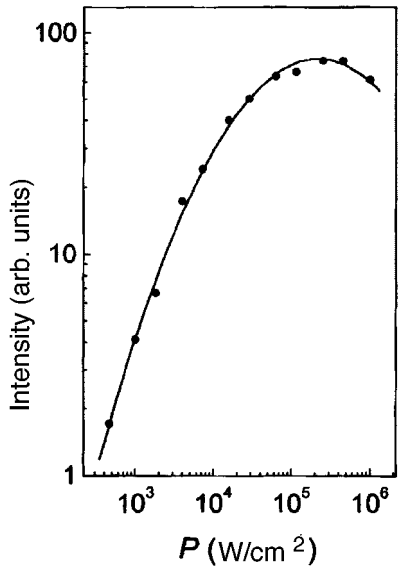

FIG. 2. Intensity of the $\hbar\omega \simeq 1.88$ eV band versus laser excitation density P.

second band increases substantially with increasing excitation level; this is accompanied by a strong blue shift of the band, exceeding 0.5 eV with maximum excitation densities $P_{\max} \approx 1000$ kW/cm^2. The spectral position of the band near $\hbar\omega \simeq 1.88$ eV remains practically unchanged and the intensity of the band saturates with increasing laser pump density P (Fig. 2) and even decreases slightly near $P_{\max}$.

The measurements of the photoluminescence kinetics in a ZnSe/BeTe superlattice with maximum excitation levels at different wavelengths showed that the emission times $\tau(\omega)$ vary by more than two orders of magnitude depending on the spectral interval (points in Fig. 1). The duration of the emission pulses in the region of direct optical transitions ($\hbar\omega \approx 2.8$ eV) and in the blue wing of the spectral band in the region of indirect transitions ($\hbar\omega \sim 2.4-2.6$ eV) are close in magnitude and equal ≈ 1.5 ns, which is at the limit of the temporal resolution of the measuring system ~ 1.2 ns and does not permit us to determine the emission time τ in this region of the spectrum but permits only estimating the upper limit, $\tau \leqslant 1.5$ ns. The photoluminescence emission time increases rapidly with increasing wavelength.

To explain the nature of the emission lines we also investigated the changes occurring in the emission spectra with increasing temperature. We found that when the temperature increases up to $T = 40$ K, the spectral band with a maximum at $\hbar\omega \simeq 1.88$ eV vanishes almost completely. At the same time, the nonmonotonic dependence $\tau(\omega)$ observed at low temperatures in this spectral region also vanishes: τ changes from ≈ 225 ns to ≈ 90 ns (open circle in Fig. 1). Changes of this character in the emission spectra and the emission time with increasing temperature together with the pump dependence of the intensity indicate that the spectral band with a maximum at $\hbar\omega \simeq 1.88$ eV is due to impurities.

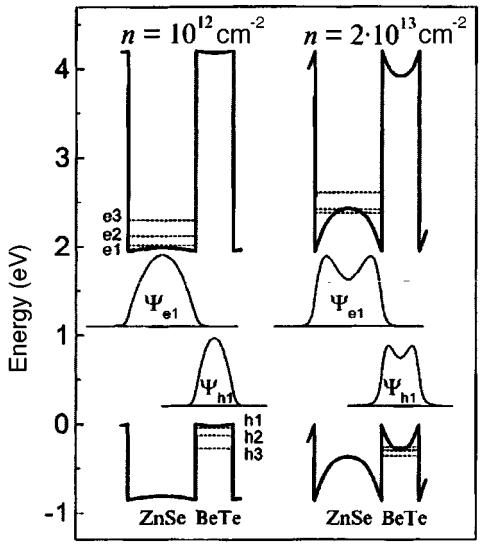

FIG. 3. Band diagram of a ZnSe/BeTe (7.2 nm/4.0 nm) superlattice calculated for two values of the carrier density n. The dotted straight lines show the positions of the first three levels for electrons in the ZnSe ($e1-e3$) layer and holes in the BeTe ($h1-h3$) layer; light solid lines — electron (Ψ_{e1}) and hole (Ψ_{h1}) wave functions, respectively, for the lowest levels.

The virtually temperature-independent emission band in the region 2.0–2.6 eV corresponds to indirect interband transitions of electrons from the ZnSe layers into the BeTe valence band. To explain its spectral-temporal features, it is necessary to take into consideration the fact that as the photoexcited carriers in the ZnSe layer relax they spread out in space, since holes strive to be localized in the BeTe layer. This leads to the appearance of electric fields in the system which in turn give rise to bending of the valence and conduction band and change the overlapping of the electron and hole wave functions. We performed numerical calculations based on which we determined, by solving a self-consistent problem,[6] the positions of the energy levels and wave functions of the electrons (in the ZnSe layer) and holes (in the BeTe layer) with different carrier densities taking account of the bending of the conduction and valence bands. The computational results are presented in Fig. 3 for two densities $n=10^{12}$ cm^{-2} and $n=2\times10^{13}$ cm^{-2}. One can see that as the carrier density increases, a large shift of the electron (e) and hole (h) energy levels, as a result of increasing band bending, as well as a strong change in the wave functions occur.

Figure 4 displays the computational results for the positions of the first three levels of the electrons ($e1-e3$) and holes ($h1-h3$) with the density varying from $n=10^{10}$ to $n=2\times10^{13}$cm^{-2}. The arrows indicate for several values of the carrier densities the energy of the spatially indirect optical transition accompanying radiative recombination of electrons and holes occupying the lower level. The Fermi energy estimated for carrier density $n=2\times10^{13}$ cm^{-2} is $E_F\approx200$ meV,[c)] which agrees well with the width of the emission band at the maximum excitation level (Fig. 1, curve *4*). It should be noted that

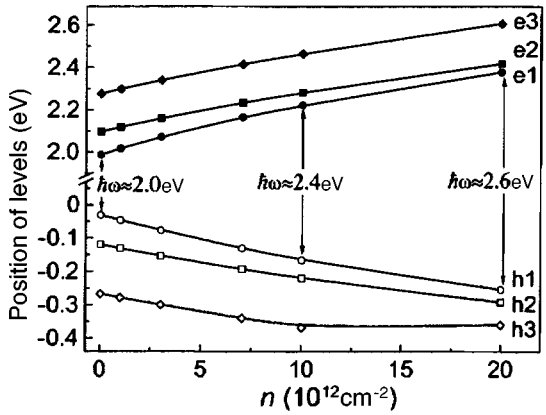

FIG. 4. Computed positions of the first three levels for electrons in the ZnSe ($e1-e3$) layer and holes in the BeTe ($h1-h3$) layer versus carrier density n.

in our calculations we neglected the renormalization of the bands by the multiparticle Coulomb interactions. This approximation is entirely justified for a semiquantitative description of dense electron–hole systems, since in this case the Fermi energy E_F greatly exceeds the total exchange-correlation energy E_{xc}.[8,9] At the same time, it is evident from Fig. 1 that for high excitation densities the observed blue shift reaches values >0.5 eV, which greatly exceeds our estimate for $E_F \approx 0.2$ eV. Therefore the experimentally observed spectral shifts into the short-wavelength region agree reasonably with the computational results and can thereby be attributed to band bending caused by a high density of photoexcited carriers.

Figure 3 also displays the computational results for the wave functions of the lowest electron and hole levels at high carrier densities. It is evident from the figure that as the carrier density increases, the Coulomb attraction of the electrons and holes results in strong carrier localization near the boundary of the interface, substantially increasing the overlapping of their wave functions. This decreases the radiative recombination time on the blue wing of the spectral band in the region of spatially indirect optical transitions, as is observed experimentally.

It should be noted that at sufficiently high laser excitation levels the time-integrated photoluminescence spectrum is a superposition of spectra corresponding to different carrier densities. Indeed, at the end of the laser pulse the carrier density in the system is initially maximum. Maximum band bending occurs and, correspondingly, the blue shift for indirect optical transitions reaches its highest values. As the carrier density decreases after the laser pulse ends, the radiative recombination spectrum in the region of indirect optical transitions shifts continuously in the direction of lower energies. In principle, such an evolution of the spectral composition of the photoluminescence can be traced in time-resolved spectra. However, in our case of a superlattice with a large number of periods the level of laser excitation is substantially nonuniform for layers lying at different depths from the surface of the sample. For this reason, to obtain quantitative results we plan to perform in the near future measurements of time-resolved emission spectra on

superlattices with a small number of periods or on a single quantum well.

In summary, we have established that a giant blue shift of the spectral band in the region of spatially indirect optical photoluminescence transitions and a sharp decrease of the radiative recombination time on the blue wing of the band are observed in a type-II ZnSe/BeTe superlattice at high optical pumping levels. Numerical calculations showed that the observed effects are due to strong bending of the conduction band in ZnSe and the valence band in BeTe which occurs as high-density photoexcited carriers relax. Such effects should be observed in any type-II two-dimensional structures with deep potential wells.

This work was sponsored by Deutsche Forschungsgemeinschaft (SFB 410) and the Russian Fund for Fundamental Research Grant NNIO 96-00100.

[a)]e-mail: maksimov@issp.ac.ru
[b)]Permanent address: A. F. Ioffe Physicotechnical Institute, Russian Academy of Sciences, St. Petersburg, Russia
[c)]In estimating the density, it was assumed that the electron effective mass in ZnSe $m^* \approx 0.17 m_e$ (Ref. 7) is much less than the hole mass in BeTe.

[1] F. C. Zhang, H. Luo, N. Dai *et al.*, Phys. Rev. B **47**, 3806 (1993).
[2] N. Dai, L. R. Ram–Mohan, H. Luo *et al.*, Phys. Rev. B **50**, 18153 (1994).
[3] E. Finkman and R. Planel, *Proceedings of the 23rd International Conference on the Physics of Semiconductors*, edited by M. Scheffler and R. Zimmermann, World Scientific, Singapore, 1996, Vol. 3, p. 1723.
[4] A. Waag, F. Fisher, Th. Litz *et al.*, Appl. Phys. Lett. **70**, 280 (1997).
[5] A. V. Platonov, D. R. Yakovlev, U. Zehnder *et al.*, Acta Polonica A, to be published.
[6] N. F. Gippius, S. G. Tikhodeev, M. Bayer *et al.*, *Proceedings of the 23rd International Conference on the Physics of Semiconductors*, edited by M. Scheffler and R. Zimmermann, World Scientific, Singapore, 1996, Vol. 3, p. 2075.
[7] V. I. Gavrilenko, A. M. Grekhov, D. V. Korbutyak, and V. G. Litovchenko, *Optical Properties of Semiconductors* [in Russian], Naukova Dumka, Kiev, 1987.
[8] G. Träkle, T. Lach, A. Forchel *et al.*, Phys. Rev. Lett. **58** 419 (1987).
[9] V. D. Kulakovskii, E. Lach, A. Forchel, and D. Grützmacher, Phys. Rev. B **40**, 8087 (1989).

Translated by M. E. Alferieff

Anomalous evolution of photoluminescence in porous silicon in an electric field

B. M. Kostishko[a)] and L. I. Gonchar
Ul'yanovsk State University, 432700 Ul'yanovsk, Russia

(Submitted 7 August 1997)
Pis'ma Zh. Éksp. Teor. Fiz. **66**, No. 5, 357–361 (10 September 1997)

The change produced in the photoluminescence (PL) of *n*-type porous silicon (por-Si) by irradiation with ultraviolet laser radiation in the presence of an external electric field has been investigated. A field effect, consisting of a large change in the integrated PL intensity when the field is switched on or off, was observed. When the field intensity E exceeds a critical value, the change in the PL becomes anomalous — an alternating saw-tooth signal. A kinetic model is proposed wherein the experimental results are explained by a change in the density of neutral acceptor and hole surface states formed by hydrogen, oxygen, and fluorine atoms adsorbed on the surfaces of pores. © *1997 American Institute of Physics.* [S0021-3640(97)01517-X]

PACS numbers: 78.55.Ap, 78.55.Mb

The discovery by Canham[1] of visible-range photoluminescence (PL) of porous silicon (por-Si) has aroused great interest in porous silicon as a promising material for optoelectronics. Even though investigations showed that the practical application of porous silicon as light-emitting elements[2] is held back by the instability of its optical properties,[3] the number of studies of the PL mechanism in porous silicon continues to increase. There is still no generally accepted theory describing the mechanism of photo- and electroluminescence in porous silicon. The most complete model, both on a theoretical level and supported by experimental results, is currently the model of excitonic annihilation on surface states of quantum-size structures.[4,5]

As is well known,[6] radiative annihilation of excitons occurs on neutral surface states whose number can be controlled by an electric field. In the present work we investigate in this connection the change produced in the photoluminescence of porous silicon in an external electric field by laser irradiation.

Phosphorus-doped (100) silicon plates with resistivity $\rho = 2.4\ \Omega\cdot$cm ($N_a = 1.5\times 10^{15}$ cm^{-3}) served as the starting material for the por-Si samples. Porous silicon was produced by the standard technology in a process of electrochemical etching in an electrolyte consisting of 48% hydrofluoric (HF) acid and ethyl alcohol in a 1:1 ratio. The electrochemical etch time was equal to 40 min with a current density of 20 mA/cm^2. The initial PL intensity and its uniformity over the surface were checked in advance for each freshly prepared sample. The por-Si was irradiated with a LGN-409 He–Cd laser ($\lambda = 325$ nm, $P = 20$ mW/cm^2) in the electric field (with intensity up to 2×10^4 V/cm) of a flat capacitor whose electrodes were separated by a distance of 1.5 mm. A quartz plate with an In

 © 1997 American Institute of Physics

$_2O_3$ film was used as the top plate of the capacitor, through which the integrated intensity of the PL was monitored. A 0.6 μm thick layer of indium oxide was formed by thermal evaporation of metallic indium (99.999% purity) with a resistively heated evaporator in an oxygen atmosphere. To improve the adhesion properties and transparency the film was subjected to additional thermal oxidation. As a result, the quartz plate with a conducting In_2O_3 layer possessed transmittance $T=60\%$ at the wavelength employed.

Laser irradiation of the por-Si surface was started at the moment the electric field was switched on. The electric field **E** was oriented perpendicular to the surface and directed away from the experimental sample. During irradiation the field was switched off at definite moments in time and then switched on once again. The moments when the intensity of the electric field changed are marked in the figure by the symbols *A* and *B*. As a result, a change in the integrated PL intensity I_L was obtained as a function of the laser irradiation time in the presence or absence of an external electric field.

The investigations showed that the field defect appears when the electric field strength reaches the value $E\approx 8\times 10^3$ V/cm. Irradiation of por-Si in such a field for several minutes and then switching the field off resulted in a sharp change in the integrated PL intensity I_L (see Fig. 1a). In addition, the character of the change in the intensity, i.e., an increase or decrease, depended on a large number of factors — the sample storage time and conditions, the location of the surface section which was investigated, the intensity of the laser irradiation, the intensity of the electric field, and finally the time elapsed from the start of irradiation up to the moment the field was switched off. The contribution of each of these factors is a subject of future investigations. Figure 1a displays the most typical case, when switching off the field resulted in the excitation of PL. Subsequently, $I_L(t)$ exhibited the standard degradation form characteristic for laser treatment.[7,8]

Irradiation of the sample in the presence of fields exceeding 1.2×10^4 V/cm resulted in the appearance of an alternating saw-tooth component in the time dependence $I_L(t)$ (see Fig. 1b). In addition, the period of the alternating signal depended only on the intensity of the field and assumed the values $T=110\pm 7$ s at $E=12$ kV/cm, $T=30\pm 3$ s at $E=16$ kV/cm (see Fig. 1c), and $T=26\pm 3$ s at $E=18$ kV/cm. As one can see, increasing the intensity of the field decreased the period *T*. The characteristic decay time τ of the alternating component also depended on the laser irradiation time. For example, for $E=12$ kV/cm τ doubled over 10 lasing periods.

To explain the experimental data we propose a model that takes account of adsorption–desorption processes as well as electron exchange in the adatom–substrate system. The hydrogen, oxygen, and fluorine atoms adsorbed on the por-Si surface can be acceptors and/or donors. As a result, some donors (N_D^0) and acceptors (N_A^0) on the surface are in a neutral state, forming a ''weak'' bond with the lattice, and they remaining donors and acceptors (N_D^+, N_A^-) are ionized and ''strongly'' bound with the surface. The ratio between the concentrations of the neutral and charged phases is determined by their lifetimes, which depend on the charge-exchange rates, which in turn are functions of the positions of the Fermi quasilevels.[6] Quasilevels are introduced because the change in the state of the surface is studied during the process of laser irradiation.

Thus, the change in the density of adatoms, taking account of electron exchange

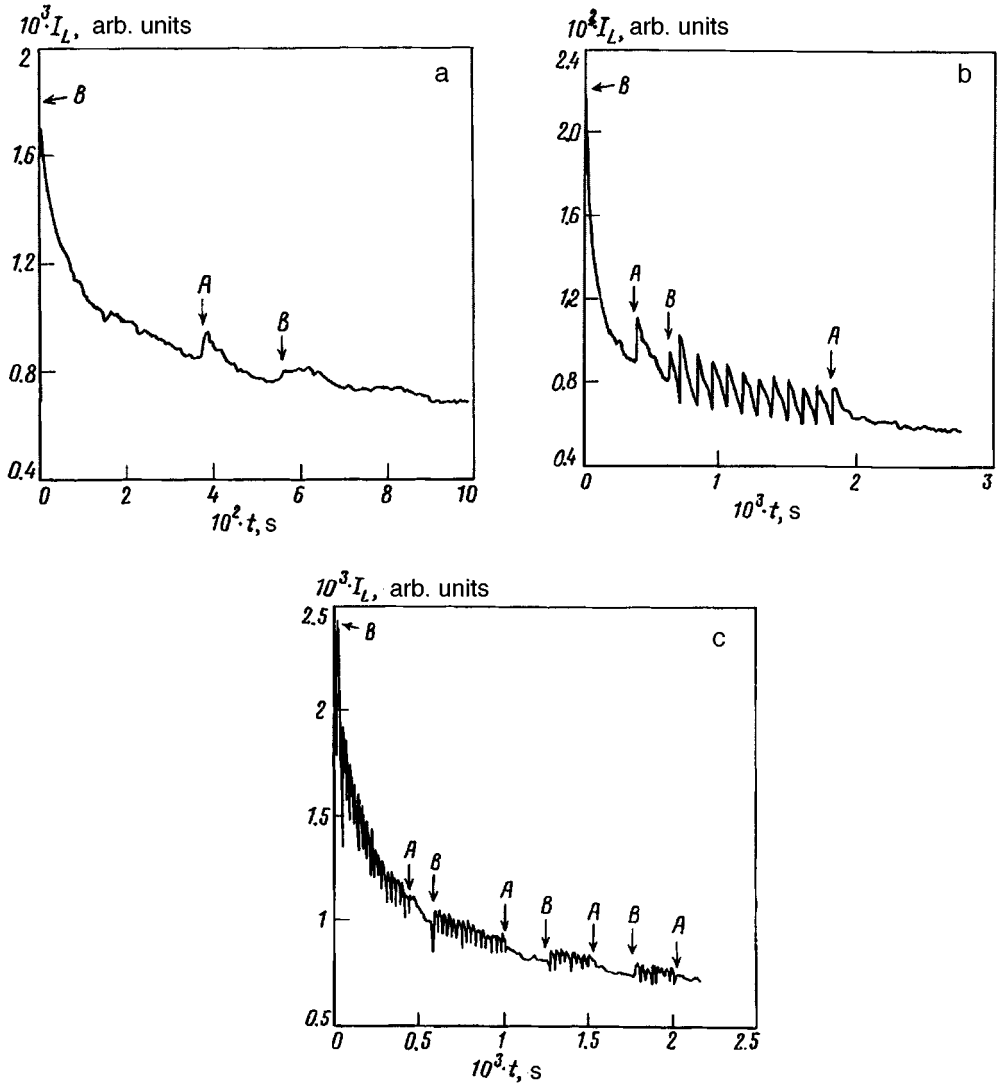

FIG. 1. Integrated intensity of photoluminescence in *n*-type porous silicon versus laser irradiation time in the presence of an electric field with intensity: a — 8×10^3 V/cm, intensity 12×10^4 V/cm, and c — intensity 16×10^3 V/cm. The symbols *A* and *B* mark the moments when the electric field is switched off and on, respectively.

processes, can be determined from the system of kinetic equations

$$dN_D^0/dt = -N_D^0/\tau_D - N_D^0/\tau_D^0 + N_D^+/\tau_D^+ ,$$

$$dN_D^+/dt = N_D^0/\tau_D^0 - N_D^+/\tau_D^+ , \qquad (1)$$

$$dN_A^0/dt = -N_A^0/\tau_A - N_A^0/\tau_A^0 + N_A^-/\tau_A^- ,$$

$$dN_A^-/dt = N_A^0/\tau_A^0 - N_A^-/\tau_A^- ,$$

where τ_D and τ_A are the lifetimes of the neutral adatoms, which depend on their desorption rates (it is assumed, by analogy to Ref. 6, that only particles which are weakly bound with the lattice can be desorbed); τ_D^0 and τ_A^0 are the lifetimes of the adsorbed atoms in the neutral state, taking account of ionization of the atoms; and, τ_D^+ and τ_A^- are the lifetimes of the ionized surface states, characterizing the probability of trapping of mobile charge carriers.

The system of equations (1) is a logical extension of the kinetic model of the evolution of PL with ultraviolet and electronic processing of porous silicon.[8,9] Adsorption processes are neglected in this system. This makes it possible to obtain an analytic solution of the system, assuming that the lifetimes are constants whose values change abruptly only at the moment when the field is switched on or off:

$$\begin{aligned} N_D^0 &= C_{D1}^0 \exp(-\lambda_1 l) + C_{D2}^0 \exp(-\lambda_2 l), \\ N_D^+ &= C_{D1}^+ \exp(-\lambda_1 l) + C_{D2}^+ \exp(-\lambda_1 l), \\ N_A^0 &= C_{A1}^0 \exp(-q_1 l) + C_{A2}^0 \exp(-q_1 l), \\ N_A^- &= C_{A1}^- \exp(-q_1 l) + C_{A2}^- \exp(-q_1 l), \end{aligned} \tag{2}$$

where the pre-exponential factors are functions of the initial concentration and lifetime of each component studied and the arguments of the exponentials are functions of the lifetimes only.

In the model of radiative annihilation of excitons in a system of donors and acceptors, the intensity of photoluminescence can be can be written in the form

$$I_L = A_{ex} n_{ex} (\beta_D N_D^0 + \beta_A N_A^0), \tag{3}$$

where n_{ex} is the exciton density, β_D and β_A are the probabilities of radiative annihilation of excitons on neutral states of donors and acceptors, and A_{ex} is a dimensional constant.

It can be concluded on the basis of the the experimental data that irradiation of the surface of *n*-type por-Si with 325 nm light results in the accumulation of a negative space charge near the surface. Optical charging of porous silicon was observed earlier by Petrov.[10] Therefore, laser irradiation and the presence of an electric field directed away from the por-Si surface cause the bands to curve downwards. For strong fields E the following relations between the lifetimes hold in this case:

$$\tau_D^0 \gg \tau_D^+ , \quad \tau_A^0 \ll \tau_A^- . \tag{4}$$

After the field is switched off, the surface potential decreases and the inequalities (4) are reversed. Using these assumptions, the necessary conditions under which switching the field on or off would result in the experimentally observed change in the PL intensity can be determined. For example, for the case shown in Fig. 1a, the condition that I_L increases when the field is switched off is

$$\beta_D N_D^0(l_0)/\beta_A N_A^0(l_0) < \tau_D^0/\tau_A^- , \tag{5}$$

where τ_D^0 and τ_A^- are the lifetimes established after the moment τ_0 when the field is switched off. As one can see, in order for PL to be excited por-Si the density of neutral acceptor levels must increase at a rate higher than the rate of ionization of the donor states.

The appearance of an alternating signal in the degradation curves is explained by the fact that the photostimulated charging of the surface of porous silicon and the external electric field result in the accumulation of a critical level of electric charge, accompanied by relatively slow quenching of PL. The subsequent formation of drain channels and the rapid decrease of the surface charge result in rectification of the bands and an abrupt increase in the PL intensity. But if the external conditions did not change, i.e., laser irradiation continues and an electric field is present, the entire process repeats (Figs. 1b and 1c). It is obvious that in this case the period of the oscillations of the PL intensity should depend only on the magnitude of the field, the structure of the surface, and the intensity of the laser radiation. This is confirmed by the experimental results.

In summary, we have investigated in the present work the evolution of photoluminescence in porous silicon under laser irradiation in an electric field. It was found that in fields exceeding 8×10^3 V/cm, switching an electric field on or off results in an abrupt change in the PL intensity. For stronger fields $E\geqslant1.2\times10^4$ V/cm the integrated intensity becomes an alternating function of the irradiation time, the period of the oscillations decreasing with increasing E. To explain the observed effect, a model which describes on the basis of radiative annihilation of excitons the change in I_L as being due to adsorption–desorption processes and electron exchange in the system of donor and acceptor surface states was proposed.

This work was supported by the Grants ''Conversion and high technologies'' and ''Fundamental studies in high technologies.''

[a)]e-mail: Kost@ftf.univ.simbirsk.su

---

[1] L. T. Canham, Appl. Phys. Lett. **57**, 1046 (1990).
[2] I. N. Sorokin, S. A. Gavrilov, and N. F. Grevtsev, Élektronnaya Promyshelennost' **29,** 72 (1995).
[3] V. Grivickas, J. Kolenda, A. Bernussi *et al.*, Braz. J. Phys. **24**, 349 (1994).
[4] G. D. Sanders, and Yia-Chung, Phys. Rev. B **45,** 9202 (1992).
[5] P. K. Kashkarov, E. A. Konstantinova, and V. Yu. Timoshenko, Fiz. Tekh. Poluprovodn. **30,** 1479 (1996) [Semiconductors **30**, 778 (1996)].
[6] F. F. Vol'kenshteĭn, *Electronic Processes Accompanying Chemisorption on Semiconductor Surfaces* [in Russian], Nauka, Moscow, 1987.
[7] I. M. Chang, G. S. Chuo, D. C. Chang *et al.*, J. Appl. Phys. **77**, 5365 (1995).
[8] B. M. Kostishko, A. M. Orlov, and T. G. Emel'yanova, Pis'ma Zh. Tekh. Fiz. **22,** 68 (1996) [Tech. Phys. Lett. **22** 417 (1996)].
[9] B. M. Kostishko, A. M. Orlov, and T. G. Emel'yanova, Izv. Ross. Akad. Nauk, Neorg. Mater. **32,** 1432 (1996).
[10] A. V. Petrov and A. G. Petrukhin, Fiz. Tekh. Poluprovodn. **28,** 82 (1994) [Semiconductors **28**, 49 (1994)].

Translated by M. E. Alferieff

Annihilation of Brownian particles on randomly distributed traps during anisotropic diffusion

A. M. Berezhkovskii[a)]
L. Ya. Karpov Scientific-Research Physicochemical Institute, 103064 Moscow, Russia

Yu. A. Makhnovskii
A. V. Topchiev Institute of Petrochemical Synthesis, Russian Academy of Sciences, 117912 Moscow, Russia

A. A. Ovchinnikov
N. M. Émanuél' Joint Institute of Chemical Physics, Russian Academy of Sciences, 117334 Moscow, Russia

(Submitted 5 August 1997)
Pis'ma Zh. Éksp. Teor. Fiz. **66**, No. 5, 362–365 (10 September 1997)

The effect of diffusion anisotropy on the long-time asymptotic behavior of the survival probability of a Brownian particle among randomly distributed traps is discussed. © *1997 American Institute of Physics.* [S0021-3640(97)01617-4]

PACS numbers: 05.40.+j

1. The problem of the survival of a Brownian particle in a medium with randomly distributed traps arises in the study of different phenomena in physics and chemistry. The Smoluchowski theory,[1,2] which is a mean-field approximation in this problem, describes the survival probability satisfactorily at not too long times.[3] This approximation is no longer valid at long times. The $t\to\infty$ asymptotic behavior of the exact solution has been obtained independently by a number of authors.[4–8] They all used the ideas proposed by Lifshitz[9] for calculating the tail of the density of states of a quantum particle in the field produced by randomly distributed scatterers. In the analysis it was assumed that the diffusion is isotropic. The asymptotic behavior of the survival probability $S(t)$ of a particle in a d-dimensional space has the form[4–8]

$$-\ln S(t)\propto(c^{2/d}Dt)^{d/(d+2)}, \tag{1}$$

where c is the trap density and D is the diffusion coefficient of a Brownian particle. To obtain expression (1) one must study the survival of particles created in large fluctuation cavities with no traps. If a particle resides for the entire time t inside such a cavity, then the particle will certainly not be annihilated. Both the fraction of large fluctuation cavities and the probability of avoiding an escape from a cavity over the time t are small. Nonetheless, of the particles that survive for long times the overwhelming majority are particles that were always located in fluctuation cavities.[4–8]

Our objective in the present letter is to investigate the influence of diffusion anisotropy on the asymptotic behavior of the survival probability. Our analysis shows how expression (1) is modified a) in the presence of anisotropic diffusion (when the diffusion

 © 1997 American Institute of Physics

coefficients are finite in all directions) and b) when the coefficients in some directions vanish and essentially the spatial dimension of the problem changes.

2. We start with an analysis of the annihilation of Brownian particles in three-dimensional space on spherical traps of radius b in the limiting anisotropic situation when diffusion occurs only along the x direction and $D_y = D_z = 0$. Let L be the amplitude of a one-dimensional Wiener trajectory of a Brownian particle (the sum of the maximum deviations to the left and right of the starting point over the observation time t). The survival probability of a particle realizing such a trajectory equals a fraction of the trap configurations for which all traps are located quite far from the trajectory. In other words, this probability equals the probability that no trap falls within a cylinder of radius b surrounding a trajectory. In the case of a Poisson distribution of traps the probability equals $\exp(-\pi b^2 cL)$. The amplitude L is a random quantity. Introducing its probability density $F(t|L)$, we can represent the desired survival probability in the form

$$S(t) = \int_0^\infty \exp(-\pi b^2 cL) F(t|L)\, dL. \tag{2}$$

Using the results of Ref. 10, it can be shown that expression (2) is the exact solution, first obtained in Ref. 4, of the one-dimensional problem with an effective one-dimensional density $\tilde{c}_1 = \pi c b^2$:

$$S(t) = \frac{4}{\pi^2} \int_0^\infty \exp\left(-\frac{\pi^2 \tilde{c}_1^{\,2} D_x t}{x^2} \right) \frac{x}{\sinh x}\, dx. \tag{3}$$

An important feature of the one-dimensional case is that the quantities $\tilde{c}_1$, D_x, and t form the dimensionless combination $\tilde{c}_1^2 D_x t$. Therefore the quantity $(\tilde{c}_1^2 D_x)^{-1} = (\pi^2 b^4 c^2 D_x)^{-1}$ is a natural time scale of the problem. For $t < (\pi^2 b^4 c^2 D_x)^{-1}$ the mean-field description works, while for $t > (\pi^2 b^4 c^2 D_x)^{-1}$ the survival probability is described well by the asymptotic expression (1) with $d = 1$ and $c = \tilde{c}_1$: $-\ln S(t) \propto (\tilde{c}_1 D_x t)^{1/3}$.

3. If the diffusion coefficients D_y and D_z are different from zero but small, expression (3) for the survival probability is applicable as long as the observation time t is not too large, specifically, the displacement in the perpendicular direction must be small compared with b, i.e., for $t \ll b^2 D_\perp^{-1}$, where we assumed that $D_y = D_z = D_\perp$. If $D_\perp \to 0$, expression (3) is applicable in the entire time interval. Comparing the two time scales $b^2 D_\perp^{-1}$ and $(\pi^2 b^4 c^2 D_x)^{-1}$ shows that the deviations from the one-dimensional behavior of $S(t)$ appear after expression (3) reaches the asymptotic behavior (1) with $d = 1$ and $c = \tilde{c}_1$, if $D_\perp < D_x \Psi^2$, where $\Psi = 4\pi c b^3$ is the volume fraction of traps, assumed to be a small parameter of the problem, $\Psi \ll 1$. However, if $D_\perp > D_x \Psi^2$, then the deviation from the one-dimensional behavior of $S(t)$ occurs at times when the mean-field description is valid.

To estimate the asymptotic survival probability for $D_\perp \neq 0$ we note that the probabilities that the displacement amplitudes in the x and $r = \sqrt{y^2 + z^2}$ directions do not exceed L and R, respectively, equal $\exp(-a_1 D_x t/L^2)$ and $\exp(-a_2 D_\perp t/R^2)$, where a_1 and a_2 are numerical factors expressed in terms of the first zeros of the corresponding Bessel

functions.[3] The probability that a cylinder of radius R and length L contains no traps equals $\exp(-\pi R^2 cL)$. The particles created and residing in such a cylinder at all times certainly survive. Therefore, to estimate the long-time asymptotic behavior of the survival probability the following expression (product of the probabilities mentioned above) must be optimized with respect to L and R:

$$\exp\left\{-\left[\left(\frac{a_1 D_x}{L^2}+\frac{a_2 D_\perp}{R^2}\right)t+\pi R^2 cL\right]\right\}\equiv\exp[-f(L,R|t)]. \tag{4}$$

Varying $f(L,R|t)$ with respect to L and R we obtain the system of equations

$$-\frac{2a_1 D_x t}{L^3}+\pi cR^2=0, \quad -\frac{a_2 D_\perp t}{R^3}+\pi cRL=0, \tag{5}$$

whence we find the optimum values of L_t and R_t as functions of time:

$$L_t\propto\left(\frac{D_x^2}{cD_\perp}t\right)^{1/5}, \quad R_t\propto\left(\frac{D_\perp^{3/2}}{cD_x^{1/2}}t\right)^{1/5}. \tag{6}$$

Substituting the obtained optimal values into $f(L,R|t)$, we obtain the desired asymptotics

$$-\ln S(t)\simeq f(L_t,R_t|t)\propto(c^{2/3}D_x^{1/3}D_\perp^{2/3}t)^{3/5}. \tag{7}$$

In the case of isotropic diffusion ($D_x=D_\perp=D$) the relation (7) passes into the well-known result (1), which in the three-dimensional case has the form $-\ln S(t)\propto(c^{2/3}Dt)^{3/5}$.

The estimate (7) holds under the condition that the optimal values of L_t and R_t are large compared with b. This is essentially a restriction on the times at which the asymptotic relation (7) is justified:

$$t\gg cb^5\max\left\{\frac{D_x^{1/2}}{D_\perp^{3/2}};\frac{D_\perp}{D_x^2}\right\}. \tag{8}$$

If one of the diffusion coefficients vanishes, then the relation (7) is not realized. For example, if $D_\perp=0$, the problem is one-dimensional.

4. Performing a similar analysis in the d-dimensional case, we find that the expression to be optimized is

$$\exp\left\{-\left[a_1 t\left(\sum_{i=1}^{d}\frac{D_i}{L_i^2}\right)+c\left(\prod_{i=1}^{d}L_i\right)\right]\right\}\equiv\exp[-f(\{L_i\}|t)], \tag{9}$$

analogous to expression (4). Minimizing $f(\{L_i\}|t)$ with respect to all L_i, $i=1, 2, \ldots, d$, we arrive at the system of equations

$$\frac{\partial f}{\partial L_i}=-\frac{2a_1 D_i}{L_i^3}+\frac{c}{L_i}\left(\prod_{j=1}^{d}L_j\right)=0, i=1,2,\ldots,d, \tag{10}$$

whence we find the optimal values of $L_{i,t}$

$$L_{i,t}=\left[\frac{2DL_i^{(d+2)/2}t}{c\left(\prod_{j=1}^{d}D_j\right)^{1/2}}\right]^{1/(d+2)}, \quad i=1,2,\ldots,d. \tag{11}$$

Substituting the optimal values into $f(\{L_i\}|t)$ we obtain the asymptotic expression for the survival probability

$$-\ln S(t)\simeq f(\{L_{i,t}\}|t)\propto\left[c^{2/d}\left(\prod_{j=1}^{d}D_j\right)^{1/d}t\right]^{d/(d+2)}. \tag{12}$$

This expression is an extension of the relation (1) to the case of anisotropic diffusion. If diffusion is isotropic, both expressions are identical. The estimate (12) holds if all $L_{i,t}$ are much greater than the trap size, $L_{i,t}\gg b$, $i=1, 2, \ldots,d$. This holds at times satisfying the inequality

$$t\gg cb^{d+2}\max\left\{\left[\frac{1}{D_1^{d+2}}\left(\prod_{j=1}^{d}D_j\right)^{1/2},\frac{1}{D_2^{d+2}}\left(\prod_{j=1}^{d}D_j\right)^{1/2},\ldots,\frac{1}{D_d^{d+2}}\left(\prod_{j=1}^{d}D_j\right)^{1/2}\right]\right\}. \tag{13}$$

If at least one of the diffusion coefficients D_i, $i=1, 2, \ldots,d$ vanishes, then the asymptotic behavior (12) is not realized, since the dimension of the problem in this case is lower than the dimension of the d-space.

This work was sponsored by the Russian Fund for Fundamental Research (Grants Nos. 96-03-3218a and 97-03-33683a).

[a)]e-mail: berezh@cc.nifhi.ac.ru

[1]M. von Smoluchowski, Phys. Z. **17**, 557, 585 (1916).
[2]A. A. Ovchinnikov, S. F. Timashev, and A. A. Belyĭ, *Kinetics of Diffusion-Controlled Chemical Processes* [in Russian], Khimiya, Moscow, 1986.
[3]A. M. Berezhkovskii, Yu. A. Makhnovskii, and R. A. Suris, Chem. Phys. **137**, 41 (1989); J. Stat. Phys. **65**, 1025 (1991).
[4]B. Ya. Balagurov and V. G. Vaks, Zh. Éksp. Teor. Fiz. **65**, 1939 (1973) [Sov. Phys. JETP **38**, 968 (1974)].
[5]M. D. Donsker and S. R. S. Varadhan, Commun. Pure Appl. Math. **28**, 525 (1975).
[6]A. A. Ovchinnikov and Ya. B. Zeldovich, Chem. Phys. **28**, 215 (1978).
[7]P. Grassberger and I. Procaccia, J. Chem. Phys. **77**, 6281 (1982).
[8]R. F. Kayser and J. B. Hubbard, Phys. Rev. Lett. **51**, 79 (1983).
[9]I. M. Lifshitz, S. A. Gredeskul, and L. A. Pastur, *Introduction to the Theory of Disordered Systems*, Wiley, New York, 1988 [Russian original, Nauka, Moscow, 1982]; I. M. Lifshitz, Usp. Fiz. Nauk **83**, 617 (1964) [Sov. Phys. Usp. **7**, 549 (1965)]; Zh. Éksp. Teor. Fiz. **44**, 1723 (1963) [Sov. Phys. JETP **17**, 1159 (1963)].
[10]A. M. Berezhkovskii, Yu. A. Makhnovskii, and G. E. Chudinov, Chem. Phys. Lett. **161**, 507 (1989).

Translated by M. E. Alferieff